



Measurements of the production cross-section for a Z boson in association with b - or c -jets in proton–proton collisions at $\sqrt{s} = 13$ TeV with the ATLAS detector

The ATLAS Collaboration

This paper presents a measurement of the production cross-section of a Z boson in association with b - or c -jets, in proton–proton collisions at $\sqrt{s} = 13$ TeV with the ATLAS experiment at the Large Hadron Collider using data corresponding to an integrated luminosity of 140 fb^{-1} . Inclusive and differential cross-sections are measured for events containing a Z boson decaying into electrons or muons and produced in association with at least one b -jet, at least one c -jet, or at least two b -jets with transverse momentum $p_T > 20$ GeV and rapidity $|y| < 2.5$. Predictions from several Monte Carlo generators based on next-to-leading-order matrix elements interfaced with a parton-shower simulation, with different choices of flavour schemes for initial-state partons, are compared with the measured cross-sections. The results are also compared with novel predictions, based on infrared and collinear safe jet flavour dressing algorithms. Selected $Z + \geq 1$ c -jet observables, optimized for sensitivity to intrinsic-charm, are compared with benchmark models with different intrinsic-charm fractions.

Contents

1	Introduction	3
2	ATLAS detector	5
3	Data and simulated event samples	6
3.1	Data sample description	6
3.2	Simulated event samples for signal and background processes	7
3.3	Theoretical predictions	8
4	Object definitions and event selections	9
5	Background estimation	13
5.1	Data-driven estimation of $t\bar{t}$ contribution	13
5.2	Extraction of Z+jets background	13
5.3	Estimation of multijet background contribution	15
6	Kinematic distributions	16
7	Correction to particle level	16
8	Uncertainties in the cross-section measurement	20
8.1	Detector-level systematic uncertainties	20
8.2	Background systematic uncertainties	21
8.3	Unfolding systematic uncertainties	22
9	Results	23
9.1	Inclusive fiducial cross-sections	24
9.2	Differential cross-sections for $Z + \geq 1$ b -jet	25
9.3	Differential cross-sections for $Z + \geq 2$ b -jets	29
9.4	Differential cross-sections for $Z + \geq 1$ c -jet	30
10	Conclusion	34

1 Introduction

The measurement of the production rate of a Z boson in association with jets generated from heavy-flavour quarks, namely c -quarks and b -quarks,¹ leading to $Z + c$ -jets and $Z + b$ -jets final states, in proton–proton (pp) collisions provides an important test of perturbative quantum chromodynamics (pQCD) and of the proton internal structure. Measurements of $Z + c$ -jets and $Z + b$ -jets production provide a benchmark to probe the modelling from Monte Carlo (MC) generators used to estimate the background contribution of these processes to other topologies, such as Higgs boson measurements or searches for new physics which often feature resonant decay into a pair of b -quarks.

State-of-the-art MC predictions for $Z + b$ -jets and $Z + c$ -jet production are available for different flavour and mass schemes and typically based on next-to-leading-order (NLO) matrix elements combined with a parton shower (PS). In the 4-flavour number scheme (4FS), b -quarks can only be generated perturbatively from an explicit gluon splitting ($g \rightarrow b\bar{b}$) in the partonic matrix element, are typically treated as massive, and do not contribute to the parton distribution functions (PDFs) of the proton. This method does not resum logarithms of the type $\alpha_s \ln(Q^2/m_b^2)$, where Q is the hard process scale and m_b the quark mass, making it suitable for processes close to the b -quark mass scale. In the 5-flavour number scheme (5FS), the b -quark density is allowed in the initial state via a b -quark PDF, allowing the resummation of the $\alpha_s \ln(Q^2/m_b^2)$ terms to all orders in α_s . This method is suitable for predictions where the scale of the process is much larger than the b -quark mass, by treating the b -quark as massless. The ambiguity among the schemes is an intrinsic property of the calculation and is expected to reduce with the inclusion of higher-order perturbative corrections [1]. While infrared-safe algorithms are routinely used for inclusive jets at the Large Hadron Collider (LHC), a variety of such algorithms has now also been developed for flavoured jets [2–5].

Inclusive and differential cross-sections of $Z + b$ -jets production were measured in proton–anti-proton collisions at the centre-of-mass energy of $\sqrt{s} = 1.96$ TeV by the CDF and D0 experiments [6, 7]. Measurements of $Z + b$ -jets processes were performed at the LHC in pp collisions at $\sqrt{s} = 7$ TeV by the ATLAS, CMS and LHCb experiments [8–12], at $\sqrt{s} = 8$ TeV by the CMS experiment [13] and at $\sqrt{s} = 13$ TeV by the ATLAS experiment with a partial dataset in both resolved [14] and boosted [15] regimes, and by the CMS experiment with the full Run 2 dataset [16].

Predictions for $Z + c$ -jets production are derived either in a 3-flavour scheme (3FS) or in a 4/5FS. Similarly to the discussion for $Z + b$ -jets production, the two approaches differ by the presence of resummation of $\alpha_s \ln(Q^2/m_c^2)$ terms. The 4/5FS calculations that resum these logarithms are suitable for calculations where the scale of the process is much larger than the mass of c -quark, treating them as massless. In this context, the hypothesis of a valence-like, or intrinsic, component of charm quarks in a proton was first proposed nearly 40 years ago [17, 18]. Although major PDF fitters also provide PDF sets including intrinsic charm (IC) [19, 20], its existence and amount is still subject of a long-standing debate, lacking experimental observations. It was shown that the measurement of photon and Z boson production in association with c -jets in the forward rapidity region is sensitive to the effect of IC [21, 22]. Inclusive and differential cross-sections of $Z + c$ -jets production were measured in $\sqrt{s} = 13$ TeV pp collisions by CMS with a partial dataset [23]. The LHCb experiment has measured $Z + c$ -jets cross-sections in the forward region [24] demonstrating a sizeable excess over predictions made with no-IC PDF in the region of high Z boson rapidity, which was later interpreted as evidence of the IC in the proton [25].

¹ Throughout the paper it is implicitly assumed that c -quark and b -quark refer to both quark and antiquark.

This paper presents measurements of the inclusive and differential production cross-sections of a Z boson, decaying into electrons or muons, in association with at least one c -jet, at least one b -jet or at least two b -jets using the full pp collision dataset collected by the ATLAS experiment at $\sqrt{s} = 13$ TeV and corresponding to 140 fb^{-1} . Measurements of the inclusive $Z + \geq 1$ c -jet, $Z + \geq 1$ b -jet and $Z + \geq 2$ b -jets cross-sections in a fiducial phase space are performed. Differential measurements are performed for observables selected for their sensitivity to pQCD, PDF models and MC generator validation, as detailed in Table 1. In particular: the transverse momentum, p_T , of the Z boson and of the highest- p_T (leading) heavy-flavour jet are able to probe both the pQCD predictions and MC modelling for $Z + \geq 1$ b -jet or $Z + \geq 1$ c -jet production; $\Delta\tilde{R}_{Zb}$ is chosen as it is sensitive to the presence of additional radiation in the event, a substantially different feature of 4FS versus 5FS calculations; the $x_F(c)$ and $R(p_T(Z))$ observables, for $Z + \geq 1$ c -jet events, are sensitive to PDF models and focus on IC sensitivity; finally, m_{bb} and $\Delta\phi_{bb}$ are sensitive to various features of MC generators, in particular $g \rightarrow b\bar{b}$ modelling, in the $Z + \geq 2$ b -jets final state, relevant for Higgs boson measurements or searches for new physics.

Table 1: List of observables used to perform differential cross-section measurements.

Final state	Observable	Notation
$Z + \geq 1$ b -jet	p_T of the leading b -jet	$p_{T,b}^0$
	p_T of the Z boson	$p_T(Z)$
	$\Delta\tilde{R} = \sqrt{(\Delta\phi)^2 + (\Delta y)^2}$ between the Z boson and leading b -jet, where $\Delta\phi$ (Δy) is the azimuthal angle (rapidity) difference	$\Delta\tilde{R}_{Zb}$
$Z + \geq 1$ c -jet	p_T of the leading c -jet	$p_{T,c}^0$
	p_T of the Z boson	$p_T(Z)$
	Feynman- x variable $x_F = 2 p_z(c) /\sqrt{s}$ [26]	$x_F(c)$
	Cross-section ratio of $p_T(Z)$ in $ y(Z) < 1.2$ and $ y(Z) > 1.2$	$R(p_T(Z))$
$Z + \geq 2$ b -jets	Invariant mass of the two leading b -jets	m_{bb}
	Azimuthal angle difference between the two leading b -jets	$\Delta\phi_{bb}$

In comparison with the previous ATLAS measurement [14], more extreme regions of the phase space are explored. The higher integrated luminosity contributes to increase the number of selected events for rare final states with c -jets or two b -jets. Advances in jet reconstruction and b -tagging and the new data-driven methodologies developed for the estimate of main backgrounds allow a reduction of the leading experimental and modelling uncertainties, and thus increase the sensitivity to the signal processes. In addition, the measurement of $R(p_T(Z))$, i.e. the $p_T(Z)$ differential cross-section ratio of forward over central $Z + \geq 1$ c -jet events,² allows further cancellation of systematic uncertainties enhancing sensitivity to IC effects. Finally, recent advances in the theory sector permit a comparison of data with MC predictions using next-to-leading-order matrix elements, expected to provide a better description of the processes.

The strategy of the measurement is the following. Events with a Z boson candidate decaying into an electron or muon pair produced in association with at least one or at least two jets identified as containing a b - or a c -hadron (flavour-tagged) are selected based on variables measured at detector level. Top quark pair and multijet backgrounds are estimated via data-driven techniques, while the remaining non- Z +jets backgrounds (mainly dibosons) are estimated via MC simulations. Selected events containing processes

² The separation of the central and forward $Z + \geq 1$ c -jet event categories for $|y(Z)| = 1.2$ is optimized on the basis of sensitivity to IC models and statistical precision of the expected measurement.

with a genuine Z boson are categorized as $Z + b$ -jets, $Z + c$ -jets and $Z +$ light jets through a likelihood fit on a flavour-sensitive observable (“flavour fit”). The fit is done separately for events with ≥ 1 flavour-tagged jet and with ≥ 2 flavour-tagged jets. Fits are performed in each bin of each observable, using the data to constrain the shape of that observable and the normalisation. Separate electron and muon channel distributions are fitted simultaneously. The non-signal Z +jets components, normalised in the flavour fit, are then subtracted from the data together with the other electroweak (EWK) and top backgrounds. After background subtraction, data are unfolded to particle level using an iterative approach, in a fiducial phase-space close to the detector-level selection. Unfolding inputs are obtained by summing electron and muon-channel distributions. The detector-level systematic uncertainties are propagated by performing the flavour fits and unfolding separately for each systematic variation in a correlated way. Unfolded distributions of $Z + \geq 1$ or ≥ 2 b -jets and $Z + \geq 1$ c -jet are compared with available signal predictions from state-of-the-art generators and from NNLO fixed-order predictions. $Z + \geq 1$ c -jet measurements are finally compared with several PDF sets with different contributions from IC.

This paper is organized as follows. The ATLAS detector is described in Section 2, and details of the data sample and the MC simulations are provided in Section 3. The object definitions and the event selection at detector level are presented in Section 4. Backgrounds that do not contain a real Z boson are estimated via MC simulations or via data-driven techniques, while backgrounds containing a real Z boson and jets are estimated with a fit to data distributions sensitive to the flavour of the jet; both are described in Section 5. Distributions of the kinematic variables are presented in Section 6. After background subtraction, the data are unfolded to particle level in a fiducial phase space, as detailed in Section 7. Systematic uncertainties in the unfolded data are discussed in Section 8. The results are presented in Section 9, and conclusions are drawn in Section 10.

2 ATLAS detector

The ATLAS detector [27] at the LHC covers nearly the entire solid angle around the collision point.³ It consists of an inner tracking detector surrounded by a thin superconducting solenoid, electromagnetic and hadronic calorimeters, and a muon spectrometer incorporating three large superconducting air-core toroidal magnets.

The inner-detector system (ID) is immersed in a 2 T axial magnetic field and provides charged-particle tracking in the range $|\eta| < 2.5$. The high-granularity silicon pixel detector covers the vertex region and typically provides four measurements per track, the first hit generally being in the insertable B-layer (IBL) installed before Run 2 [28, 29]. It is followed by the SemiConductor Tracker (SCT), which usually provides eight measurements per track. These silicon detectors are complemented by the transition radiation tracker (TRT), which enables radially extended track reconstruction up to $|\eta| = 2.0$. The TRT also provides electron identification information based on the fraction of hits (typically 30 in total) above a higher energy-deposit threshold corresponding to transition radiation.

The calorimeter system covers the pseudorapidity range $|\eta| < 4.9$. Within the region $|\eta| < 3.2$, electromagnetic calorimetry is provided by barrel and endcap high-granularity lead/liquid-argon (LAr) calorimeters, with an additional thin LAr presampler covering $|\eta| < 1.8$ to correct for energy loss in material

³ ATLAS uses a right-handed coordinate system with its origin at the nominal interaction point (IP) in the centre of the detector and the z -axis along the beam pipe. The x -axis points from the IP to the centre of the LHC ring, and the y -axis points upwards. Polar coordinates (r, ϕ) are used in the transverse plane, ϕ being the azimuthal angle around the z -axis. The pseudorapidity is defined in terms of the polar angle θ as $\eta = -\ln \tan(\theta/2)$. Angular distance is measured in units of $\Delta R \equiv \sqrt{(\Delta\eta)^2 + (\Delta\phi)^2}$.

upstream of the calorimeters. Hadronic calorimetry is provided by the steel/scintillator-tile calorimeter, segmented into three barrel structures within $|\eta| < 1.7$, and two copper/LAr hadronic endcap calorimeters. The solid angle coverage is completed with forward copper/LAr and tungsten/LAr calorimeter modules optimised for electromagnetic and hadronic energy measurements respectively.

The muon spectrometer (MS) comprises separate trigger and high-precision tracking chambers measuring the deflection of muons in a magnetic field generated by the superconducting air-core toroidal magnets. The field integral of the toroids ranges between 2.0 and 6.0 T m across most of the detector. Three layers of precision chambers, each consisting of layers of monitored drift tubes, cover the region $|\eta| < 2.7$, complemented by cathode-strip chambers in the forward region, where the background is highest. The muon trigger system covers the range $|\eta| < 2.4$ with resistive-plate chambers in the barrel, and thin-gap chambers in the endcap regions.

The luminosity is measured mainly by the LUCID-2 [30] detector that records Cherenkov light produced in the quartz windows of photomultipliers located close to the beam pipe.

Events are selected by the first-level trigger system implemented in custom hardware, followed by selections made by algorithms implemented in software in the high-level trigger [31]. The first-level trigger accepts events from the 40 MHz bunch crossings at a rate below 100 kHz, which the high-level trigger further reduces in order to record complete events to disk at about 1 kHz.

A software suite [32] is used in data simulation, in the reconstruction and analysis of real and simulated data, in detector operations, and in the trigger and data acquisition systems of the experiment.

3 Data and simulated event samples

3.1 Data sample description

The data used in this measurement were collected with the ATLAS detector at the LHC between 2015 and 2018 in pp collisions at $\sqrt{s} = 13$ TeV (LHC Run 2). Crossings of proton bunches occurred every 25 ns, the collisions achieved a peak instantaneous luminosity of $2.1 \times 10^{34} \text{ cm}^{-2}\text{s}^{-1}$, and the mean number of pp interactions per bunch crossing (pile-up) was $\langle \mu \rangle = 34$.

The recorded data correspond to a total integrated luminosity of 140 fb^{-1} with an uncertainty of 0.83% [33], obtained using the LUCID-2 detector [30] for the primary luminosity measurements, complemented by measurements using the inner detector and calorimeters. Data quality requirements are applied to ensure that all detector components were in good operating conditions.

The candidate events are selected by either a single-electron or single-muon trigger with minimum transverse momentum threshold, quality and isolation requirements [34–36]. The p_T threshold in 2015 is 24 (20) GeV for the electrons (muons), satisfying loose isolation requirements. Due to the higher instantaneous luminosity in 2016–2018, the p_T threshold is increased to 26 GeV for both the electrons and the muons, and more restrictive isolation requirements are imposed on both leptons along with more restrictive identification requirements for electrons. Triggers with higher p_T thresholds but with no isolation requirement or with loosened identification criteria were also used to increase the efficiency.

Table 2: Summary of signal and background MC samples. The generator programs used in the simulation are listed in the second column. The QCD order in the calculation of the matrix elements (ME) is indicated in the third column, where np denotes the number of real parton emissions, and FS refers to the flavour scheme used. The precision in QCD calculation for the inclusive production cross-section (σ_{prod}) is provided in the fourth column.

Process	Generator	Order of pQCD in ME (FS)	Order σ_{prod} calculation
$Z \rightarrow \ell\ell$	MGAMC+PY8 FxFx	0–3p NLO (5FS)	
$Z \rightarrow \ell\ell$	SHERPA 2.2.11	0–2p NLO, 3–5p LO (5FS)	
$t\bar{t}$	NNLO+NNLL		
single top ($s/t/Wt$ -channel)	POWHEG+PY8	NLO	NLO
$qg/q\bar{q} \rightarrow VV \rightarrow \ell\ell/\ell\nu/\nu\nu + q\bar{q}$	SHERPA 2.2.1	1p NLO, 2–3p LO	NLO
$qq \rightarrow ZH \rightarrow \ell\ell/\nu\nu + b\bar{b}$	POWHEG+PY8	NLO	NNLO (QCD), NLO (EWK)
$gg \rightarrow ZH \rightarrow \ell\ell/\nu\nu + b\bar{b}$	POWHEG+PY8	NLO	NLO+NLL

3.2 Simulated event samples for signal and background processes

MC simulations are used to describe signal events, to estimate the contribution of background processes, to unfold the data yield to the particle level, to estimate systematic uncertainties and in comparison with the unfolded data distributions. Generated events are processed using a full detector simulation [37] based on GEANT4 [38], for the detector response to final-state particles, and then reconstructed using the same algorithms as the data. To account for pile-up, multiple overlaid inelastic pp collisions are simulated with PYTHIA 8.186 [39] using the A3 tune [40] and the NNPDF 2.3 LO PDF set [41]. The distribution of the average number of interactions per bunch crossing in the simulations is weighted to reflect the one in data.

An overview of all signal and background processes and the generators used for the production of nominal results is given in Table 2.

Inclusive Z boson production in association with both light- and heavy-flavour jets is simulated using the MADGRAPH5_AMC@NLO v2.6.5 [42] generator, combined with PYTHIA v8.245 [43] parton shower using the FxFx [44] merging procedure (MGAMC+PY8 FxFx). This program generates matrix elements for Z boson production, with up to three additional partons in the final state at NLO accuracy in the strong coupling constant [45]. The showering and subsequent hadronisation is performed using PYTHIA v8.245 with the A14 tune [46], using the NNPDF 2.3 LO PDF set with $\alpha_s = 0.130$. The different jet multiplicities are merged using the FxFx NLO matrix element and parton shower merging prescription. The MGAMC+PY8 FxFx calculation uses the 5FS with massless b - and c -quarks at the matrix element level, and massive quarks in the PYTHIA 8 parton shower. At the generation level, the jet momentum is required to be at least 10 GeV. The PDF set used for event generation is NNPDF3.1LUXQED with $\alpha_s = 0.118$ [47]. The merging scale is set to $Q_{\text{cut}} = 20$ GeV. MGAMC+PY8 FxFx Z +jets samples are used for the nominal signal and background determination, unfolding of the data distributions, to estimate the uncertainties and are compared with the final cross-section measurements. $Z(\rightarrow \tau\tau)$ +jets background samples are also modelled by MGAMC+PY8 FxFx.

Additional $Z(\rightarrow \ell\ell)$ +jets ($\ell = e, \mu$) samples are simulated with the ATLAS configuration of SHERPA 2.2.11 [45], which computes NLO-accurate matrix elements for up to two partons and LO-accurate matrix elements for up to five partons with the Comix [48] and OPENLOOPS [49–51] libraries. The default

SHERPA parton shower [52] based on a Catani–Seymour dipole factorization and the cluster hadronisation model [53] is used. SHERPA 2.2.11 performs a 5FS calculation with massless b - and c -quarks at the ME level, and massive quarks in the parton shower. The Hessian NNPDF 3.0 NNLO set of PDFs [54] is used, calculated at next-to-next-to-leading order (NNLO) in QCD with $\alpha_s = 0.118$. The samples are produced using a dedicated set of parameters developed by the SHERPA authors. The different jet multiplicities are merged using the MEPS@NLO prescription [55–58], with merging scale Q_{cut} set to 20 GeV. The samples provide an alternative in the modelling of $Z(\rightarrow \ell\ell)$ +jets processes to MGAMC+PY8 FxFx. In particular they are used to determine the uncertainty on the Z +jets background, to evaluate the modelling uncertainty in the unfolding procedure and finally in comparison with the measured data.

The $t\bar{t}$ simulations use the POWHEGBOX v2 [59–62] generator at NLO with the NNPDF3.0_{NLO} [54] PDF set and the h_{damp} parameter⁴ set to $1.5 m_{top}$ [63]. The events are interfaced to PYTHIA 8.230 [43], using the A14 tune [46] and the NNPDF2.3_{LO} set of PDFs [41]. This sample is normalized to the NNLO cross-section, including the resummation of next-to-next-to-leading logarithmic (NNLL) soft gluon terms, calculated with TOP++2.0 [64–70].

Single top quark production, in association with W bosons (tW) as well as in the s - and t - channels, is also simulated using POWHEGBOX v2 at NLO using the NNPDF3.0_{NLO} PDF set interfaced with PYTHIA 8.230 using the NNPDF 2.3 LO PDF set. To remove overlap with the $t\bar{t}$ sample, the diagram-removal [71] procedure was used.

Semileptonic diboson (VV) final states, where one W or Z boson decays leptonically and the other decays hadronically, were simulated with SHERPA v.2.2.1 [72], with NLO MEs for up to one parton emission and LO MEs for up to three parton emissions calculated using the NNPDF 3.0 NNLO PDF set. The ME calculations are matched to the SHERPA parton shower using the MEPS@NLO prescription.

Simulated events for $q\bar{q} \rightarrow ZH(\rightarrow \ell\ell + b\bar{b})$ and $g\bar{g} \rightarrow ZH(\rightarrow \ell\ell + b\bar{b})$ processes in inclusive production or in association with one jet at NLO are generated with the POWHEGBOX v2 interfaced with PYTHIA 8.230 generator with the NNPDF 3.0 NNLO PDF set. The samples include all final states where the Higgs boson decays into $b\bar{b}$ and the Z boson in a leptonic final state. The mass of the Higgs boson is set to 125 GeV and the $H \rightarrow b\bar{b}$ branching ratio is set to 58%. The $q\bar{q} \rightarrow ZH(\rightarrow \ell\ell + b\bar{b})$ cross-section is calculated at NNLO (QCD) and NLO (EWK), while $g\bar{g} \rightarrow ZH(\rightarrow \ell\ell + b\bar{b})$ cross-section is calculated at NLO+NLL (QCD). Contributions from $t\bar{t}Z$ and tZ processes are found to be negligible and are not included.

3.3 Theoretical predictions

In addition to particle-level predictions from the fully simulated MGAMC+PY8 FxFx and SHERPA 2.2.11 samples described above, the measured unfolded cross-sections are compared with several theoretical predictions, in order to test the sensitivity to different flavour schemes in the matrix element calculation, to the intrinsic-charm component in the proton PDF and to higher orders in QCD calculation.

The generator predictions, all based on MGAMC+PY8, and their respective settings are summarized in Table 3.

To test the 4FS predictions, a sample of $Z + b\bar{b}$ events generated by MADGRAPH5_AMC@NLO v3.5.3 is produced using the 4FS with massive b -quarks at NLO with two partons in the matrix element. It uses

⁴ The h_{damp} parameter is a resummation damping factor and one of the parameters that control the matching of POWHEG matrix elements to the parton shower and thus effectively regulates the high- p_T radiation against which the $t\bar{t}$ system recoils.

the 4-flavour NNPDF 3.1 NLO PDF set (with only perturbative charm contribution) with $\alpha_s = 0.118$; the sample is combined with PYTHIA v8.310 for the parton shower and hadronisation. To provide a 5FS reference for these predictions, another sample is produced with MADGRAPH5_AMC@NLO v2.7.3 in the 5FS, where $Z + b$ -jets and $Z + c$ -jets production is modelled with massless quarks in the matrix element, generated at NLO accuracy with one parton. It uses the NNPDF 2.3 NLO PDF with $\alpha_s = 0.118$. The showering and subsequent hadronisation is performed with PYTHIA v8.243 where b -quarks are treated as massive.

For the 3FS prediction of $Z + c$ -jets production, a $Z + c\bar{c}$ event sample is generated with MADGRAPH5_AMC@NLO v3.5.3 at NLO with two partons, treating c -quarks as massive in the matrix element. It uses the 3-flavour NNPDF 3.1 NLO PDF set (with only perturbative charm contribution) with $\alpha_s = 0.118$. The showering and subsequent hadronisation is done with PYTHIA v8.310 with massive c -quarks.

Finally, a variety of predictions testing several IC models were produced using the PDF reweighting technique according to the prescriptions in Ref. [73]. The standard MGAMC+PY8 FxFx sample is used as a baseline for PDF reweighting. One possibility to include the IC is provided by the NNPDF group and allows a fraction of IC already in the nominal NNPDF3.1LUXQED PDF used in the MGAMC+PY8 FxFx sample. A later analysis still allows it in the nominal NNPDF4.0 PDF sets [74]. Moreover, fits including the LHCb Z +charm measurement [24] and EMC data [75] on top of the baseline NNPDF dataset have been performed [25]. In the latter case, the NNPDF group has claimed a 3σ evidence of presence of the intrinsic charm in the proton. Predictions for the $Z + c$ -jets processes are produced using the nominal NNPDF 4.0 NNLO PDF and the one including the LHCb and EMC data. To produce a no-IC reference to those, another prediction is made using the NNPDF4.0 NNLO (pCH) PDF that includes only perturbative charm contribution.

Two predictions are produced using the CTEQ-TEA PDF sets including IC contributions under various assumptions [76]. One of them is made using a PDF based on the CT18NNLO fit implementing the BHPS3 model of IC [20, 77]. The other one uses a CT18NNLO variant including IC following a meson-baryon model based on the effective-mass (MBME) quark model [78]. As a reference for these, a no-IC prediction is made using the nominal CT18NNLO PDF that includes only perturbative charm contribution.

Lastly, two predictions are made using earlier PDFs from CT14 fits that include a fixed amount of IC. They are based on the CT14NNLO baseline fit and correspond to BHPS1 and BHPS2 models that include IC with an average fraction of proton momentum carried by intrinsic c -quarks of 0.6% and 2.1%, respectively [20]. A no-IC prediction with the nominal CT14NNLO PDF is also provided as no-IC reference.

In addition, fixed-order NLO and NNLO QCD Z +jets predictions with massless quarks are obtained for signal comparisons, following the numerical set-up of [3]. Notably, the flavour of the jets are assigned following an infrared and collinear (IRC) safe algorithm referred to as the flavour-dressing algorithm [2].⁵

4 Object definitions and event selections

In this measurement, events are required to have a signature consistent with a Z boson, decaying into two electrons or two muons, in association with at least one or at least two b -jets or at least one c -jet.

⁵ Numerically, the main difference of this definition is that jets containing a $b\bar{b}$ or a $c\bar{c}$ pair (i.e. double tagged jets) are considered flavour-less, a contribution which becomes more relevant in the high $p_T(Z)$ regime.

Table 3: Summary of all MC prediction along with the flavour schemes (FS) and PDFs they use. PDF ID numbers are given according to LHAPDF [79] numbering scheme.

Generator/settings	Flav. scheme	PDF	LHAPDF ID
Main MC samples			
MGAMC+Py8 FxFx	5FS	NNPDF3.1 (NNLO) LuxQED	325100
SHERPA 2.2.11	5FS	NNPDF3.0 (NNLO)	303200
Predictions to test various flavour schemes			
MGAMC+Py8	5FS	NNPDF2.3 (NLO)	229800
MGAMC+Py8 Zbb	4FS	NNPDF3.1 (NLO) _{PCH}	321500
MGAMC+Py8 Zcc	3FS	NNPDF3.1 (NLO) _{PCH}	321300
Intrinsic charm (IC) predictions			
MGAMC+Py8 FxFx	5FS	NNPDF4.0 (NNLO) _{PCH} (no IC)	332100
		NNPDF4.0 (NNLO)	331100
		NNPDF4.0 (NNLO) EMC+LHCbZc	– [25]
		CT18 (NNLO) (no IC)	14000
		CT18FC – CT18 BHPS3	14087
		CT18FC – CT18 MCM-E	14093
		CT14 (NNLO) (no IC)	13000
		CT14 (NNLO)IC – BHPS1	13082
		CT14 (NNLO)IC – BHPS2	13083
		Fixed-order predictions [3]	
NLO	5FS	PDF4LHC21	93000
NNLO	5FS	PDF4LHC21	93000

Events are selected if they are recorded during stable beam conditions and if they satisfy detector and data-quality requirements [80]. Candidate events are required to have a primary vertex (PV), defined as the vertex with the highest sum of track p_T^2 , with at least two associated tracks measured in the ID, each with $p_T > 500$ MeV [81].

Electron candidates are reconstructed from ID tracks coming from the PV, which are matched to clusters of energy deposited in the electromagnetic calorimeters. Electrons must fulfil the following PV conditions: the longitudinal impact parameter (z_0) is required to satisfy $|z_0 \sin(\theta)| < 0.5$ mm, where θ is the angle of the track with respect to the beam-line, and the transverse impact parameter significance (d_0/σ_{d_0}) is required to satisfy $d_0/\sigma_{d_0} < 5$. Electrons must satisfy requirements on the shape of the electromagnetic shower in the calorimeter, track quality and track-cluster matching, using a likelihood-based identification with a ‘Tight’ working-point [82]. Electrons must be isolated, passing the ‘Tight-Var’ working point, built from tracking and calorimeter information, with a energy-dependent variable cone [82]. Electron are required to have $p_T > 27$ GeV and $|\eta| < 2.47$. Candidates in the transition region between the barrel and end-caps of the electromagnetic calorimeters ($1.37 < |\eta| < 1.52$) are excluded.

Muon candidates are identified by matching ID tracks coming from the PV to either full tracks or track segments reconstructed in the muon spectrometer. The candidates must pass the following PV requirements: the longitudinal impact parameter must satisfy $|z_0 \sin(\theta)| < 0.5$ mm and the transverse impact parameter significance must satisfy $|d_0|/\sigma(d_0) < 3$. Muons are required to fulfil ‘Medium’ identification requirements [83] based on quality criteria applied to the inner-detector and muon-spectrometer tracks. Muons must be isolated, passing the ‘FCTight’ working point, built from tracking and calorimeter information, with a p_T -dependent variable cone [84]. Muon candidates are required to have $p_T > 27$ GeV

and $|\eta| < 2.5$.

Hadronic jets are reconstructed using the anti- k_t algorithm [85] implemented in the FASTJET package [86], with radius parameter $R = 0.4$, from particle-flow objects [87]. Jets are calibrated using a simulation-based calibration scheme, followed by in situ corrections to account for differences between simulation and data [88]. To eliminate jets coming from pile-up vertices, jets with $p_T < 60$ GeV and $|\eta| < 2.4$ are required to have a significant fraction of their tracks with origin compatible with the PV, as defined by a jet vertex tagger (JVT) discriminant [89]. Selected jets must have $p_T > 20$ GeV and rapidity $|y| < 2.5$.

Jets containing heavy-flavour hadrons are identified using a cut on the DL1r b -tagging discriminant [90], a deep-learning multivariate algorithm trained using information about tracks and the secondary vertexes within a jet. Jets are selected if they pass the 85% working point, which corresponds to an efficiency of 85% in selecting jets containing a b -hadron, of 30% for jets containing a c -hadron (and no b -hadrons) and of 2.5% for jets containing only light hadrons. Flavour-tagged jets are required to have $p_T > 20$ GeV and pseudorapidity $|\eta| < 2.5$.

Electrons, muons and jets are reconstructed and identified independently. An overlap-removal procedure is then applied to uniquely identify these objects in an event. Preselected jets with a high probability to be initiated by an electron or a radiated photon, such that ΔR between the jet and a lepton is smaller than 0.2, are removed. In a second step, leptons closer than $\Delta R = 0.4$ to any remaining jet are removed.

The missing transverse momentum \vec{p}_T^{miss} , with magnitude E_T^{miss} , is defined as the negative vector sum of the transverse momentum of all identified hard physics objects (electrons, muons, jets), as well as an additional track-based soft term accounting for the contribution of unclustered particles, as in Ref. [91].

Events are required to have exactly two leptons of the same flavour (ee or $\mu\mu$) and of opposite charge with dilepton invariant mass in the range of $76 \text{ GeV} < m_{\ell\ell} < 106 \text{ GeV}$. At least one of the lepton candidates is required to match the lepton that triggered the event. To reject the large contribution from $t\bar{t}$ background, events with $p_T^{\ell\ell} < 150$ GeV must have $E_T^{\text{miss}} < 60$ GeV. For events passing these selection criteria two signal regions are defined: those with at least one flavour-tagged jet form the “1-tag” region; and those with at least two flavour-tagged jets form the “2-tag” region.

A summary of the object definitions and the event selections used in the analysis is given in Table 4.

Table 4: Summary of object definitions and event selections defining the signal regions of the analysis at detector level.

Object definition		
	Electron channel	Muon channel
Leptons	Single electron trigger Tight Isolated $d_0/\sigma_{d_0} < 5$, $ z_0 \sin(\theta) < 0.5$ mm $p_T > 27$ GeV $ \eta < 1.37$ or $1.52 < \eta < 2.47$	Single muon trigger Medium Isolated $d_0/\sigma_{d_0} < 3$, $ z_0 \sin(\theta) < 0.5$ mm $p_T > 27$ GeV $ \eta < 2.5$
Jets	$p_T > 20$ GeV and $ y < 2.5$ $\Delta R(\text{jet}, \ell) > 0.4$	
Flavour-tagged jets	$p_T > 20$ GeV and $ y < 2.5$ DLIr@85%	
Event selection		
Leptons	Exactly 2, same-flavour, opposite-charge	
$m_{\ell\ell}$	$76 \text{ GeV} < m_{\ell\ell} < 106 \text{ GeV}$	
E_T^{miss}	$E_T^{\text{miss}} < 60 \text{ GeV}$ if $p_T^{\ell\ell} < 150 \text{ GeV}$	
Flavour-tagged jets	≥ 1 or ≥ 2 jets, DLIr@85%	
Signal regions		
1-tag	≥ 1 flavour-tagged jets	
2-tag	≥ 2 flavour-tagged jets	
Rapidity regions		
Central rapidity	Z boson rapidity $ y(Z) < 1.2$	
Forward rapidity	Z boson rapidity $ y(Z) \geq 1.2$	

In MC samples, events passing the selection in Table 4 are furthermore categorised according to the flavour of the underlying hadron generating the jet. First, the selected jets are classified as either b -, c - or light jets using cone-based criteria as follows. They are labelled as b -jets if they lie within $\Delta R = 0.3$ of at least one b hadron with $p_T > 5$ GeV. If a b hadron matches two jets, only the closest jet in ΔR is labelled as b -jet. Jets not identified as b -jets are considered to be c -jets if they lie within $\Delta R = 0.3$ of any c hadron with $p_T > 5$ GeV. All other jets are classified as light jets. Then, simulated events are sequentially classified as follows. If they have heavy-flavour jets and the leading one is a b -jet, they are classified as $Z + b$ or $Z + bb$ when there is exactly one or more than one b -jet, respectively. If the leading heavy-flavour jet is a c -jet, they are classified as $Z + c$. Finally, they are classified as $Z + l$ when only light jets are present.

In the 1-tag signal region, $Z + \geq 1$ b -jet and $Z + \geq 1$ c -jet analyses are performed. In the former, the sum of $Z + b$ and $Z + bb$ samples is used to define the signal, while the Z +jets background corresponds to the sum of the $Z + c$ and $Z + l$ samples. In the latter, $Z + c$ is used to define the signal, while the sum of the $Z + b$, $Z + bb$ and $Z + l$ samples is treated as Z +jets background. In the 2-tag signal region, $Z + \geq 2$ b -jets analysis is performed, where the signal is given by the $Z + bb$ sample, while the sum of the $Z + b$, $Z + c$, and $Z + l$ samples form the Z +jets background.

5 Background estimation

The dominant background in both the 1-tag and 2-tag signal regions is composed by events with a Z boson produced in association with jets where jet flavour is different from the one targeted in the measurement, i.e. light jets and either c -jets for $Z + \geq 1$ b -jet and $Z + \geq 2$ b -jets measurements or b -jets for $Z + \geq 1$ c -jet measurement. This is determined using a fit to data, as detailed in Section 5.2. Dileptonic $t\bar{t}$ events represent the second largest background, especially important in 2-tag region. Its contribution is estimated with a data-driven method, as explained in Section 5.1. Smaller background contributions from dibosons, ZH , single top quark and $Z \rightarrow \tau\tau$ productions are estimated using simulation, as described in Section 3.2. Background contributions from multijet events are estimated with a data-driven technique and found to be negligible as described in Section 5.3.

5.1 Data-driven estimation of $t\bar{t}$ contribution

A control region enriched with $t\bar{t}$ events is constructed using the same event selection of Table 4, but requiring opposite-flavour $e^\pm\mu^\mp$ final states, instead of same-flavour e^+e^- and $\mu^+\mu^-$ ones, and a wider dilepton mass window $71 \text{ GeV} < m_{\ell\ell} < 111 \text{ GeV}$. This control region contains only percent-level contributions from single-top production events and other processes. Examples of $t\bar{t}$ control region distributions are shown in Figure 1.

The prediction for the $t\bar{t}$ distributions⁶ in the signal regions is obtained by subtracting all non- $t\bar{t}$ simulated backgrounds from the data in the control region and multiplying by $ee/e\mu$ and $\mu\mu/e\mu$ transfer factors. The transfer factors are derived as the ratio of the simulated $t\bar{t}$ distribution in the signal region to that in the control region for each observable.

All detector systematic uncertainties described in Section 8 are propagated to the $t\bar{t}$ estimate by applying corresponding variation to the simulated $t\bar{t}$ sample used for deriving the transfer factors, and to the non- $t\bar{t}$ simulated backgrounds in the control region. The propagation of theoretical uncertainties associated with the simulated $t\bar{t}$ sample was found to have negligible effect. An additional uncertainty is introduced to evaluate possible bias from the extrapolation of $t\bar{t}$ contribution to the signal region. It is evaluated in a validation region defined to be similar to the signal region but requiring $E_{\text{T}}^{\text{miss}} \geq 60 \text{ GeV}$, irrespective of the value of $p_{\text{T}}^{\ell\ell}$, and requiring the dilepton mass to satisfy $71 \text{ GeV} < m_{\ell\ell} < 76 \text{ GeV}$ or $106 \text{ GeV} < m_{\ell\ell} < 111 \text{ GeV}$. The uncertainty is computed as difference between the $t\bar{t}$ estimate by extrapolation from the control region and the result of subtracting simulated non- $t\bar{t}$ contributions in the validation region. This difference reaches 10% for low transverse momenta of Z boson and of leading tagged jet and is mostly consistent with zero elsewhere.

5.2 Extraction of Z +jets background

The flavour fit consists in a set of maximum-likelihood fits to data used to correct the simulated shape and rate of Z +jets background components. The individual fits are based on templates of a jet-flavour sensitive distribution built using events falling in kinematic regions corresponding, in most of the cases, to the bins of the observable used in the cross-section measurement. In statistically limited kinematic regions, events

⁶ This data-driven estimate automatically includes minor processes where $t\bar{t}$ dileptonic events are produced in association with vector bosons.

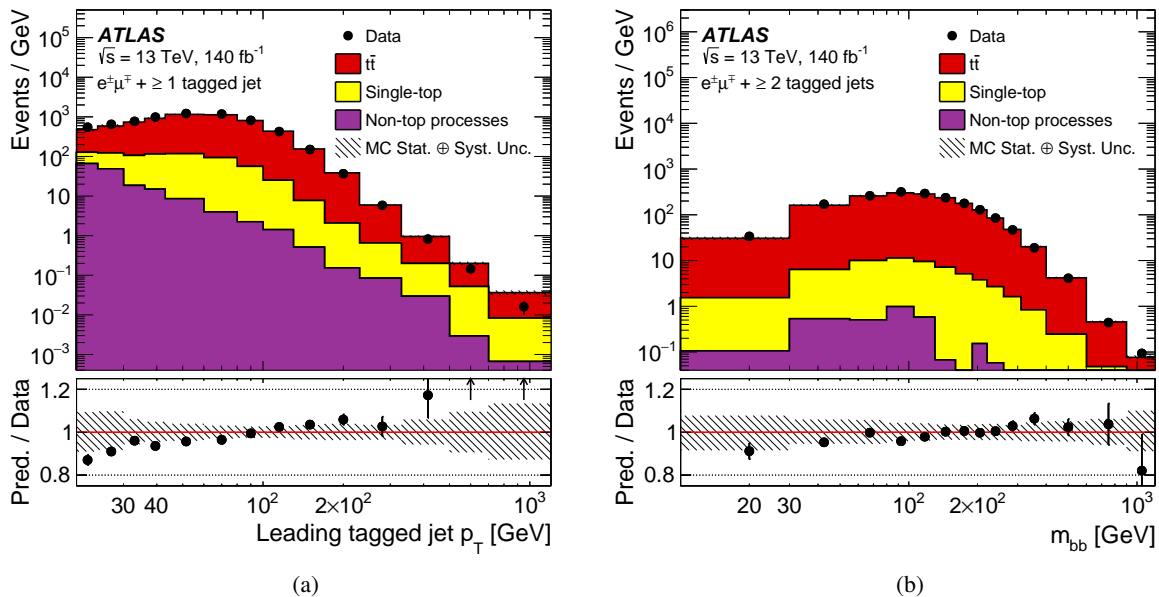


Figure 1: Distribution of events in the $t\bar{t}$ control region as a function of (a) leading tagged jet p_T for the 1-tag selection, and (b) m_{bb} for the 2-tag selection. The lower panels display the ratio of the predictions of MC simulations for signal plus background to data. The statistical uncertainty of the data is shown as error bars and the total uncertainty of the prediction as a hatched band (MC theory uncertainties are not included).

from up to four cross-section bins can be merged to produce the templates. Such merged bin boundaries are always aligned with those of the cross-section bins. Each individual fit is done simultaneously in the electron and muon channels, while fits using each lepton channel independently are checked to yield consistent results.

In the 1-tag region, the DL1r b -tagging discriminant output of the leading flavour-tagged jet is used as the flavour-sensitive distribution. This observable is split in four intervals corresponding to certain ranges of b -tagging efficiencies, namely 85–77% (bin 1 – loosest b -jet selection, lowest purity), 77–70% (bin 2), 70–60% (bin 3), and < 60% (bin 4 – tightest b -jet selection, highest purity). Separate templates are built for simulated $Z + \geq 1$ b -jet, $Z + \geq 1$ c -jet and $Z +$ light jets events. All non- Z +jets backgrounds are combined to build a single template.

In the 2-tag region, the previously described four intervals of the DL1r discriminant outputs of the leading and the sub-leading flavour-tagged jets are combined to give a new ten-bin distribution used for fitting.⁷ Templates are built separately for $Z + \geq 2$ b -jets, $Z + 1$ b -jet, $Z + \geq 1$ c -jet and $Z +$ light jets events, while all non- Z +jets backgrounds are again combined in a single template.

For all the fits, the normalisation of each Z +jets template is left unconstrained, while non- Z +jets backgrounds are fixed to their MC estimate (and to the data-driven estimate for the $t\bar{t}$ background). For each measured observable, the fits result in a set of scale factors for each Z +jets component, which are the ratios of their

⁷ The first four bins include events with one jet in the 85–77% efficiency range and the other in one of the four bins as ordered above; bins 5–7 include those with one jet in the 77–70% range and the other in one of the three ranges with efficiency below 77%; bins 8 and 9 correspond to one jet in the 70–60% range and the other in the same or < 60% range; finally, in bin 10 both jets are in the < 60% efficiency range.

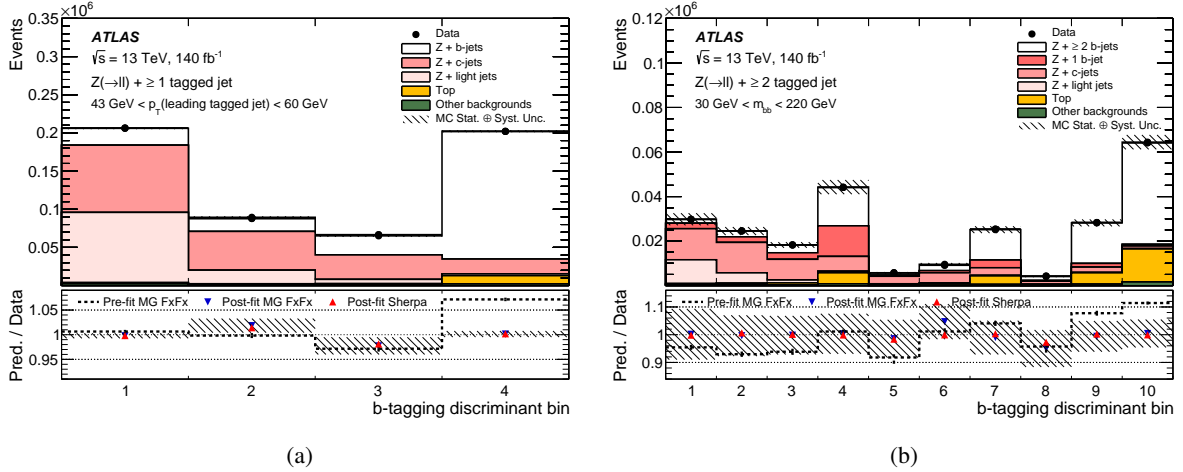


Figure 2: Flavour-sensitive distributions for (a) the 1-tag region fit in the interval $[43, 60]$ GeV of $p_{T,b}^0$ and (b) the 2-tag region fit in the interval $[30, 220]$ GeV of m_{bb} . The main panel compares data and post-fit distribution. The bottom panels show the ratio of the pre-fit and post-fit distributions to data when using MGAMC+PY8 FxFx and SHERPA for Z+jets simulated samples. The total uncertainty of the MGAMC+PY8 FxFx post-fit distribution is shown as a hatched band.

post-fit and pre-fit yields in each bin. Figure 2 shows two examples of flavour-sensitive distributions after the fit in 1-tag and 2-tag regions.

In order to perform the background subtraction from data, the initial MC-based templates of the Z+jets background components, i.e. only Z+light jets and Z+c-jets for $Z + \geq 1$ b-jet measurement, same and Z+1 b-jet for $Z + \geq 2$ b-jets measurement, or only Z+light jets and Z+b-jets for $Z + \geq 1$ c-jet measurement, are modified using the scale factors in each bin of the flavour fit. Normalisation scale factors obtained for the signal are not applied to the data. In cases where binning for the flavour fit is coarser than for the cross-section measurements, the same scale factor is applied to all bins belonging to the merged one used for the flavour fit. The effect of detector-level systematic uncertainties due to the object selection efficiencies and calibrations, discussed in Section 8, are assessed by repeating the fits with the templates varied according to each of the uncertainties. The fit is also repeated for each of the uncertainties affecting the $t\bar{t}$ background and theory uncertainties of Z+jets and other simulated processes. An additional systematic uncertainty affecting the Z+jets background shape is derived by taking the difference between the post-fit Z+jets background evaluated using MGAMC+PY8 FxFx and SHERPA simulated samples.

5.3 Estimation of multijet background contribution

Background contributions from multijet events is studied separately in the electron and muon channels using a data-driven technique. Control regions enriched with such events are defined to derive the expected shapes of this background. These control region definitions are similar to those of the signal regions in Table 4 and only lepton selection requirements are different. In the muon channel, the multijet-enriched control region is characterized by removing the muon isolation criteria and requiring both muon candidates to have the same charge. In the electron channel, the identification and impact parameter cuts for electrons are removed, isolation requirement is inverted, and electrons are required to have the same charge.

In both lepton channels, contributions from non-multijet sources in the control regions are estimated from simulation and subtracted from the data, with the remaining distributions used as shape templates. A simultaneous fit of the $m_{\ell\ell}$ distribution to data in the signal and multijet control region is performed within the $40 \text{ GeV} < m_{\ell\ell} < 160 \text{ GeV}$ window, in the 1-tag and 2-tag regions separately. The normalisation of the Z +jets processes and of the multijet background templates is left unconstrained in the fit, while the normalisation of the other processes is fixed.

Systematic uncertainties in the multijet contribution are assessed by excluding the Z boson peak from the fit, performing the fit in the regions without requiring the jets to satisfy flavour tagging selection (with subsequent extrapolation to the signal regions using normalisation factors equal to the fraction of events in the multijet control region that satisfy the 1-tag and 2-tag requirements) and by allowing the processes other than Z +jets to be varied independently in the fit. All these fit variations still yield multijet background estimates consistent with zero. This background is therefore neglected in the analysis.

6 Kinematic distributions

After requiring the event selection described in Section 4, the measured and expected distributions are compared at the detector level. Pre-fit distributions are used for the signal samples. The Z +jets background components are scaled using the respective normalization factors derived from the flavour fit.

Figure 3 shows the distributions of events in the 1-tag signal region as a function of leading tagged jet p_T (a) and of leading tagged jet x_F (b), when considering $Z + \geq 1$ b -jet and $Z + \geq 1$ c -jet as signal, respectively. The distribution of the events in the 2-tag signal region is presented as a function of m_{bb} (c), when considering $Z + \geq 2$ b -jets as signal. In each distribution, the Z +jets processes are modelled with MGAMC+PY8 FxFx, and SHERPA 2.2.11 is presented in comparison. The uncertainty bands include the uncertainties on the statistics of the simulated sample, on the event-selection (omitting the common luminosity uncertainty) and on the background, as described in Section 8. Theory uncertainties on the generators are not included. The agreement between the data and the sum of the estimated signal and backgrounds is generally within 10% for the measurements in the 1-tag region and within 20% for the $Z + \geq 2$ b -jets measurement (where the signal purity is higher).

The total numbers of selected events in data and in predictions are presented in Table 5, separately for $Z + \geq 1$ b -jet, $Z + \geq 1$ c -jet and $Z + \geq 2$ b -jets measurements, together with the prediction of signal and background process, expressed as a fraction of the total number of predicted events.

7 Correction to particle level

The signal event yields are determined by subtracting the estimated background contributions from the data. The resulting distributions are corrected for detector-level effects, to the fiducial phase space at particle level, as defined in Table 6. Particle-level objects are selected with requirements close to the reconstruction level selection described in Section 4 to limit the dependence of the measurement on theoretical predictions. In this definition, the lepton kinematic variables are computed using final-state leptons from the Z boson decay. Radiated photons within a cone of $\Delta R = 0.1$ around the direction of a final-state lepton are added to the lepton, and the sum is referred to as the ‘dressed’ lepton. Particle-level jets are identified by applying the anti- k_r algorithm with $R = 0.4$ to all final-state particles with a lifetime longer than 30 ps, excluding

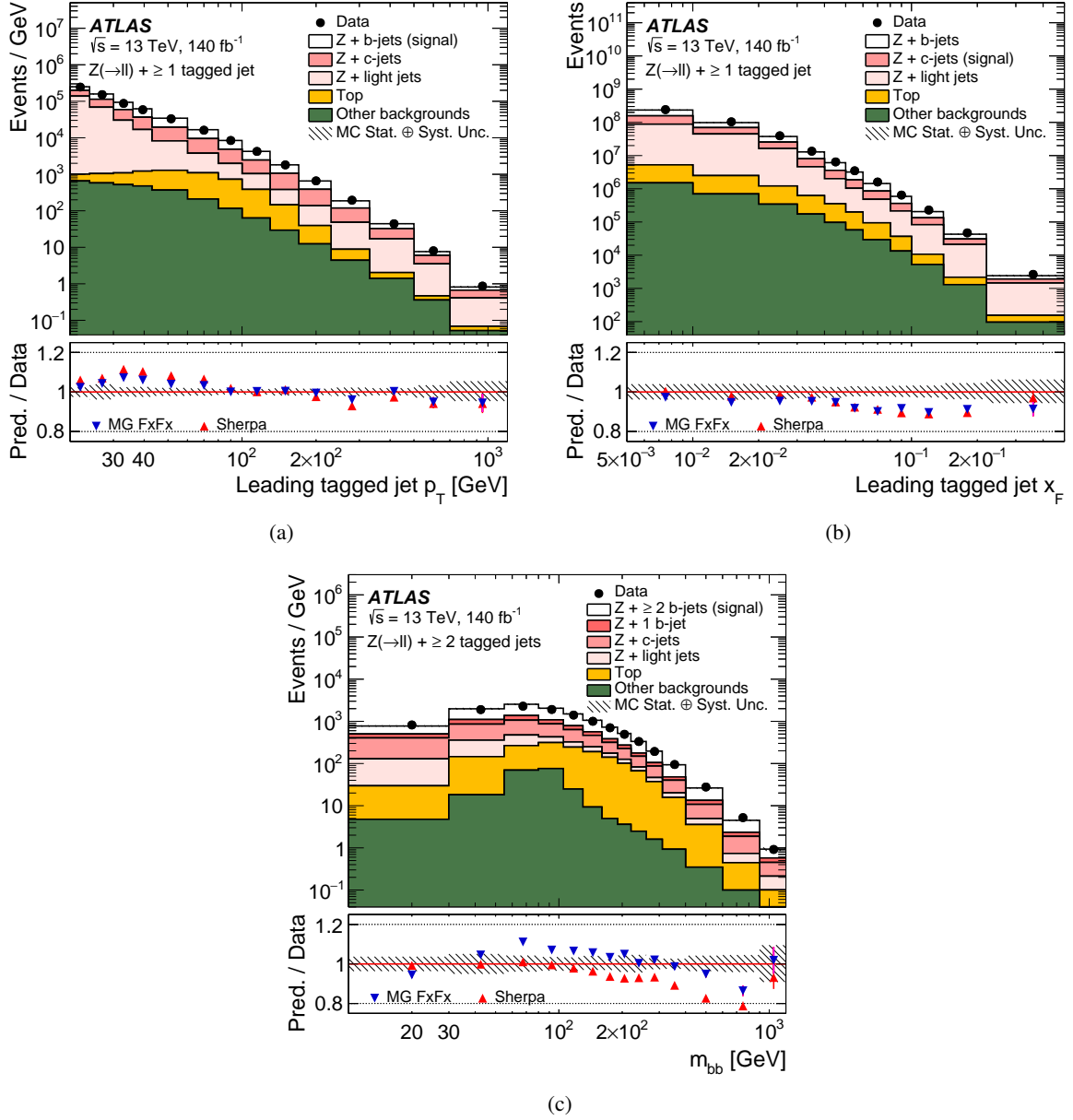


Figure 3: Distribution of events passing the event selection as a function of (a) leading tagged jet p_T for $Z + \geq 1$ b -jet as signal and (b) leading tagged jet x_F for $Z + \geq 1$ c -jet as signal in the 1-tag region and (c) invariant mass of the leading and sub-leading tagged jets for $Z + \geq 2$ b -jets as signal in the 2-tag region. The lower panels display the ratio of the predictions for signal plus background to data using either MGAMC+Py8 FxFx or SHERPA 2.2.11 as the signal simulation. The statistical uncertainty of the data is shown as error bars and the total uncertainty of the prediction as a hatched band (MC theory uncertainties are not included).

the dressed Z boson decay products. Particle-level jets are classified as b -jets or c -jets following the same logic as described for reconstructed jets in Section 4. The correction to particle-level accounts for selection efficiencies, resolution effects and differences between the fiducial and the detector-level phase spaces.

Table 5: The expected size of the signal and backgrounds, expressed as a fraction of the total number of predicted events for 1-tag and 2-tag signal regions, when considering (a) $Z + \geq 1$ b -jet, (b) $Z + \geq 2$ b -jets or (c) $Z + \geq 1$ c -jet as signal. The signal and Z +jets background predictions are from the MGAMC+PY8 FxFx generator, with the Z +jets background estimate obtained after applying the normalization scale factors obtained from the flavour fit. The total numbers of predicted and observed events are also shown. The uncertainty in the total predicted number of events is statistical only.

1-tag region		2-tag region		1-tag region	
Signal $Z + \geq 1$ b -jet		Signal $Z + \geq 2$ b -jets		Signal $Z + \geq 1$ c -jet	
$Z + b, Z + bb$	34%	$Z + bb$	46%	$Z + c$	28%
Backgrounds		Backgrounds		Backgrounds	
$Z + c$	29%	$Z + b$	11%	$Z + b, Z + bb$	33%
$Z + l$	35%	$Z + c$	23%	$Z + l$	37%
		$Z + l$	7%		
Top	2%	Top	12%	Top	2%
Others	1%	Others	2%	Others	1%
Total predicted	$4\,294\,900 \pm 2100$	Total predicted	$325\,300 \pm 600$	Total predicted	$3\,994\,400 \pm 2000$
Data	4 145 168	Data	309 199	Data	4 145 168
(a)		(b)		(c)	

Table 6: Fiducial regions of the $Z + \geq 1$ b -jet, $Z + \geq 2$ b -jets and $Z + \geq 1$ c -jet measurements at particle level. The assignment of a b -jet or a c -jet is explained in Section 4.

Object Selection	Acceptance cuts
Lepton	$p_T > 27$ GeV, $ \eta < 2.5$
b -jet	2 same flavour and opposite charge, 76 GeV $< m_{\ell\ell} < 106$ GeV
c -jet	$p_T > 20$ GeV, $ y < 2.5$, $\Delta R(b\text{-jet}, \ell) > 0.4$
	$p_T > 20$ GeV, $ y < 2.5$, $\Delta R(c\text{-jet}, \ell) > 0.4$
Event Selection	Acceptance cuts
$Z + \geq 1$ b -jet	$Z + \geq 1$ b -jet and a b -jet is the leading heavy-flavour jet
$Z + \geq 2$ b -jets	$Z + \geq 2$ b -jets and a b -jet is the leading heavy-flavour jets
$Z + \geq 1$ c -jet	$Z + \geq 1$ c -jet and a c -jet is the leading heavy-flavour jet
Rapidity regions	Acceptance cuts
Central rapidity	Z boson rapidity $ y(Z) < 1.2$
Forward rapidity	Z boson rapidity $ y(Z) \geq 1.2$

Differential distributions are corrected to the particle level by using an iterative Bayesian unfolding [92] with two iterations. Simulated signal events, passing the selection defined in Section 4, are used to generate a response matrix for each distribution. The matrix is filled with the events that pass both the detector-level and particle-level selections and accounts for bin-to-bin migration effects between the detector-level and particle-level distributions. Figure 4 shows two examples of these response matrices. In the first iteration of the Bayesian unfolding, the particle-level prediction is used as the initial prior. From the second iteration, the prior is given by the unfolded distribution of the previous iteration and the unfolding matrix is derived on the basis of the Bayes' theorem, from the response matrix and the prior. The use of more than two

iterations has not been found to change significantly the final results, but it would have increased the statistical uncertainty.

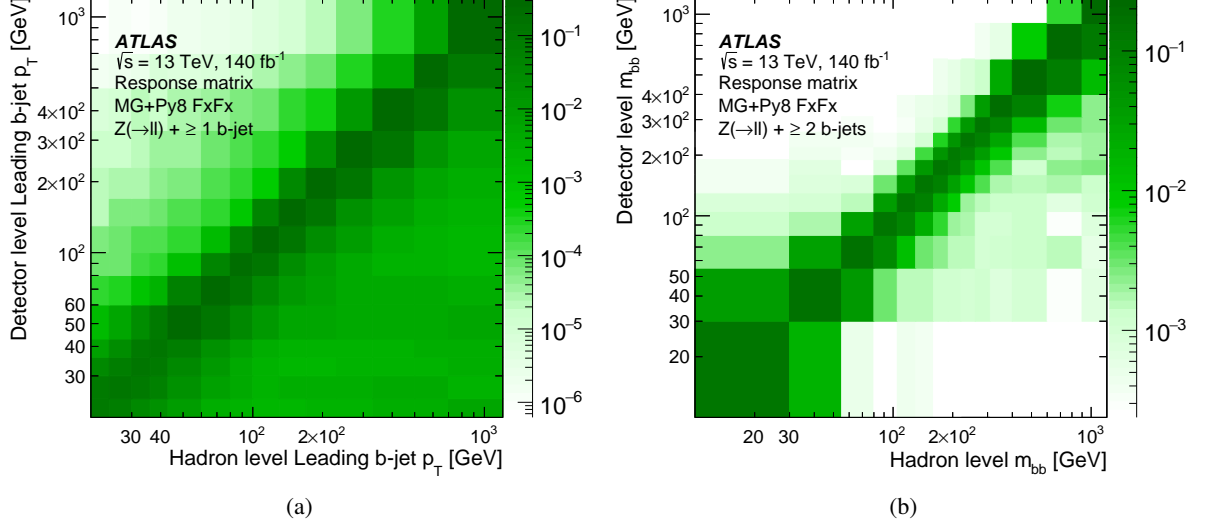


Figure 4: Response matrix of (a) leading b -jet p_T for $Z + \geq 1 b$ -jet events and (b) m_{bb} for $Z + \geq 2 b$ -jets events. The matrix is created from the MGAMC+PY8 FxFx sample and used for the nominal unfolding of the data. The sum of the entries in each column is normalised to the reconstruction efficiency in corresponding bin.

The pre-fit distributions of the MGAMC+PY8 FxFx signal samples are used to perform the unfolding procedure. The background-subtracted data are corrected for the expected fraction of events that pass the detector-level selection, but not the particle-level one (unmatched events), before entering the iterative unfolding. To obtain the cross-sections, the unfolded event yields are divided by the integrated luminosity of the data sample and by the bin width in each bin of each differential distribution. The differential cross-section measurement of a given observable in the i -th bin is given by:

$$\sigma_i = \frac{1}{\epsilon_i L} \sum_j U_{ij} f_j N_j^{\text{bsD}},$$

where L is the integrated luminosity, ϵ_i is the reconstruction efficiency in the i -th bin, N_j^{bsD} is the number of background-subtracted data events in the reconstructed j -th bin, f_j is the factor that corrects for unmatched events in the j -th bin, and U_{ij} is the element (i, j) of the unfolding matrix calculated after two iterations, using the updated prior from the first iteration and the response matrix. The efficiency is defined as a fraction of simulated events in i -th particle-level bin that pass the detector-level selection, and the f_j is a fraction of simulated events reconstructed in j -th bin that also pass the fiducial particle-level selection.

The measurement of $R(p_T(Z))$, as defined in Table 6, is performed as follows: At reconstruction level, the background subtraction is performed separately for events passing the central and forward rapidity selection, as defined in Table 4. Resulting distributions of Z boson p_T are then unfolded simultaneously in the full fiducial phase space, to obtain the corresponding particle-level distributions, accounting for migrations between the rapidity regions via the unfolding matrix (in addition to migrations between the Z boson p_T bins). Finally, the unfolded distribution for the forward region is divided by the one for the central region. In this way all systematic uncertainties are treated coherently between the rapidity regions, allowing a significant cancellation of the correlated ones.

The measurement of the inclusive fiducial cross-section for $Z + \geq 1$ b -jet, $Z + \geq 2$ b -jets and $Z + \geq 1$ c -jet processes is obtained by applying a particle-level correction to the number of events in data passing the selection in Section 4, after background subtraction⁸. The correction, which is applied as a divisor of the background-subtracted data, is derived from the ratio of the total number of reconstructed events in the detector-level phase space to the number of particle-level events in the fiducial phase space. Integration of the unfolded differential cross-sections yield consistent results, but the described procedure is adopted as the one independent of the choice of binning for the flavour fit and the unfolding.

Since the electron and muon decay channels are combined to increase the precision of the signal fits to data, the corrections and response matrices are made using electron and muon signal samples to obtain combined particle-level yields. To validate this procedure, the analysis is performed for each of the two lepton channels separately. The results obtained from the individual channels are compatible within 1σ for the inclusive fiducial cross-section of $Z + \geq 1$ b -jet and $Z + \geq 1$ c -jet production and within 2σ for the $Z + \geq 2$ b -jets cross-section. This comparison uses only the sum in quadrature of the statistical and uncorrelated systematic uncertainties. The differential cross-section measurements in the two channels also agree over the full range of each distribution.

8 Uncertainties in the cross-section measurement

Uncertainties in the $Z + \geq 1$ b -jet, $Z + \geq 2$ b -jets and $Z + \geq 1$ c -jet cross-section measurements arise from systematic effects related to detector-level selection, background determination and unfolding method and from the statistical uncertainty of the analysed data sample. Uncertainties are considered correlated, when appropriate, between lepton channels, signal and background processes and over the observables.

8.1 Detector-level systematic uncertainties

Detector-level systematic uncertainties are defined to be the uncertainties in the selection of the physics objects entering the measurement and in the luminosity. They are derived for each observable by propagating shifts from each systematic source through both the unfolding inputs (response matrices, reconstruction efficiency and the unmatched events correction) and the subtracted background into the unfolded data, after the flavour fit.

Systematic uncertainties on the leptons are related to the trigger, reconstruction, identification and isolation criteria adopted in the selection of electrons and muons [82, 84]. Variations in the electron energy scale and resolution are taken into account, as are those related to the muon momentum scale, the inner-detector and muon spectrometer resolution, and the sagitta-bias corrections. These uncertainties are specific for each leptonic final state and therefore uncorrelated between the two lepton channels. The contribution of the lepton uncertainties is less than 1% of the final measurements.

The uncertainties associated to the reconstructed jets take into account corrections to the energy scale (JES) and resolution (JER) [88]. They are estimated by scaling and smearing the jet four-momentum in the simulation by the associated uncertainties in the calibration procedure. The JVT selection efficiency is also considered. Jet systematic uncertainties are among the largest uncertainties in the measured cross-sections, with an average contribution of 5% which increases in specific regions of phase space (i.e. high m_{bb}).

⁸ For the purpose of flavour fit and data-driven $t\bar{t}$ background evaluation procedure, all events are treated as belonging to a single bin.

The systematic uncertainty on E_T^{miss} accounts for the energy scale and resolution of the soft hadronic activity reconstructed in the event [93] and contribute to less than 1%.

The flavour tagging uncertainties are derived from the calibration of the DL1r tagger using data control samples enriched in b [94], c [95], or light-jets [96], up to a jet p_T of several hundreds GeV. Any difference in the flavour-tagging performance measured in data events and MC samples is used to correct the flavour-tagging efficiency in the MC as a function of the jet flavour, the different b -tagging discriminant output thresholds, and of the jet p_T . In the case of b -jets, correction factors are close to unity and their uncertainties, described by a set of 45 independent parameters, are as low as 1% for jet p_T of about 60 GeV, but reach 7% for jet p_T of about 20 GeV and up to 3% at 400 GeV. In the case of c -jets, correction factors range from about 1 to about 1.3, their uncertainties are described by a set of 20 independent parameters, and are about 3-4% in the bulk of the phase space, but reach up to 15% for low jet p_T and for the largest values of the b -tagging discriminant output. In the case of light-flavour jets, correction factors for light-jets range from about 1 to about 1.3, with uncertainties described by a set of 20 independent parameters and ranging from 10% to 20%. The uncertainties in the flavour-tagging calibration are extrapolated to high p_T on the basis of MC simulations.

The flavour tagging systematic is the second largest uncertainty in $Z + \geq 1$ b -jet and $Z + \geq 2$ b -jets inclusive cross-sections, with average contributions of respectively 3.6% and 5.7%, and it becomes the largest uncertainty in the $Z + \geq 1$ c -jet measurement with an average contribution of 10.3% to the final precision.

The uncertainty of the imperfect modelling of the pile-up effects is assessed by varying the average number of pile-up interactions. It contributes to less than 1% to the cross-section measurements. The uncertainty in the combined 2015–2018 integrated luminosity is 0.83% [33], obtained using the LUCID-2 detector for the primary luminosity measurements [30].

8.2 Background systematic uncertainties

The uncertainty from each background source is determined by applying shifts to the subtracted background contributions and to the nominal unfolding inputs.

The uncertainty related to the determination of the Z +jets background ranges from 0.6% to 1.6% in the measured inclusive cross-sections. It is determined as an envelope of two separate but related variations. The first accounts for the differences between the post-fit Z +jets backgrounds evaluated using MGAMC+PY8 FxFx or SHERPA 2.2.11, as described in Section 5.2. The second source accounts for the MGAMC+PY8 FxFx theoretical uncertainties, which are determined by varying independently the QCD renormalisation (μ_R) and factorisation (μ_F) scales by a factor 0.5 and 2 with an additional constraint of $0.5 < \mu_R/\mu_F < 2$. For each of these scale variations the flavour fit is repeated and an envelope of the post-fit result is used for the error estimate. Effects due to PDF and α_s uncertainties have a negligible impact and are not propagated to the final measurements.

The systematic uncertainty in the data-driven $t\bar{t}$ background accounts for the extrapolation from the $e^\pm\mu^\mp$ control region to the signal region, as explained in Section 5.1. The contribution of this uncertainty is less than 1% in the inclusive cross-sections.

The uncertainty in the other backgrounds is given by the sum in quadrature of the uncertainties in the MC-modelled diboson, single-top, ZH and $Z \rightarrow \tau\tau$ backgrounds. Diboson uncertainty is determined by varying independently the QCD scales μ_R and μ_F by a factor 0.5 and 2 with an additional constraint of

$0.5 < \mu_R/\mu_F < 2$ and by taking the envelope of the predicted variations as error estimate. For the smaller single-top, ZH and $Z \rightarrow \tau\tau$ contaminations, overall normalization uncertainties covering QCD scale, PDF and α_s variations, are considered. The contribution to the measured cross-sections is negligible.

8.3 Unfolding systematic uncertainties

The uncertainties in the unfolding procedure originate from the statistical uncertainty of MGAMC+PY8 FxFx used as nominal MC in the unfolding, the intrinsic bias introduced by the unfolding method and the modelling and theoretical uncertainties of the MGAMC+PY8 FxFx signal samples.

The uncertainty due to the limited statistics of MGAMC+PY8 FxFx samples is propagated using 100 MC pseudo-experiments: the unfolding inputs are fluctuated independently according to Gaussian distributions and the RMS of the results is taken as error estimate.

The dependence of the Bayesian unfolding regularisation procedure on the choice of the initial prior is determined by reweighting the generator-level distribution of each observable in the MGAMC+PY8 FxFx samples to provide a better description of the data at detector level. The modified MGAMC+PY8 FxFx samples are then used to emulate data and are unfolded with the nominal matrix.

The signal modelling uncertainty accounts for the mis-modelling of the migrations, the reconstruction efficiency and the unmatched events corrections. It is evaluated by comparing unfolded results when using different MC generators. First, for each measured observable, SHERPA 2.2.11 signal sample is reweighted to match the MGAMC+PY8 FxFx particle-level distribution of that observable and used to unfold its distribution in data. The reweighting is performed to avoid double-counting with the estimate of the effect of the initial prior choice described above. Second, theoretical uncertainties related to modelling the signal in MGAMC+PY8 FxFx are evaluated by the same variations of QCD scales as described above and taking an envelope of the unfolded results using the varied matrices.

The contributions to the unfolding uncertainty are summed in quadrature and represent one of the dominant uncertainties for the $Z + \geq 1$ b -jet, $Z + \geq 2$ b -jets and $Z + \geq 1$ c -jet inclusive cross-sections with contributions of respectively 3.3%, 5.8% and 5.0%.

Table 7 summarizes the systematic uncertainties in the measured inclusive fiducial cross-sections for the $Z + \geq 1$ b -jet, $Z + \geq 2$ b -jets and $Z + \geq 1$ c -jet production. Figures 5–6 show, as examples, the breakdown of the systematic uncertainties in the cross-section as a function of Z boson p_T for events with at least one b -jet, m_{bb} for events with at least two b -jets, leading c -jet p_T for events with at least one c -jet, and in the ratio of the cross-sections as functions of Z boson p_T in forward and central Z boson rapidity regions.

The total systematic uncertainty in the inclusive cross-sections is 5.6% in $Z + \geq 1$ b -jet events, 9.4% in $Z + \geq 2$ b -jets events and 13.2% in $Z + \geq 1$ c -jet events. In the differential distributions it is less than 5% in the $Z + \geq 1$ b -jet, except in some bins of $p_T(Z)$. In $Z + \geq 2$ b -jets and $Z + \geq 1$ c -jet measurements it is at a level of 10%–15%, except in some bins at the edges of the distributions.

The statistical uncertainty of the data is propagated through the unfolding by using 1000 pseudo-experiments. The flavour fit and the unfolding is repeated for each data replica. The statistical uncertainty in the inclusive cross-sections of $Z + \geq 1$ b -jet, $Z + \geq 2$ b -jets and $Z + \geq 1$ c -jet is 0.2%, 0.4% and 0.3% respectively.

Table 7: Relative systematic uncertainties in the measured production cross-sections of $Z + \geq 1$ b -jet, $Z + \geq 2$ b -jets and $Z + \geq 1$ c events. The “Jet” term includes the JES, JER and JVT uncertainties. The “Lepton” term includes the lepton trigger, efficiency, scale and resolution uncertainties.

Source of uncertainty	$Z(\rightarrow \ell\ell) + \geq 1$ b -jet [%]	$Z(\rightarrow \ell\ell) + \geq 2$ b -jets [%]	$Z(\rightarrow \ell\ell) + \geq 1$ c -jet
Flavour tagging	3.6	5.7	10.3
Jet	2.4	4.3	6.5
Lepton	0.3	0.3	0.4
E_T^{miss}	0.4	0.5	0.3
Z+jets background	0.6	1.5	1.6
Top background	0.1	0.3	<0.1
Other backgrounds	<0.1	0.2	0.1
Pile-up	0.6	0.6	0.2
Unfolding	3.3	5.8	5.0
Luminosity	0.8	0.9	0.7
Total [%]	5.6	9.4	13.2

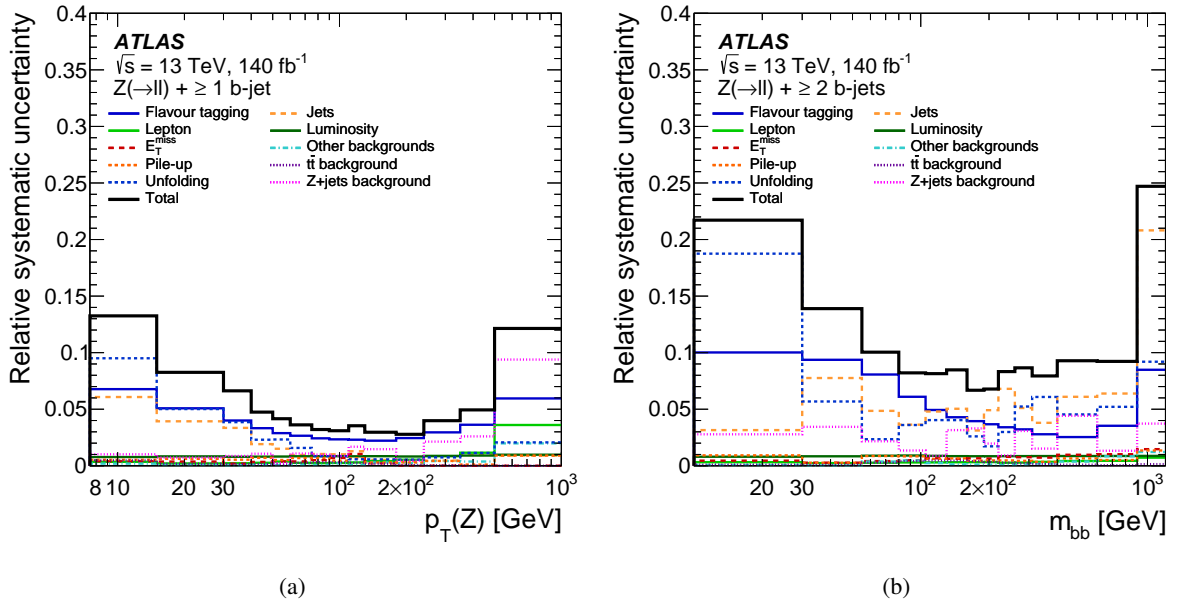


Figure 5: Relative systematic uncertainties in the fiducial cross-section (a) as a function of $p_T(Z)$ in events with at least one b -jet and (b) as a function of m_{bb} in events with at least two b -jets. The total uncertainty is shown with solid black line while the different components listed in Table 7 are shown in different line styles and colours.

9 Results

The inclusive and differential cross-section measurements for $Z + \geq 1$ b -jet, $Z + \geq 2$ b -jets and $Z + \geq 1$ c -jet are shown in Figures 7–14. The measurements are compared with standard 5FS multi-leg MGAMC+PY8

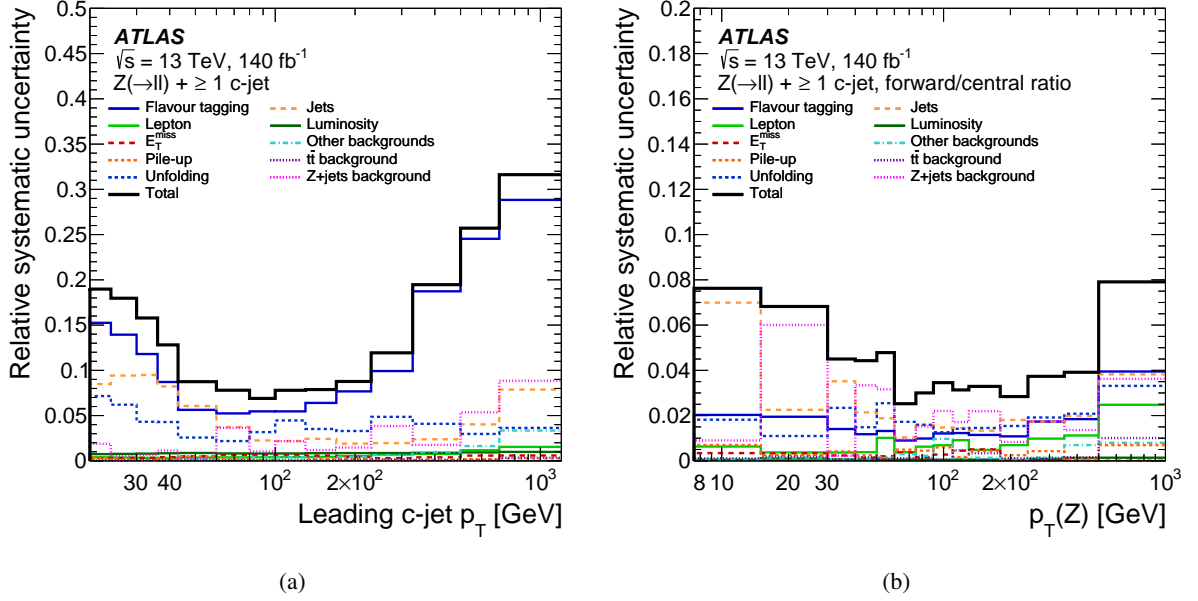


Figure 6: Relative systematic uncertainties in (a) the fiducial cross-section as a function of leading c -jet p_T ($p_{T,c}^0$) and (b) the ratio of the cross-sections as functions of Z boson p_T in forward and central Z boson rapidity regions in events with at least one c -jet. The total uncertainty is shown with solid black line while the different components listed in Table 7 are shown in different line styles and colours.

FxFx and SHERPA 2.2.11 predictions, MGAMC+PY8 FxFx variations with several PDFs using different intrinsic charm models, with NLO MGAMC+PY8 predictions of various flavour schemes and with fixed-order 5FS NLO and NNLO predictions using the flavour-dressing algorithm (see Section 3).

Theoretical uncertainties of the various samples, computed as described in Section 3, are shown in the comparison with data. In this section, all predictions are normalised to their own cross-section to allow an unbiased comparison among different generators.

9.1 Inclusive fiducial cross-sections

The measured inclusive cross-sections in the fiducial phase space for $Z + \geq 1 b$ -jet, $Z + \geq 2 b$ -jets and $Z + \geq 1 c$ -jet, shown in Figures 7 and 8, are $10.49 \pm 0.02(\text{stat.}) \pm 0.59(\text{syst.})$ pb, $1.39 \pm 0.01(\text{stat.}) \pm 0.13(\text{syst.})$ pb, and $20.9 \pm 0.1(\text{stat.}) \pm 2.8(\text{syst.})$ pb, respectively.

The 5FS simulations, in general, adequately predict the inclusive cross-sections for both the $Z + \geq 1 b$ -jet and $Z + \geq 2 b$ -jets whereas the 4FS simulation shows an underestimate of about 2σ for the $Z + \geq 1 b$ -jet inclusive cross-section, while predicting the $Z + \geq 2 b$ -jets cross-sections accurately. Overall, these results are consistent with the ones presented in the ATLAS measurement on a partial Run 2 data set [14], based on previous generator versions. All 5FS multi-leg predictions considered here, as well as MGAMC+PY8 4FS (NLO), are in agreement with the measured $Z + \geq 1 c$ -jet cross-section. The MGAMC+PY8 3FS (NLO) prediction drastically underestimates the measured cross-section by about 50%, consistent with the lack of resummation of $\ln(Q^2/m_c^2)$ in the collinear PDF evolution.

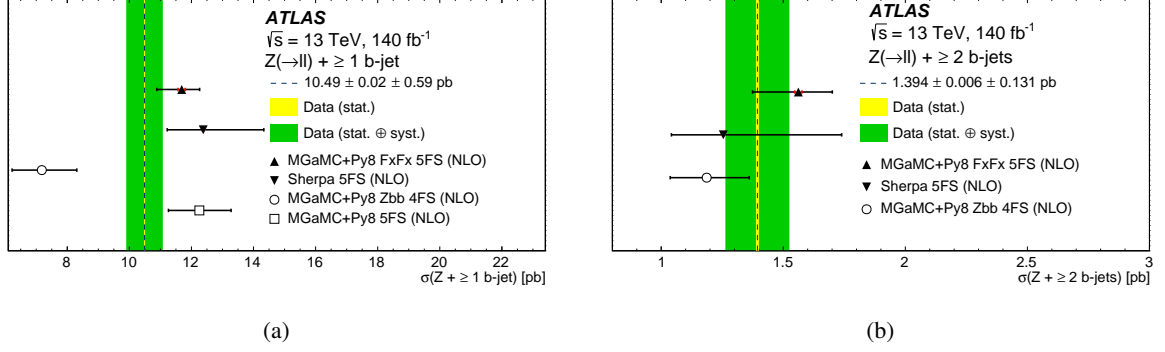


Figure 7: Measured fiducial cross-section for (a) $Z + \geq 1$ b -jet and (b) $Z + \geq 2$ b -jets production. The data are compared with the predictions from the 5FS multi-leg generators MGaMC+Py8 FxFx and SHERPA 2.2.11, with MGaMC+Py8 4FS (NLO), and with MGaMC+Py8 5FS (NLO). The thin inner band corresponds to the statistical uncertainty of the data, and the outer band to statistical and systematic uncertainties of the data, added in quadrature. The error bars on the MGaMC+Py8 FxFx, SHERPA 2.2.11, and MGaMC+Py8 predictions correspond to the statistical and theoretical uncertainties added in quadrature. The sum in quadrature of statistical and PDF related uncertainties are shown as inner bars.

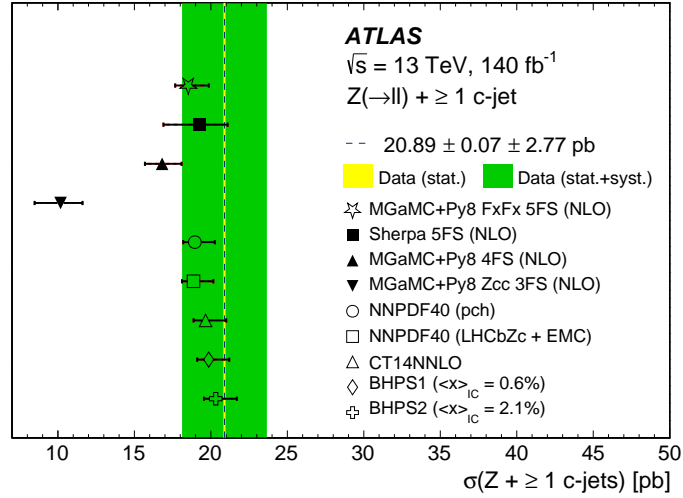


Figure 8: Measured fiducial cross-section for $Z + \geq 1$ c -jet production. The data are compared with the 5FS predictions from MGaMC+Py8 FxFx and SHERPA 2.2.11, with MGaMC+Py8 3FS (NLO), and with MGaMC+Py8 4FS (NLO), and with various PDFs based on different intrinsic charm models (see Section 3). The thin inner band corresponds to the statistical uncertainty of the data, and the outer band to statistical and systematic uncertainties of the data, added in quadrature. The error bars on the MGaMC+Py8 FxFx, and SHERPA 2.2.11 predictions correspond to the statistical and theoretical uncertainties added in quadrature.

9.2 Differential cross-sections for $Z + \geq 1$ b -jet

The differential cross-section measurements for the $Z + \geq 1$ b -jet process are shown in Figures 9–10. They are compared with the predictions from the 5FS multi-leg generators MGaMC+Py8 FxFx and

SHERPA 2.2.11, with MGAMC+PY8 4FS (NLO) and MGAMC+PY8 5FS (NLO), and with NLO and NNLO fixed-order predictions [3].

As the fixed-order predictions are made at parton level and, moreover, use a different jet flavour definition [2], the unfolded cross-sections cannot be compared with them directly. To allow for a proper comparison, two corrections are applied to the predictions. The first one accounts for the hadronisation and multi-parton-interaction (MPI) effects. It is calculated as the ratio of the simulated distributions at hadron level with MPI enabled to those at parton level with MPI disabled, using a dedicated sample of Z +jets events generated with PYTHIA 8.310 at LO accuracy. The jet flavour definition in this case uses the flavour-dressing algorithm [2]. The second correction accounts for the effect of different jet flavour classification algorithms. It is calculated as the ratio of hadron-level distributions using the jet flavour definition described in Section 7 to those made with the flavour-dressing algorithm, using MGAMC+PY8 FxFx sample. This correction is also derived using the SHERPA 2.2.11 sample and the difference with MGAMC+PY8 FxFx is treated as its uncertainty. Both corrections are applied to the fixed-order predictions as bin-by-bin multiplicative factors. Uncertainties in these predictions shown on the plot correspond to the sum of the intrinsic theory uncertainty of the predictions and the total uncertainty of the corrections, while the former are also shown separately.

The distributions of the transverse momentum of the Z boson and of the b -jets probe pQCD over a wide range of scales and provide important input to the background prediction for other SM processes and searches beyond the SM.

The differential cross-section as a function of $p_T(Z)$ for events with at least one b -jet is shown in Figure 9(a). In general, the measured spectrum is harder than all predicted spectra. Overall, the prediction from MGAMC+PY8 FxFx demonstrates the best agreement with data, while the SHERPA 2.2.11 prediction still describes the data within larger theory uncertainties. MGAMC+PY8 5FS (NLO) predicts a softer $p_T(Z)$ spectrum resulting in an overestimate of the low- p_T range, while MGAMC+PY8 4FS (NLO) is below data in the entire range. The NLO fixed-order computation predicts a noticeably softer spectrum than in data. This discrepancy reduces with NNLO prediction, however, it still cannot describe the entire spectrum.

Figure 9(b) shows the leading b -jet p_T distribution. Both MGAMC+PY8 FxFx and SHERPA 2.2.11 predictions agree with data within their theory uncertainties. The MGAMC+PY8 5FS (NLO) prediction overestimates the data cross-section in the low p_T regime, while for higher p_T values the data are modelled well. Both NLO and NNLO fixed-order calculations describe well almost the entire spectrum, only slightly underpredict the data at p_T values above 500 GeV.

It is noticeable that the uncertainty of the NNLO predictions is dominated by the that of the correction described above, while their own uncertainty evaluated by varying the QCD scales is small. This indicates the importance of using IRC-safe jet flavour definitions in future precision measurements of similar processes.

The distribution of $\Delta\tilde{R}_{Zb}$ is sensitive to the presence of additional radiation in the event. It is shown in Figure 10. Both MGAMC+PY8 FxFx and SHERPA 2.2.11 predictions describe data rather well, only overestimating data in the $\Delta\tilde{R}_{Zb} \approx \pi$ region corresponding to the $Z + b$ back-to-back topology. The same trend is present in the MGAMC+PY8 5FS (NLO) prediction, with the discrepancy being even larger. The worst agreement with data is shown by MGAMC+PY8 4FS (NLO), where topologies in the tail of the distribution – i.e. collinear and at large $\Delta\tilde{R}_{Zb}$ – undershoot the data by more than 50%. Fixed-order calculations suffer from divergences at $\Delta\tilde{R}_{Zb} \approx \pi$ and their uncertainties are high in that region. The NLO calculation tends to underestimate the cross-section for $\Delta\tilde{R}_{Zb}$ between 1 and 2.5 and above 4, but the description becomes almost perfect when moving to NNLO.

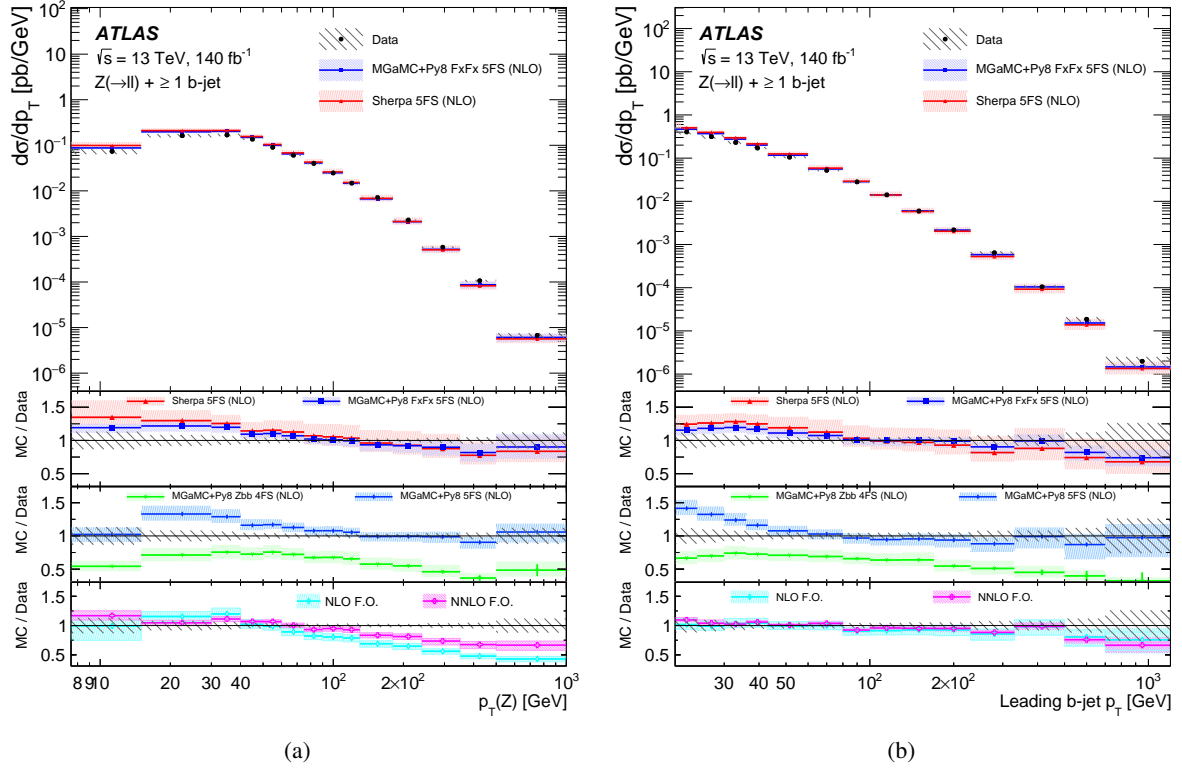


Figure 9: Measured fiducial cross-section for $Z + \geq 1$ b -jet production as a function of (a) $p_T(Z)$ and (b) leading b -jet p_T . The data are compared with the predictions from the 5FS multi-leg generators MGAMC+PY8 FxFx and SHERPA 2.2.11, with MGAMC+PY8 4FS (NLO) and MGAMC+PY8 5FS (NLO), and with NLO and NNLO fixed-order (F.O.) predictions [3]. The error bars correspond to the statistical uncertainty, and the hatched bands to the data statistical and systematic uncertainties added in quadrature. The shaded bands correspond to the statistical and theoretical uncertainties of the predictions added in quadrature. For the fixed-order predictions, the uncertainties in the hadronisation and MPI and flavour definition algorithm corrections are also added in quadrature to the total, while pure theory uncertainty of the predictions are shown as the range between the horizontal lines.

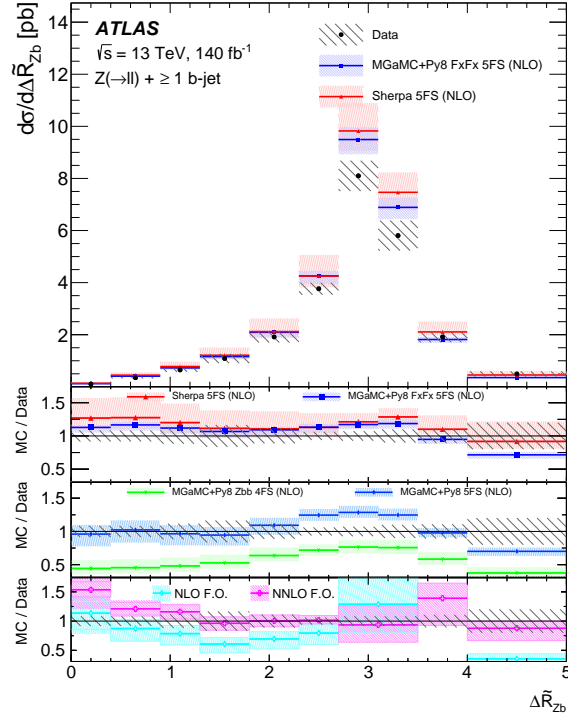


Figure 10: Measured fiducial cross-section for $Z + \geq 1$ b -jet production as a function of ΔR_{Zb} . The data are compared with the predictions from the 5FS multi-leg generators MGaMC+Py8 FxFx and SHERPA 2.2.11, with MGaMC+Py8 4FS (NLO) and MGaMC+Py8 5FS (NLO), and with NLO and NNLO fixed-order (F.O.) predictions [3]. The error bars correspond to the statistical uncertainty, and the hatched bands to the data statistical and systematic uncertainties added in quadrature. The shaded bands correspond to the statistical and theoretical uncertainties of the predictions added in quadrature. For the fixed-order predictions, the uncertainties in the hadronisation and MPI and flavour definition algorithm corrections are also added in quadrature to the total, while pure theory uncertainty of the predictions are shown as the range between the horizontal lines.

9.3 Differential cross-sections for $Z + \geq 2$ b -jets

Events with a Z boson produced in association with two b -jets constitute an important background for other SM and beyond-SM processes, such as Higgs boson production in association with a Z boson or potential new physics signatures with similar final states. Furthermore, they probe the mechanism of gluon splitting into b -quarks. The differential cross-section measurements for $Z + \geq 2$ b -jets are shown in Figure 11. They are compared with predictions from the 5FS multi-leg generators MGAMC+PY8 FxFx and SHERPA 2.2.11 and with MGAMC+PY8 4FS (NLO). No fixed-order calculations are provided for $Z + \geq 2$ b -jets observables within the framework used in Ref. [3].

A measurement of the angular separation between the two leading b -jets allows characterisation of the hard radiation at large angles and the soft radiation for collinear emissions. The distribution of the azimuthal angle between the two leading b -jets, $\Delta\phi_{bb}$, is chosen as an example of such an observable and the corresponding differential cross-section is shown in Figure 11(a). All predictions generally agree with data within their theory uncertainties. Both MGAMC+PY8 FxFx and SHERPA 2.2.11 describe the data shape well, while MGAMC+PY8 4FS (NLO) tends to underestimate small and large $\Delta\phi_{bb}$ values corresponding to collinear and back-to-back b -jets.

The invariant mass of the two leading b -jets is an important observable in the measurement of associated ZH production with the Higgs boson decaying into $b\bar{b}$, and in searches for physics beyond the SM in the same final state. The differential cross-section as a function of m_{bb} is shown in Figure 11(b). In general, all calculations predict steeper growth below 80 GeV and steeper decrease for higher values. MGAMC+PY8 4FS (NLO) provides a good description of the data in the widest range between 60 and 600 GeV, but still fails to describe them for smaller and larger m_{bb} . MGAMC+PY8 FxFx overestimates the data near the maximum of the distribution at 60–100 GeV and underestimates them above 600 GeV. SHERPA 2.2.11 is in agreement with the data within its large uncertainty up to 400 GeV and deviates from the data at higher values.

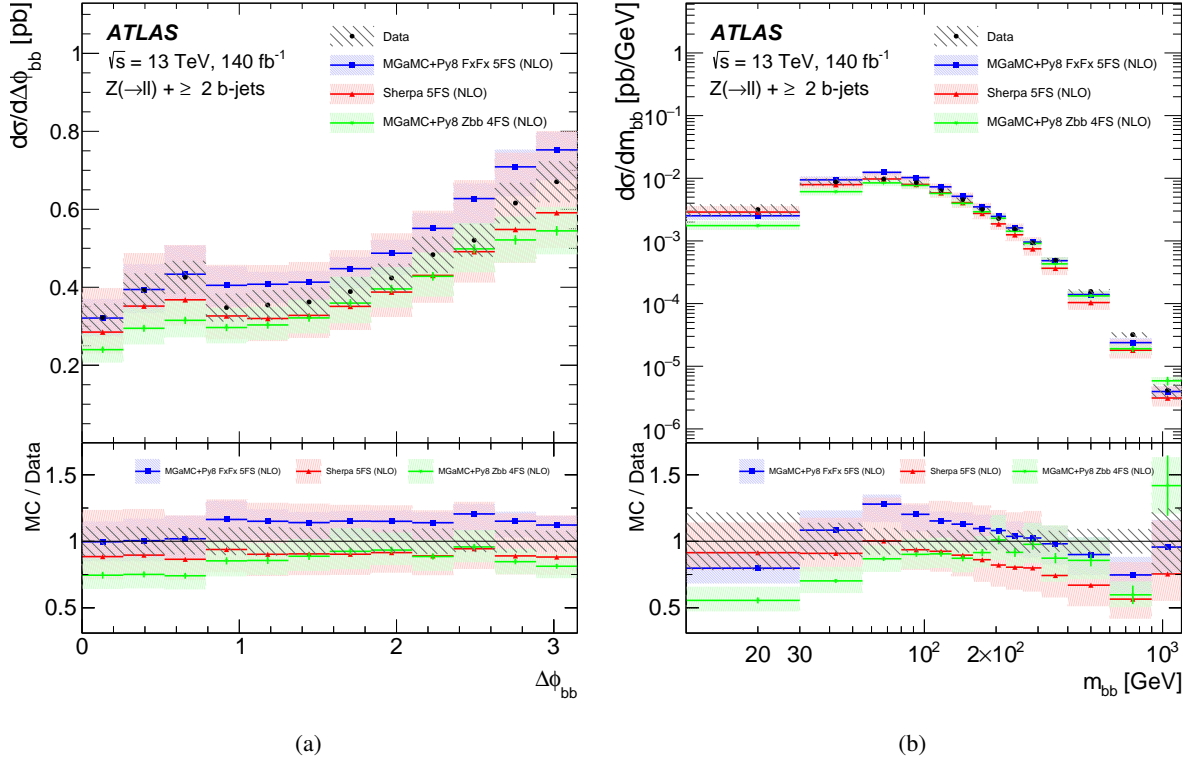


Figure 11: Measured fiducial cross-section for $Z + \geq 2$ b -jets production as a function of (a) $\Delta\phi_{bb}$ and (b) m_{bb} . The data are compared with the predictions from the 5FS multi-leg generators MGaMC+Py8 FxFx and SHERPA 2.2.11, and with MGaMC+Py8 4FS (NLO). The error bars correspond to the statistical uncertainty, and the hatched bands to the data statistical and systematic uncertainties added in quadrature. The shaded bands correspond to the statistical and theoretical uncertainties of the predictions added in quadrature.

9.4 Differential cross-sections for $Z + \geq 1$ c -jet

Differential cross-section measurements for the $Z + \geq 1$ c -jet process constitute an important probe of pQCD and of the charm PDF. The results are presented in Figures 12–14. The differential $Z + c$ -jets cross-section measurements are compared with the predictions from the 5FS multi-leg generators SHERPA 2.2.11 and MGaMC+Py8 FxFx, with MGaMC+Py8 3FS (NLO) and MGaMC+Py8 4FS (NLO), and with NLO and NNLO fixed-order predictions [3]. The latter are corrected for the effects related to the hadronisation and MPI and to the different jet flavour classification algorithms as described in Section 9.2. These comparisons are shown in Figures 12–13.

Besides, the measurements are compared to MGaMC+Py8 FxFx predictions with various PDFs, probing the IC models as listed in Section 3.3. Comparisons to those predictions are shown in Figure 14.

Differential cross-sections as function of p_T of the Z boson and the leading c -jet are shown in Figure 12. Both p_T spectra are described well by MGaMC+Py8 FxFx and SHERPA 2.2.11 in the soft part, while above 40–50 GeV (80–100 GeV) for Z boson (c -jet) p_T the data cross-section is significantly underestimated by these predictions. A better description of the data shape overall is provided by MGaMC+Py8 4FS (NLO), however, it is generally near or beyond the lower edge of the data uncertainty band. The MGaMC+Py8

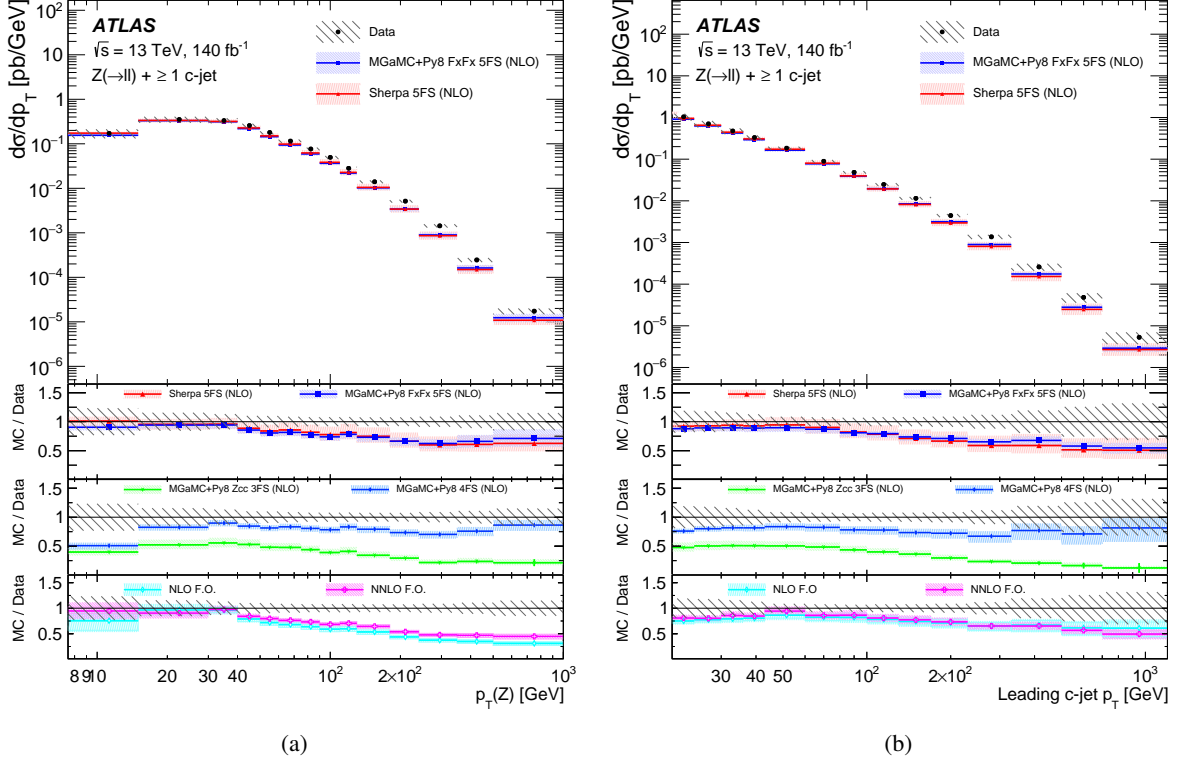


Figure 12: Measured fiducial cross-section for $Z + \geq 1$ c -jet production as a function of (a) $p_T(Z)$ and (b) leading c -jet p_T . The data are compared with the predictions from the 5FS multi-leg generators MGaMC+Py8 FxFx and SHERPA 2.2.11, with MGaMC+Py8 3FS (NLO) and MGaMC+Py8 4FS (NLO), and with NLO and NNLO fixed-order (F.O.) predictions [3]. The error bars correspond to the statistical uncertainty, and the hatched bands to the data statistical and systematic uncertainties added in quadrature. The shaded bands correspond to the statistical and theoretical uncertainties of the predictions added in quadrature. For the fixed-order predictions, the uncertainties in the hadronisation and MPI and flavour definition algorithm corrections are also added in quadrature to the total, while pure theory uncertainty of the predictions are shown as the range between the horizontal lines.

3FS (NLO) prediction is significantly below the data as mentioned above when discussing the inclusive cross-sections. This discrepancy is noticeably larger than that between the MGaMC+Py8 4FS (NLO) prediction and the $Z + \geq 1$ b -jet measurement, which can be attributed to the different masses of b - and c -quarks, causing those logarithmic terms to be larger for the latter.

The NLO fixed-order calculation predicts softer spectra of both Z boson and leading c -jet p_T than that in data. The discrepancy is the most noticeable for $p_T(Z)$ above 50–100 GeV. Moving to NNLO precision improves the agreement only slightly for $p_T(Z)$ and has no impact on $p_{T,c}^0$.

Figure 13 shows the distribution of x_F of the leading c -jet. MGaMC+Py8 FxFx and SHERPA 2.2.11 predict a steeper slope of the x_F spectrum compared to the data. At the same time, the MGaMC+Py8 4FS (NLO) prediction and both NLO and NNLO fixed-order calculations describe the data shape well, while systematically underestimating the overall normalization.

Figure 14 presents comparisons of the measured cross-section as a function of leading c -jet x_F and of $R(p_T(Z))$ for events with at least one c -jet with various IC models. The x_F distribution is more sensitive

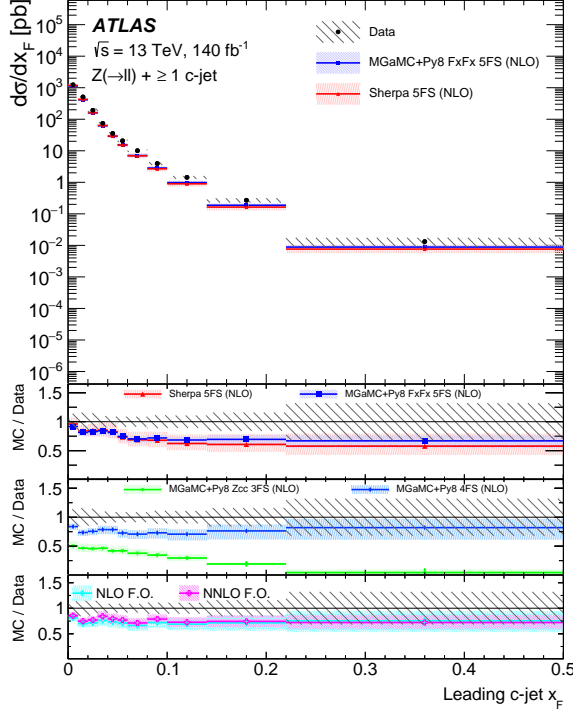


Figure 13: Measured fiducial cross-section for $Z + \geq 1$ c -jet production as a function of leading c -jet x_F . The data are compared with the predictions from the 5FS multi-leg generators MGAMC+Py8 FxFx and SHERPA 2.2.11, with MGAMC+Py8 3FS (NLO) and MGAMC+Py8 4FS (NLO), and with NLO and NNLO fixed-order (F.O.) predictions [3]. The error bars correspond to the statistical uncertainty, and the hatched bands to the data statistical and systematic uncertainties added in quadrature. The shaded bands correspond to the statistical and theoretical uncertainties of the predictions added in quadrature. For the fixed-order predictions, the uncertainties in the hadronisation and MPI and flavour definition algorithm corrections are also added in quadrature to the total, while pure theory uncertainty of the predictions are shown as the range between the horizontal lines.

to the IC contribution. The large amount of IC in the BHPS2 model noticeably improves the agreement to data. However, for more realistic IC scenarios, such as BHPS1 and the IC PDFs from the NNPDF and CT18 families, the improvement is still marginal, being noticeable only in the last 1–2 bins. In the measurement of $R(p_T(Z))$ the effect of IC is more significant compared to both experimental and theory uncertainties, thanks to their significant cancellation in this ratio. However, only the BHPS2 model has a non-negligible effect on the agreement to data, making it slightly better in some bins but worse in others compared to the predictions with no-IC CT14NNLO PDF. Other IC PDFs from NNPDF and CT18 families do not make significant difference in modelling these observables.

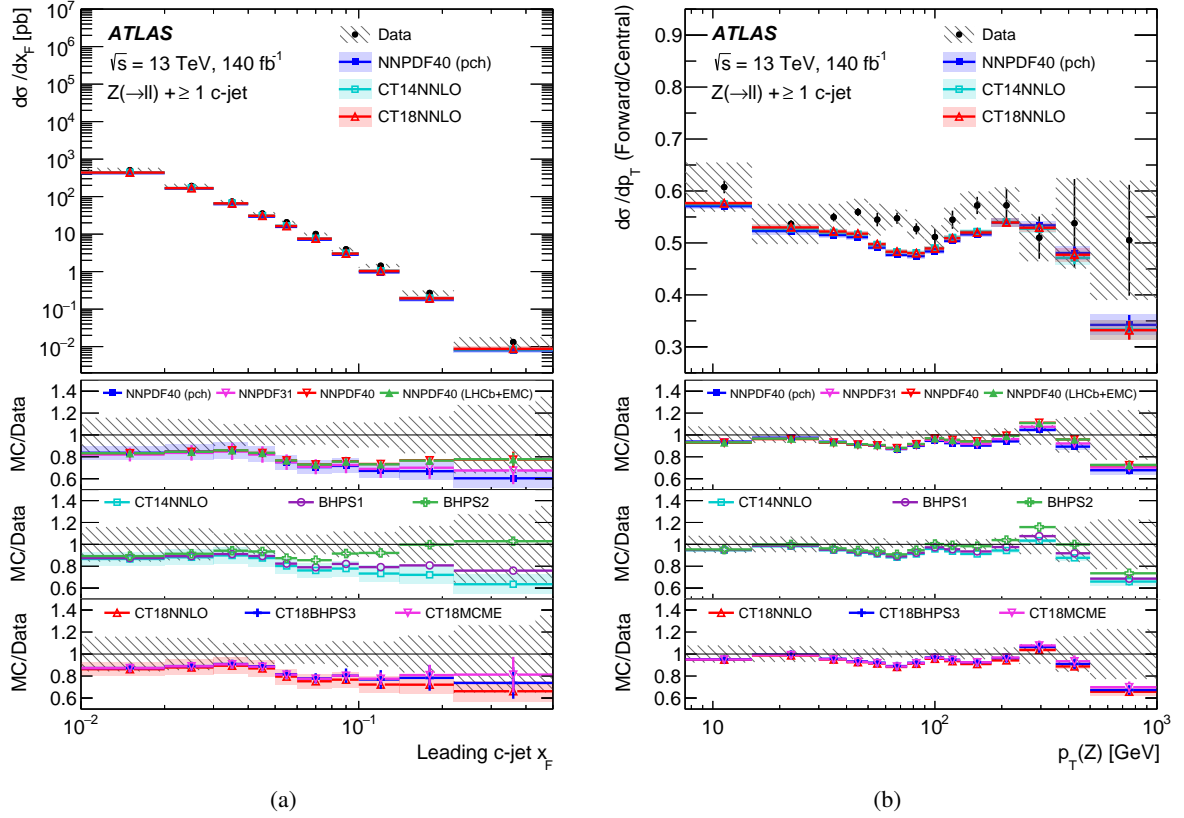


Figure 14: Measured fiducial cross-section for $Z + \geq 1$ c -jet production as a function of (a) leading c -jet x_F and (b) $R(p_T(Z))$. The data are compared with the nominal MG_{AMC}+PY8 FxFx predictions and with those using the PDFs testing several IC models. The error bars correspond to the statistical uncertainty, and the hatched bands to the data statistical and systematic uncertainties added in quadrature. The shaded bands correspond to the statistical and theoretical uncertainties of the predictions added in quadrature.

10 Conclusion

This paper presents a measurement of the production rate of a Z boson in association with jets originating from b -quarks and c -quarks ($Z + b$ -jets and $Z + c$ -jets) in proton–proton collisions at $\sqrt{s} = 13$ TeV, using data corresponding to an integrated luminosity of 140 fb^{-1} collected by the ATLAS experiment at the CERN LHC.

The cross-sections are measured using the electron and muon decay modes of the Z boson in a fiducial phase space. Inclusive cross-sections in a fiducial phase space are measured for events with at least one or at least two b -jets and for events with at least one c -jet. Differential cross-sections are measured as a function of p_T of the leading b -jet, the p_T of the Z boson and the difference in angular separation between the Z boson and the leading b -jet for events with at least one b -jet. Measurements are also performed as a function of the p_T of the leading c -jet, the p_T of the Z boson, and the Feynman- x variable x_F for events with at least one c -jet. A separate measurement is performed of the ratio of $Z + c$ -jets production cross-sections as a function of the p_T of the Z boson measured in two ranges of Z boson rapidity, central and forward. Finally, the differential cross-sections are measured as a function of the invariant mass of the two leading b -jets and as a function of the azimuthal angle difference between the two leading b -jets for events with at least two b -jets.

Measurements of the $Z + c$ -jets production cross-section are performed for the first time at the ATLAS experiment while the $Z + b$ -jets production measurements significantly improve on the precision of the previous ATLAS results [14]. Both types of measurements significantly extend to wider kinematic ranges compared to similar measurements performed at $\sqrt{s} = 13$ TeV by other experiments [16, 23].

The measurements are compared with predictions from a variety of Monte Carlo generators. In general, the 5FS MGAMC+PY8 FxFx and SHERPA 2.2.11 predictions describe the $Z + b$ -jets data within the experimental and theory uncertainties whereas the 5FS SHERPA 2.2.11 predictions show larger theory uncertainties than MGAMC+PY8 FxFx. The MGAMC+PY8 Z_{BB} 4FS (NLO) generator systematically underestimates the $Z + \geq 1$ b -jet distributions and does not provide a good description of the angular separation between the Z boson and the leading b -jet, but describes the $Z + \geq 2$ b -jets cross-sections. All generators underestimate the $Z + c$ -jet cross-sections: the 5FS MGAMC+PY8 FxFx and SHERPA 2.2.11 predictions underestimate the data for medium ranges of Z boson and c -jet p_T , whereas the MGAMC+PY8 Z_{CC} 3FS (NLO) predictions systematically underestimate all kinematic $Z + c$ -jet regions by a large factor. The 5FS NNLO $Z + \geq 1$ b -jet predictions with flavour dressing show a similar performance as the 5FS multi-leg MGAMC+PY8 FxFx and SHERPA generators but predict a softer b -jet p_T spectrum than the data. The 5FS NNLO $Z + c$ -jet predictions underestimate the data cross-sections even more than their 5FS multi-leg counterparts. MGAMC+PY8 FxFx versions with PDFs with different IC content were compared to $Z + c$ -jet distributions and for a given observable no significant difference in the modelling between the various PDFs was found.

This measurement provides important input for the improvement of theoretical predictions and Monte Carlo generators of Z boson production in association with b -jets and c -jets, allowing a better quantitative understanding of perturbative QCD.

Acknowledgements

We thank CERN for the very successful operation of the LHC and its injectors, as well as the support staff at CERN and at our institutions worldwide without whom ATLAS could not be operated efficiently.

The crucial computing support from all WLCG partners is acknowledged gratefully, in particular from CERN, the ATLAS Tier-1 facilities at TRIUMF/SFU (Canada), NDGF (Denmark, Norway, Sweden), CC-IN2P3 (France), KIT/GridKA (Germany), INFN-CNAF (Italy), NL-T1 (Netherlands), PIC (Spain), RAL (UK) and BNL (USA), the Tier-2 facilities worldwide and large non-WLCG resource providers. Major contributors of computing resources are listed in Ref. [97].

We gratefully acknowledge the support of ANPCyT, Argentina; YerPhI, Armenia; ARC, Australia; BMWFW and FWF, Austria; ANAS, Azerbaijan; CNPq and FAPESP, Brazil; NSERC, NRC and CFI, Canada; CERN; ANID, Chile; CAS, MOST and NSFC, China; Minciencias, Colombia; MEYS CR, Czech Republic; DNRF and DNSRC, Denmark; IN2P3-CNRS and CEA-DRF/IRFU, France; SRNSFG, Georgia; BMBF, HGF and MPG, Germany; GSRI, Greece; RGC and Hong Kong SAR, China; ISF and Benozzi Center, Israel; INFN, Italy; MEXT and JSPS, Japan; CNRST, Morocco; NWO, Netherlands; RCN, Norway; MNiSW, Poland; FCT, Portugal; MNE/IFA, Romania; MESTD, Serbia; MSSR, Slovakia; ARRS and MIZŠ, Slovenia; DSI/NRF, South Africa; MICINN, Spain; SRC and Wallenberg Foundation, Sweden; SERI, SNSF and Cantons of Bern and Geneva, Switzerland; MOST, Taipei; TENMAK, Türkiye; STFC, United Kingdom; DOE and NSF, United States of America.

Individual groups and members have received support from BCKDF, CANARIE, CRC and DRAC, Canada; PRIMUS 21/SCI/017, CERN-CZ and FORTE, Czech Republic; COST, ERC, ERDF, Horizon 2020, ICSC-NextGenerationEU and Marie Skłodowska-Curie Actions, European Union; Investissements d’Avenir Labex, Investissements d’Avenir Idex and ANR, France; DFG and AvH Foundation, Germany; Herakleitos, Thales and Aristeia programmes co-financed by EU-ESF and the Greek NSRF, Greece; BSF-NSF and MINERVA, Israel; Norwegian Financial Mechanism 2014-2021, Norway; NCN and NAWA, Poland; La Caixa Banking Foundation, CERCA Programme Generalitat de Catalunya and PROMETEO and GenT Programmes Generalitat Valenciana, Spain; Göran Gustafssons Stiftelse, Sweden; The Royal Society and Leverhulme Trust, United Kingdom.

In addition, individual members wish to acknowledge support from CERN: European Organization for Nuclear Research (CERN PJA5); Chile: Agencia Nacional de Investigación y Desarrollo (FONDECYT 1190886, FONDECYT 1210400, FONDECYT 1230812, FONDECYT 1230987); China: Chinese Ministry of Science and Technology (MOST-2023YFA1605700), National Natural Science Foundation of China (NSFC - 12175119, NSFC 12275265, NSFC-12075060); Czech Republic: Czech Science Foundation (GACR - 24-11373S), Ministry of Education Youth and Sports (FORTE CZ.02.01.01/00/22_008/0004632), PRIMUS Research Programme (PRIMUS/21/SCI/017); EU: H2020 European Research Council (ERC - 101002463); European Union: European Research Council (ERC - 948254, ERC 101089007), Horizon 2020 Framework Programme (MUCCA - CHIST-ERA-19-XAI-00), European Union, Future Artificial Intelligence Research (FAIR-NextGenerationEU PE00000013), Italian Center for High Performance Computing, Big Data and Quantum Computing (ICSC, NextGenerationEU); France: Agence Nationale de la Recherche (ANR-20-CE31-0013, ANR-21-CE31-0013, ANR-21-CE31-0022), Investissements d’Avenir Labex (ANR-11-LABX-0012); Germany: Baden-Württemberg Stiftung (BW Stiftung-Postdoc Eliteprogramme), Deutsche Forschungsgemeinschaft (DFG - 469666862, DFG - CR 312/5-2); Italy: Istituto Nazionale di Fisica Nucleare (ICSC, NextGenerationEU); Japan: Japan Society for the Promotion of Science (JSPS KAKENHI JP21H05085, JSPS KAKENHI JP22H01227, JSPS

KAKENHI JP22H04944, JSPS KAKENHI JP22KK0227); Netherlands: Netherlands Organisation for Scientific Research (NWO Veni 2020 - VI.Veni.202.179); Norway: Research Council of Norway (RCN-314472); Poland: Polish National Agency for Academic Exchange (PPN/PPO/2020/1/00002/U/00001), Polish National Science Centre (NCN 2021/42/E/ST2/00350, NCN OPUS nr 2022/47/B/ST2/03059, NCN UMO-2019/34/E/ST2/00393, UMO-2020/37/B/ST2/01043, UMO-2021/40/C/ST2/00187, UMO-2022/47/O/ST2/00148, UMO-2023/49/B/ST2/04085); Slovenia: Slovenian Research Agency (ARIS grant J1-3010); Spain: Generalitat Valenciana (Artemisa, FEDER, IDIFEDER/2018/048), Ministry of Science and Innovation (MCIN & NextGenEU PCI2022-135018-2, MICIN & FEDER PID2021-125273NB, RYC2019-028510-I, RYC2020-030254-I, RYC2021-031273-I, RYC2022-038164-I), PROMETEO and GenT Programmes Generalitat Valenciana (CIDEAGENT/2019/023, CIDEAGENT/2019/027); Sweden: Swedish Research Council (Swedish Research Council 2023-04654, VR 2018-00482, VR 2022-03845, VR 2022-04683, VR 2023-03403, VR grant 2021-03651), Knut and Alice Wallenberg Foundation (KAW 2018.0157, KAW 2018.0458, KAW 2019.0447, KAW 2022.0358); Switzerland: Swiss National Science Foundation (SNSF - PCEFP2_194658); United Kingdom: Leverhulme Trust (Leverhulme Trust RPG-2020-004), Royal Society (NIF-R1-231091); United States of America: U.S. Department of Energy (ECA DE-AC02-76SF00515), Neubauer Family Foundation. We thank R. Gauld (MPI Munich) and the NNLOJET developers for providing NLO $Z + b$ 5FS and $Z + c$ 4FS predictions with MGAMC+Py8 as well as NLO and NNLO fixed-order predictions [3] in the fiducial phase space of the analysis, and for helpful discussions.

References

- [1] F. Maltoni, G. Ridolfi and M. Ubiali, *b-initiated processes at the LHC: a reappraisal*, *JHEP* **07** (2012) 022, arXiv: [1203.6393 \[hep-ph\]](#).
- [2] R. Gauld, A. Huss and G. Stagnitto, *Flavor Identification of Reconstructed Hadronic Jets*, *Phys. Rev. Lett.* **130** (2023) 161901, arXiv: [2208.11138 \[hep-ph\]](#).
- [3] R. Gauld et al., *NNLO QCD predictions for Z-boson production in association with a charm jet within the LHCb fiducial region*, *Eur. Phys. J. C* **83** (2023) 336, arXiv: [2302.12844 \[hep-ph\]](#).
- [4] M. Czakon, A. Mitov and R. Poncelet, *Infrared-safe flavoured anti- k_T jets*, *JHEP* **04** (2023) 138, arXiv: [2205.11879 \[hep-ph\]](#).
- [5] S. Caletti, A. J. Larkoski, S. Marzani and D. Reichelt, *Practical jet flavour through NNLO*, *Eur. Phys. J. C* **82** (2022) 632, arXiv: [2205.01109 \[hep-ph\]](#).
- [6] CDF Collaboration, *Measurement of cross sections for b jet production in events with a Z boson in $p\bar{p}$ collisions at $\sqrt{s} = 1.96$ TeV*, *Phys. Rev. D* **79** (2009) 052008, arXiv: [0812.4458 \[hep-ex\]](#).
- [7] D0 Collaboration, *Measurement of the ratio of differential cross sections $\sigma(p\bar{p} \rightarrow Z + b \text{ jet})/\sigma(p\bar{p} \rightarrow Z + \text{jet})$ in $p\bar{p}$ collisions at $\sqrt{s} = 1.96$ TeV*, *Phys. Rev. D* **87** (2013) 092010, arXiv: [1301.2233 \[hep-ex\]](#).
- [8] ATLAS Collaboration, *Measurement of differential production cross-sections for a Z boson in association with b-jets in 7 TeV proton–proton collisions with the ATLAS detector*, *JHEP* **10** (2014) 141, arXiv: [1407.3643 \[hep-ex\]](#).
- [9] CMS Collaboration, *Measurement of the production cross sections for a Z boson and one or more b jets in pp collisions at $\sqrt{s} = 7$ TeV*, *JHEP* **06** (2014) 120, arXiv: [1402.1521 \[hep-ex\]](#).

- [10] CMS Collaboration, *Measurement of the cross section and angular correlations for associated production of a Z boson with b hadrons in pp collisions at $\sqrt{s} = 7$ TeV*, *JHEP* **12** (2013) 039, arXiv: [1310.1349 \[hep-ex\]](#).
- [11] CMS Collaboration, *Measurement of the Z/γ^*+b -jet cross section in pp collisions at $\sqrt{s} = 7$ TeV*, *JHEP* **06** (2012) 126, arXiv: [1204.1643 \[hep-ex\]](#).
- [12] R. Aaij et al., *Measurement of the Z+b-jet cross-section in pp collisions at $\sqrt{s} = 7$ TeV in the forward region*, *JHEP* **01** (2015) 064, arXiv: [1411.1264 \[hep-ex\]](#).
- [13] CMS Collaboration, *Measurements of the associated production of a Z boson and b jets in pp collisions at $\sqrt{s} = 8$ TeV*, *Eur. Phys. J. C* **77** (2017) 751, arXiv: [1611.06507 \[hep-ex\]](#).
- [14] ATLAS Collaboration, *Measurements of the production cross-section for a Z boson in association with b-jets in proton–proton collisions at $\sqrt{s} = 13$ TeV with the ATLAS detector*, *JHEP* **07** (2020) 044, arXiv: [2003.11960 \[hep-ex\]](#).
- [15] ATLAS Collaboration, *Measurement of cross sections for production of a Z boson in association with a flavor-inclusive or doubly b-tagged large-radius jet in proton–proton collisions at $\sqrt{s} = 13$ TeV with the ATLAS experiment*, *Phys. Rev. D* **108** (2023) 012022, arXiv: [2204.12355 \[hep-ex\]](#).
- [16] CMS Collaboration, *Measurement of the production cross section for Z + b jets in proton–proton collisions at $\sqrt{s} = 13$ TeV*, *Phys. Rev. D* **105** (2022) 092014, arXiv: [2112.09659 \[hep-ex\]](#).
- [17] S. Brodsky, P. Hoyer, C. Peterson and N. Sakai, *The Intrinsic Charm of the Proton*, *Phys. Lett. B* **93** (1980) 451.
- [18] S. J. Brodsky, C. Peterson and N. Sakai, *Intrinsic heavy-quark states*, *Phys. Rev. D* **23** (1981) 2745.
- [19] R. D. Ball et al., *A Determination of the Charm Content of the Proton*, *Eur. Phys. J. C* **76** (2016) 647, arXiv: [1605.06515 \[hep-ph\]](#).
- [20] T.-J. Hou et al., *CT14 Intrinsic Charm Parton Distribution Functions from CTEQ-TEA Global Analysis*, *JHEP* **02** (2018) 059, arXiv: [1707.00657 \[hep-ph\]](#).
- [21] V. Bednyakov, M. Demeichev, G. Lykasov, T. Stavreva and M. Stockton, *Searching for intrinsic charm in the proton at the LHC*, *Phys. Lett. B* **728** (2014) 602, arXiv: [1305.3548 \[hep-ph\]](#).
- [22] P.-H. Beauchemin, V. Bednyakov, G. Lykasov and Y. Y. Stepanenko, *Search for intrinsic charm in vector boson production accompanied by heavy-flavor jets*, *Phys. Rev. D* **92** (2015) 034014, arXiv: [1410.2616 \[hep-ph\]](#).
- [23] CMS Collaboration, *Measurement of differential cross sections for Z bosons produced in association with charm jets in pp collisions at $\sqrt{s} = 13$ TeV*, *JHEP* **04** (2021) 109, arXiv: [2012.04119 \[hep-ex\]](#).
- [24] LHCb Collaboration, *Study of Z Bosons Produced in Association with Charm in the Forward Region*, *Phys. Rev. Lett.* **128** (2022) 082001, arXiv: [2109.08084 \[hep-ex\]](#).
- [25] NNPDF Collaboration, *Evidence for intrinsic charm quarks in the proton*, *Nature* **608** (2022) 483, arXiv: [2208.08372 \[hep-ph\]](#).

- [26] R. P. Feynman, *Very high-energy collisions of hadrons*, *Phys. Rev. Lett.* **23** (1969) 1415, ed. by L. M. Brown.
- [27] ATLAS Collaboration, *The ATLAS Experiment at the CERN Large Hadron Collider*, *JINST* **3** (2008) S08003.
- [28] ATLAS Collaboration, *ATLAS Insertable B-Layer: Technical Design Report*, ATLAS-TDR-19; CERN-LHCC-2010-013, 2010, URL: <https://cds.cern.ch/record/1291633>, Addendum: ATLAS-TDR-19-ADD-1; CERN-LHCC-2012-009, 2012, URL: <https://cds.cern.ch/record/1451888>.
- [29] B. Abbott et al., *Production and integration of the ATLAS Insertable B-Layer*, *JINST* **13** (2018) T05008, arXiv: [1803.00844](https://arxiv.org/abs/1803.00844) [[physics.ins-det](#)].
- [30] G. Avoni et al., *The new LUCID-2 detector for luminosity measurement and monitoring in ATLAS*, *JINST* **13** (2018) P07017.
- [31] ATLAS Collaboration, *Performance of the ATLAS trigger system in 2015*, *Eur. Phys. J. C* **77** (2017) 317, arXiv: [1611.09661](https://arxiv.org/abs/1611.09661) [[hep-ex](#)].
- [32] ATLAS Collaboration, *The ATLAS Collaboration Software and Firmware*, ATL-SOFT-PUB-2021-001, 2021, URL: <https://cds.cern.ch/record/2767187>.
- [33] ATLAS Collaboration, *Luminosity determination in pp collisions at $\sqrt{s} = 13$ TeV using the ATLAS detector at the LHC*, *Eur. Phys. J. C* **83** (2023) 982, arXiv: [2212.09379](https://arxiv.org/abs/2212.09379) [[hep-ex](#)].
- [34] ATLAS Collaboration, *Performance of electron and photon triggers in ATLAS during LHC Run 2*, *Eur. Phys. J. C* **80** (2020) 47, arXiv: [1909.00761](https://arxiv.org/abs/1909.00761) [[hep-ex](#)].
- [35] ATLAS Collaboration, *Performance of the ATLAS muon triggers in Run 2*, *JINST* **15** (2020) P09015, arXiv: [2004.13447](https://arxiv.org/abs/2004.13447) [[physics.ins-det](#)].
- [36] ATLAS Collaboration, *The ATLAS inner detector trigger performance in pp collisions at 13 TeV during LHC Run 2*, *Eur. Phys. J. C* **82** (2022) 206, arXiv: [2107.02485](https://arxiv.org/abs/2107.02485) [[hep-ex](#)].
- [37] ATLAS Collaboration, *The ATLAS Simulation Infrastructure*, *Eur. Phys. J. C* **70** (2010) 823, arXiv: [1005.4568](https://arxiv.org/abs/1005.4568) [[physics.ins-det](#)].
- [38] S. Agostinelli et al., *GEANT4 - a simulation toolkit*, *Nucl. Instrum. Meth. A* **506** (2003) 250.
- [39] T. Sjöstrand, S. Mrenna and P. Skands, *A brief introduction to PYTHIA 8.1*, *Comput. Phys. Commun.* **178** (2008) 852, arXiv: [0710.3820](https://arxiv.org/abs/0710.3820) [[hep-ph](#)].
- [40] ATLAS Collaboration, *The Pythia 8 A3 tune description of ATLAS minimum bias and inelastic measurements incorporating the Donnachie–Landshoff diffractive model*, ATL-PHYS-PUB-2016-017, 2016, URL: <https://cds.cern.ch/record/2206965>.
- [41] R. D. Ball et al., *Parton distributions with LHC data*, *Nucl. Phys. B* **867** (2013) 244, arXiv: [1207.1303](https://arxiv.org/abs/1207.1303) [[hep-ph](#)].
- [42] J. Alwall et al., *The automated computation of tree-level and next-to-leading order differential cross sections, and their matching to parton shower simulations*, *JHEP* **07** (2014) 079, arXiv: [1405.0301](https://arxiv.org/abs/1405.0301) [[hep-ph](#)].
- [43] T. Sjöstrand et al., *An introduction to PYTHIA 8.2*, *Comput. Phys. Commun.* **191** (2015) 159, arXiv: [1410.3012](https://arxiv.org/abs/1410.3012) [[hep-ph](#)].

- [44] R. Frederix and S. Frixione, *Merging meets matching in MC@NLO*, **JHEP** **12** (2012) 061, arXiv: [1209.6215 \[hep-ph\]](#).
- [45] ATLAS Collaboration, *Modelling and computational improvements to the simulation of single vector-boson plus jet processes for the ATLAS experiment*, **JHEP** **08** (2022) 089, arXiv: [2112.09588 \[hep-ex\]](#).
- [46] ATLAS Collaboration, *ATLAS Pythia 8 tunes to 7 TeV data*, ATL-PHYS-PUB-2014-021, 2014, URL: <https://cds.cern.ch/record/1966419>.
- [47] R. D. Ball et al., *Parton distributions from high-precision collider data*, **Eur. Phys. J. C** **77** (2017) 663, arXiv: [1706.00428 \[hep-ph\]](#).
- [48] T. Gleisberg and S. Höche, *Comix, a new matrix element generator*, **JHEP** **12** (2008) 039, arXiv: [0808.3674 \[hep-ph\]](#).
- [49] F. Buccioni et al., *OpenLoops 2*, **Eur. Phys. J. C** **79** (2019) 866, arXiv: [1907.13071 \[hep-ph\]](#).
- [50] F. Cascioli, P. Maierhöfer and S. Pozzorini, *Scattering Amplitudes with Open Loops*, **Phys. Rev. Lett.** **108** (2012) 111601, arXiv: [1111.5206 \[hep-ph\]](#).
- [51] A. Denner, S. Dittmaier and L. Hofer, *Collier: A fortran-based complex one-loop library in extended regularizations*, **Comput. Phys. Commun.** **212** (2017) 220, arXiv: [1604.06792 \[hep-ph\]](#).
- [52] S. Schumann and F. Krauss, *A Parton shower algorithm based on Catani-Seymour dipole factorisation*, **JHEP** **03** (2008) 038, arXiv: [0709.1027 \[hep-ph\]](#).
- [53] J.-C. Winter, F. Krauss and G. Soff, *A modified cluster-hadronization model*, **Eur. Phys. J. C** **36** (2004) 381, arXiv: [hep-ph/0311085](#).
- [54] NNPDF Collaboration, R.D. Ball et al., *Parton distributions for the LHC Run II*, **JHEP** **04** (2015) 040, arXiv: [1410.8849 \[hep-ph\]](#).
- [55] S. Höche, F. Krauss, M. Schönherr and F. Siegert, *A critical appraisal of NLO+PS matching methods*, **JHEP** **09** (2012) 049, arXiv: [1111.1220 \[hep-ph\]](#).
- [56] S. Höche, F. Krauss, M. Schönherr and F. Siegert, *QCD matrix elements + parton showers. The NLO case*, **JHEP** **04** (2013) 027, arXiv: [1207.5030 \[hep-ph\]](#).
- [57] S. Catani, F. Krauss, B. R. Webber and R. Kuhn, *QCD Matrix Elements + Parton Showers*, **JHEP** **11** (2001) 063, arXiv: [hep-ph/0109231](#).
- [58] S. Höche, F. Krauss, S. Schumann and F. Siegert, *QCD matrix elements and truncated showers*, **JHEP** **05** (2009) 053, arXiv: [0903.1219 \[hep-ph\]](#).
- [59] S. Frixione, G. Ridolfi and P. Nason, *A positive-weight next-to-leading-order Monte Carlo for heavy flavour hadroproduction*, **JHEP** **09** (2007) 126, arXiv: [0707.3088 \[hep-ph\]](#).
- [60] P. Nason, *A new method for combining NLO QCD with shower Monte Carlo algorithms*, **JHEP** **11** (2004) 040, arXiv: [hep-ph/0409146](#).
- [61] S. Frixione, P. Nason and C. Oleari, *Matching NLO QCD computations with Parton Shower simulations: the POWHEG method*, **JHEP** **11** (2007) 070, arXiv: [0709.2092 \[hep-ph\]](#).

- [62] S. Alioli, P. Nason, C. Oleari and E. Re, *A general framework for implementing NLO calculations in shower Monte Carlo programs: the POWHEG BOX*, **JHEP** **06** (2010) 043, arXiv: [1002.2581 \[hep-ph\]](#).
- [63] ATLAS Collaboration, *Studies on top-quark Monte Carlo modelling for Top2016*, ATL-PHYS-PUB-2016-020, 2016, URL: <https://cds.cern.ch/record/2216168>.
- [64] M. Beneke, P. Falgari, S. Klein and C. Schwinn, *Hadronic top-quark pair production with NNLL threshold resummation*, **Nucl. Phys. B** **855** (2012) 695, arXiv: [1109.1536 \[hep-ph\]](#).
- [65] M. Cacciari, M. Czakon, M. Mangano, A. Mitov and P. Nason, *Top-pair production at hadron colliders with next-to-next-to-leading logarithmic soft-gluon resummation*, **Phys. Lett. B** **710** (2012) 612, arXiv: [1111.5869 \[hep-ph\]](#).
- [66] P. Bärnreuther, M. Czakon and A. Mitov, *Percent-Level-Precision Physics at the Tevatron: Next-to-Next-to-Leading Order QCD Corrections to $q\bar{q} \rightarrow t\bar{t} + X$* , **Phys. Rev. Lett.** **109** (2012) 132001, arXiv: [1204.5201 \[hep-ph\]](#).
- [67] M. Czakon and A. Mitov, *NNLO corrections to top-pair production at hadron colliders: the all-fermionic scattering channels*, **JHEP** **12** (2012) 054, arXiv: [1207.0236 \[hep-ph\]](#).
- [68] M. Czakon and A. Mitov, *NNLO corrections to top pair production at hadron colliders: the quark-gluon reaction*, **JHEP** **01** (2013) 080, arXiv: [1210.6832 \[hep-ph\]](#).
- [69] M. Czakon, P. Fiedler and A. Mitov, *Total Top-Quark Pair-Production Cross Section at Hadron Colliders Through $O(\alpha_S^4)$* , **Phys. Rev. Lett.** **110** (2013) 252004, arXiv: [1303.6254 \[hep-ph\]](#).
- [70] M. Czakon and A. Mitov, *Top++: A program for the calculation of the top-pair cross-section at hadron colliders*, **Comput. Phys. Commun.** **185** (2014) 2930, arXiv: [1112.5675 \[hep-ph\]](#).
- [71] S. Frixione, E. Laenen, P. Motylinski, B. R. Webber and C. D. White, *Single-top hadroproduction in association with a W boson*, **JHEP** **07** (2008) 029, arXiv: [0805.3067 \[hep-ph\]](#).
- [72] E. Bothmann et al., *Event Generation with Sherpa 2.2*, **SciPost Phys.** **7** (2019) 034, arXiv: [1905.09127 \[hep-ph\]](#).
- [73] J. Butterworth et al., *PDF4LHC recommendations for LHC Run II*, **J. Phys. G** **43** (2016) 023001, arXiv: [1510.03865 \[hep-ph\]](#).
- [74] NNPDF Collaboration, R.D. Ball et al., *The path to proton structure at 1% accuracy*, **Eur. Phys. J. C** **82** (2022) 428, arXiv: [2109.02653 \[hep-ph\]](#).
- [75] J. J. Aubert et al., *Production of charmed particles in 250-GeV μ^+ -iron interactions*, **Nucl. Phys. B** **213** (1983) 31.
- [76] M. Guzzi et al., *The persistent nonperturbative charm enigma*, **Phys. Lett. B** **843** (2023) 137975, arXiv: [2211.01387 \[hep-ph\]](#).
- [77] J. Blümlein, *A Kinematic Condition on Intrinsic Charm*, **Phys. Lett. B** **753** (2016) 619, arXiv: [1511.00229 \[hep-ph\]](#).

- [78] T. J. Hobbs, J. T. Londergan and W. Melnitchouk, *Phenomenology of nonperturbative charm in the nucleon*, *Phys. Rev. D* **89** (2014) 074008, arXiv: [1311.1578 \[hep-ph\]](#).
- [79] J. Butterworth, G. Dissertori, S. Dittmaier, D. de Florian, N. Glover et al., *Les Houches 2013: Physics at TeV Colliders: Standard Model Working Group Report*, 2014, arXiv: [1405.1067 \[hep-ph\]](#).
- [80] ATLAS Collaboration, *ATLAS data quality operations and performance for 2015–2018 data-taking*, *JINST* **15** (2020) P04003, arXiv: [1911.04632 \[physics.ins-det\]](#).
- [81] ATLAS Collaboration, *Vertex Reconstruction Performance of the ATLAS Detector at $\sqrt{s} = 13$ TeV*, ATL-PHYS-PUB-2015-026, 2015, URL: <https://cds.cern.ch/record/2037717>.
- [82] ATLAS Collaboration, *Electron and photon performance measurements with the ATLAS detector using the 2015–2017 LHC proton–proton collision data*, *JINST* **14** (2019) P12006, arXiv: [1908.00005 \[hep-ex\]](#).
- [83] ATLAS Collaboration, *Muon reconstruction performance of the ATLAS detector in proton–proton collision data at $\sqrt{s} = 13$ TeV*, *Eur. Phys. J. C* **76** (2016) 292, arXiv: [1603.05598 \[hep-ex\]](#).
- [84] ATLAS Collaboration, *Muon reconstruction and identification efficiency in ATLAS using the full Run 2 pp collision data set at $\sqrt{s} = 13$ TeV*, *Eur. Phys. J. C* **81** (2021) 578, arXiv: [2012.00578 \[hep-ex\]](#).
- [85] M. Cacciari, G. P. Salam and G. Soyez, *The anti- k_r jet clustering algorithm*, *JHEP* **04** (2008) 063, arXiv: [0802.1189 \[hep-ph\]](#).
- [86] M. Cacciari, G. P. Salam and G. Soyez, *FastJet User Manual*, *Eur. Phys. J. C* **72** (2012) 1896, arXiv: [1111.6097 \[hep-ph\]](#).
- [87] ATLAS Collaboration, *Jet reconstruction and performance using particle flow with the ATLAS Detector*, *Eur. Phys. J. C* **77** (2017) 466, arXiv: [1703.10485 \[hep-ex\]](#).
- [88] ATLAS Collaboration, *Jet energy scale measurements and their systematic uncertainties in proton–proton collisions at $\sqrt{s} = 13$ TeV with the ATLAS detector*, *Phys. Rev. D* **96** (2017) 072002, arXiv: [1703.09665 \[hep-ex\]](#).
- [89] ATLAS Collaboration, *Performance of pile-up mitigation techniques for jets in pp collisions at $\sqrt{s} = 8$ TeV using the ATLAS detector*, *Eur. Phys. J. C* **76** (2016) 581, arXiv: [1510.03823 \[hep-ex\]](#).
- [90] ATLAS Collaboration, *ATLAS flavour-tagging algorithms for the LHC Run 2 pp collision dataset*, *Eur. Phys. J. C* **83** (2023) 681, arXiv: [2211.16345 \[physics.data-an\]](#).
- [91] ATLAS Collaboration, *E_T^{miss} performance in the ATLAS detector using 2015–2016 LHC pp collisions*, ATLAS-CONF-2018-023, 2018, URL: <https://cds.cern.ch/record/2625233>.
- [92] G. D’Agostini, *A Multidimensional unfolding method based on Bayes’ theorem*, *Nucl. Instrum. Meth. A* **362** (1995) 487.
- [93] ATLAS Collaboration, *The performance of missing transverse momentum reconstruction and its significance with the ATLAS detector using 140 fb^{-1} of $\sqrt{s} = 13$ TeV pp collisions*, 2024, arXiv: [2402.05858 \[hep-ex\]](#).

- [94] ATLAS Collaboration, *ATLAS b-jet identification performance and efficiency measurement with $t\bar{t}$ events in pp collisions at $\sqrt{s} = 13$ TeV*, *Eur. Phys. J. C* **79** (2019) 970, arXiv: [1907.05120](https://arxiv.org/abs/1907.05120) [[hep-ex](#)].
- [95] ATLAS Collaboration, *Measurement of the c-jet mistagging efficiency in $t\bar{t}$ events using pp collision data at $\sqrt{s} = 13$ TeV collected with the ATLAS detector*, *Eur. Phys. J. C* **82** (2022) 95, arXiv: [2109.10627](https://arxiv.org/abs/2109.10627) [[hep-ex](#)].
- [96] ATLAS Collaboration, *Calibration of the light-flavour jet mistagging efficiency of the b-tagging algorithms with Z+jets events using 139fb^{-1} of ATLAS proton–proton collision data at $\sqrt{s} = 13$ TeV*, *Eur. Phys. J. C* **83** (2023) 728, arXiv: [2301.06319](https://arxiv.org/abs/2301.06319) [[hep-ex](#)].
- [97] ATLAS Collaboration, *ATLAS Computing Acknowledgements*, ATL-SOFT-PUB-2023-001, 2023, URL: <https://cds.cern.ch/record/2869272>.

The ATLAS Collaboration

G. Aad ¹⁰³, E. Aakvaag ¹⁶, B. Abbott ¹²¹, S. Abdelhameed ^{117a}, K. Abeling ⁵⁵, N.J. Abicht ⁴⁹, S.H. Abidi ²⁹, M. Aboeela ⁴⁴, A. Aboulhorma ^{35e}, H. Abramowicz ¹⁵², H. Abreu ¹⁵¹, Y. Abulaiti ¹¹⁸, B.S. Acharya ^{69a,69b,k}, A. Ackermann ^{63a}, C. Adam Bourdarios ⁴, L. Adamczyk ^{86a}, S.V. Addepalli ²⁶, M.J. Addison ¹⁰², J. Adelman ¹¹⁶, A. Adiguzel ^{21c}, T. Adye ¹³⁵, A.A. Affolder ¹³⁷, Y. Afik ³⁹, M.N. Agaras ¹³, J. Agarwala ^{73a,73b}, A. Aggarwal ¹⁰¹, C. Agheorghiesei ^{27c}, A. Ahmad ³⁶, F. Ahmadov ^{38,x}, W.S. Ahmed ¹⁰⁵, S. Ahuja ⁹⁶, X. Ai ^{62e}, G. Aielli ^{76a,76b}, A. Aikot ¹⁶⁴, M. Ait Tamliah ^{35e}, B. Aitbenkhik ^{35a}, M. Akbiyik ¹⁰¹, T.P.A. Åkesson ⁹⁹, A.V. Akimov ³⁷, D. Akiyama ¹⁶⁹, N.N. Akolkar ²⁴, S. Aktas ^{21a}, K. Al Houry ⁴¹, G.L. Alberghi ^{23b}, J. Albert ¹⁶⁶, P. Albicocco ⁵³, G.L. Albouy ⁶⁰, S. Alderweireldt ⁵², Z.L. Alegria ¹²², M. Aleksa ³⁶, I.N. Aleksandrov ³⁸, C. Alexa ^{27b}, T. Alexopoulos ¹⁰, F. Alfonsi ^{23b}, M. Algren ⁵⁶, M. Alhroob ¹⁶⁸, B. Ali ¹³³, H.M.J. Ali ⁹², S. Ali ³¹, S.W. Alibocus ⁹³, M. Aliev ^{33c}, G. Alimonti ^{71a}, W. Alkashi ⁵⁵, C. Allaire ⁶⁶, B.M.M. Allbrooke ¹⁴⁷, J.F. Allen ⁵², C.A. Allendes Flores ^{138f}, P.P. Allport ²⁰, A. Aloisio ^{72a,72b}, F. Alonso ⁹¹, C. Alpigiani ¹³⁹, Z.M.K. Alsolami ⁹², M. Alvarez Estevez ¹⁰⁰, A. Alvarez Fernandez ¹⁰¹, M. Alves Cardoso ⁵⁶, M.G. Alvigi ^{72a,72b}, M. Aly ¹⁰², Y. Amaral Coutinho ^{83b}, A. Ambler ¹⁰⁵, C. Amelung ³⁶, M. Amerl ¹⁰², C.G. Ames ¹¹⁰, D. Amidei ¹⁰⁷, K.J. Amirie ¹⁵⁶, S.P. Amor Dos Santos ^{131a}, K.R. Amos ¹⁶⁴, S. An ⁸⁴, V. Ananiev ¹²⁶, C. Anastopoulos ¹⁴⁰, T. Andeen ¹¹, J.K. Anders ³⁶, S.Y. Andrean ^{47a,47b}, A. Andreazza ^{71a,71b}, S. Angelidakis ⁹, A. Angerami ^{41,z}, A.V. Anisenkov ³⁷, A. Annovi ^{74a}, C. Antel ⁵⁶, E. Antipov ¹⁴⁶, M. Antonelli ⁵³, F. Anulli ^{75a}, M. Aoki ⁸⁴, T. Aoki ¹⁵⁴, M.A. Aparo ¹⁴⁷, L. Aperio Bella ⁴⁸, C. Appelt ¹⁸, A. Apyan ²⁶, S.J. Arbiol Val ⁸⁷, C. Arcangeletti ⁵³, A.T.H. Arce ⁵¹, E. Arena ⁹³, J-F. Arguin ¹⁰⁹, S. Argyropoulos ⁵⁴, J.-H. Arling ⁴⁸, O. Arnaez ⁴, H. Arnold ¹⁴⁶, G. Artoni ^{75a,75b}, H. Asada ¹¹², K. Asai ¹¹⁹, S. Asai ¹⁵⁴, N.A. Asbah ³⁶, R.A. Ashby Pickering ¹⁶⁸, K. Assamagan ²⁹, R. Astalos ^{28a}, K.S.V. Astrand ⁹⁹, S. Atashi ¹⁶⁰, R.J. Atkin ^{33a}, M. Atkinson ¹⁶³, H. Atmani ^{35f}, P.A. Atmasiddha ¹²⁹, K. Augsten ¹³³, S. Auricchio ^{72a,72b}, A.D. Auriol ²⁰, V.A. Austrup ¹⁰², G. Avolio ³⁶, K. Axiotis ⁵⁶, G. Azuelos ^{109,ad}, D. Babal ^{28b}, H. Bachacou ¹³⁶, K. Bachas ^{153,o}, A. Bachi ³⁴, F. Backman ^{47a,47b}, A. Badea ³⁹, T.M. Baer ¹⁰⁷, P. Bagnaia ^{75a,75b}, M. Bahmani ¹⁸, D. Bahner ⁵⁴, K. Bai ¹²⁴, J.T. Baines ¹³⁵, L. Baines ⁹⁵, O.K. Baker ¹⁷³, E. Bakos ¹⁵, D. Bakshi Gupta ⁸, V. Balakrishnan ¹²¹, R. Balasubramanian ¹¹⁵, E.M. Baldin ³⁷, P. Balek ^{86a}, E. Ballabene ^{23b,23a}, F. Balli ¹³⁶, L.M. Baltes ^{63a}, W.K. Balunas ³², J. Balz ¹⁰¹, I. Bamwidhi ^{117b}, E. Banas ⁸⁷, M. Bandieramonte ¹³⁰, A. Bandyopadhyay ²⁴, S. Bansal ²⁴, L. Barak ¹⁵², M. Barakat ⁴⁸, E.L. Barberio ¹⁰⁶, D. Barberis ^{57b,57a}, M. Barbero ¹⁰³, M.Z. Barel ¹¹⁵, K.N. Barends ^{33a}, T. Barillari ¹¹¹, M-S. Barisits ³⁶, T. Barklow ¹⁴⁴, P. Baron ¹²³, D.A. Baron Moreno ¹⁰², A. Baroncelli ^{62a}, G. Barone ²⁹, A.J. Barr ¹²⁷, J.D. Barr ⁹⁷, F. Barreiro ¹⁰⁰, J. Barreiro Guimarães da Costa ^{14a}, U. Barron ¹⁵², M.G. Barros Teixeira ^{131a}, S. Barsov ³⁷, F. Bartels ^{63a}, R. Bartoldus ¹⁴⁴, A.E. Barton ⁹², P. Bartos ^{28a}, A. Basan ¹⁰¹, M. Baselga ⁴⁹, A. Bassalat ^{66,b}, M.J. Basso ^{157a}, R. Bate ¹⁶⁵, R.L. Bates ⁵⁹, S. Batlamous ¹⁰⁰, B. Batool ¹⁴², M. Battaglia ¹³⁷, D. Battulga ¹⁸, M. Bauce ^{75a,75b}, M. Bauer ³⁶, P. Bauer ²⁴, L.T. Bazzano Hurrell ³⁰, J.B. Beacham ⁵¹, T. Beau ¹²⁸, J.Y. Beaucamp ⁹¹, P.H. Beauchemin ¹⁵⁹, P. Bechtel ²⁴, H.P. Beck ^{19,n}, K. Becker ¹⁶⁸, A.J. Beddall ⁸², V.A. Bednyakov ³⁸, C.P. Bee ¹⁴⁶, L.J. Beemster ¹⁵, T.A. Beermann ³⁶, M. Begalli ^{83d}, M. Begel ²⁹, A. Behera ¹⁴⁶, J.K. Behr ⁴⁸, J.F. Beirer ³⁶, F. Beisiegel ²⁴, M. Belfkir ^{117b}, G. Bella ¹⁵², L. Bellagamba ^{23b}, A. Bellerive ³⁴, P. Bellos ²⁰, K. Beloborodov ³⁷, D. Benckekroun ^{35a}, F. Bendebba ^{35a}, Y. Benhammou ¹⁵²,

K.C. Benkendorfer [ID61](#), L. Beresford [ID48](#), M. Beretta [ID53](#), E. Bergeaas Kuutmann [ID162](#), N. Berger [ID4](#),
 B. Bergmann [ID133](#), J. Beringer [ID17a](#), G. Bernardi [ID5](#), C. Bernius [ID144](#), F.U. Bernlochner [ID24](#),
 F. Bernon [ID36,103](#), A. Berrocal Guardia [ID13](#), T. Berry [ID96](#), P. Berta [ID134](#), A. Berthold [ID50](#), S. Bethke [ID111](#),
 A. Betti [ID75a,75b](#), A.J. Bevan [ID95](#), N.K. Bhalla [ID54](#), S. Bhatta [ID146](#), D.S. Bhattacharya [ID167](#),
 P. Bhattarai [ID144](#), K.D. Bhide [ID54](#), V.S. Bhopatkar [ID122](#), R.M. Bianchi [ID130](#), G. Bianco [ID23b,23a](#),
 O. Biebel [ID110](#), R. Bielski [ID124](#), M. Biglietti [ID77a](#), C.S. Billingsley [ID44](#), M. Bindi [ID55](#), A. Bingul [ID21b](#),
 C. Bini [ID75a,75b](#), A. Biondini [ID93](#), G.A. Bird [ID32](#), M. Birman [ID170](#), M. Biros [ID134](#), S. Biryukov [ID147](#),
 T. Bisanz [ID49](#), E. Bisceglie [ID43b,43a](#), J.P. Biswal [ID135](#), D. Biswas [ID142](#), I. Bloch [ID48](#), A. Blue [ID59](#),
 U. Blumenschein [ID95](#), J. Blumenthal [ID101](#), V.S. Bobrovnikov [ID37](#), L. Boccardo [ID57a](#), M. Boehler [ID54](#),
 B. Boehm [ID167](#), D. Bogavac [ID36](#), A.G. Bogdanchikov [ID37](#), C. Bohm [ID47a](#), V. Boisvert [ID96](#), P. Bokan [ID36](#),
 T. Bold [ID86a](#), M. Bomben [ID5](#), M. Bona [ID95](#), M. Boonekamp [ID136](#), C.D. Booth [ID96](#), A.G. Borbély [ID59](#),
 I.S. Bordulev [ID37](#), H.M. Borecka-Bielska [ID109](#), G. Borissov [ID92](#), D. Bortoletto [ID127](#), D. Boscherini [ID23b](#),
 M. Bosman [ID13](#), J.D. Bossio Sola [ID36](#), K. Bouaouda [ID35a](#), N. Bouchhar [ID164](#), L. Boudet [ID4](#),
 J. Boudreau [ID130](#), E.V. Bouhova-Thacker [ID92](#), D. Boumediene [ID40](#), R. Bouquet [ID57b,57a](#), A. Boveia [ID120](#),
 J. Boyd [ID36](#), D. Boye [ID29](#), I.R. Boyko [ID38](#), L. Bozianu [ID56](#), J. Bracinek [ID20](#), N. Brahimi [ID4](#),
 G. Brandt [ID172](#), O. Brandt [ID32](#), F. Braren [ID48](#), B. Brau [ID104](#), J.E. Brau [ID124](#), R. Brenner [ID170](#),
 L. Brenner [ID115](#), R. Brenner [ID162](#), S. Bressler [ID170](#), D. Britton [ID59](#), D. Britzger [ID111](#), I. Brock [ID24](#),
 G. Brooijmans [ID41](#), E. Brost [ID29](#), L.M. Brown [ID166](#), L.E. Bruce [ID61](#), T.L. Bruckler [ID127](#),
 P.A. Bruckman de Renstrom [ID87](#), B. Brüers [ID48](#), A. Bruni [ID23b](#), G. Bruni [ID23b](#), M. Bruschi [ID23b](#),
 N. Bruscinò [ID75a,75b](#), T. Buanes [ID16](#), Q. Buat [ID139](#), D. Buchin [ID111](#), A.G. Buckley [ID59](#), O. Bulekov [ID37](#),
 B.A. Bullard [ID144](#), S. Burdin [ID93](#), C.D. Burgard [ID49](#), A.M. Burger [ID36](#), B. Burghgrave [ID8](#),
 O. Burlayenko [ID54](#), J.T.P. Burr [ID32](#), J.C. Burzynski [ID143](#), E.L. Busch [ID41](#), V. Büscher [ID101](#),
 P.J. Bussey [ID59](#), J.M. Butler [ID25](#), C.M. Buttar [ID59](#), J.M. Butterworth [ID97](#), W. Buttinger [ID135](#),
 C.J. Buxo Vázquez [ID108](#), A.R. Buzykaev [ID37](#), S. Cabrera Urbán [ID164](#), L. Cadamuro [ID66](#), D. Caforio [ID58](#),
 H. Cai [ID130](#), Y. Cai [ID14a,14e](#), Y. Cai [ID14c](#), V.M.M. Cairo [ID36](#), O. Cakir [ID3a](#), N. Calace [ID36](#),
 P. Calafiura [ID17a](#), G. Calderini [ID128](#), P. Calfayan [ID68](#), G. Callea [ID59](#), L.P. Caloba [ID83b](#), D. Calvet [ID40](#),
 S. Calvet [ID40](#), M. Calvetti [ID74a,74b](#), R. Camacho Toro [ID128](#), S. Camarda [ID36](#), D. Camarero Munoz [ID26](#),
 P. Camarri [ID76a,76b](#), M.T. Camerlingo [ID72a,72b](#), D. Cameron [ID36](#), C. Camincher [ID166](#), M. Campanelli [ID97](#),
 A. Camplani [ID42](#), V. Canale [ID72a,72b](#), A.C. Canbay [ID3a](#), E. Canonero [ID96](#), J. Cantero [ID164](#), Y. Cao [ID163](#),
 F. Capocasa [ID26](#), M. Capua [ID43b,43a](#), A. Carbone [ID71a,71b](#), R. Cardarelli [ID76a](#), J.C.J. Cardenas [ID8](#),
 G. Carducci [ID43b,43a](#), T. Carli [ID36](#), G. Carlino [ID72a](#), J.I. Carlotto [ID13](#), B.T. Carlson [ID130,p](#),
 E.M. Carlson [ID166,157a](#), J. Carmignani [ID93](#), L. Carminati [ID71a,71b](#), A. Carnelli [ID136](#), M. Carnesale [ID75a,75b](#),
 S. Caron [ID114](#), E. Carquin [ID138f](#), S. Carrá [ID71a](#), G. Carratta [ID23b,23a](#), A.M. Carroll [ID124](#), T.M. Carter [ID52](#),
 M.P. Casado [ID13,h](#), M. Caspar [ID48](#), F.L. Castillo [ID4](#), L. Castillo Garcia [ID13](#), V. Castillo Gimenez [ID164](#),
 N.F. Castro [ID131a,131e](#), A. Catinaccio [ID36](#), J.R. Catmore [ID126](#), T. Cavaliere [ID4](#), V. Cavaliere [ID29](#),
 N. Cavalli [ID23b,23a](#), Y.C. Cekmecelioglu [ID48](#), E. Celebi [ID21a](#), S. Cella [ID36](#), F. Celli [ID127](#),
 M.S. Centonze [ID70a,70b](#), V. Cepaitis [ID56](#), K. Cerny [ID123](#), A.S. Cerqueira [ID83a](#), A. Cerri [ID147](#),
 L. Cerrito [ID76a,76b](#), F. Cerutti [ID17a](#), B. Cervato [ID142](#), A. Cervelli [ID23b](#), G. Cesarini [ID53](#), S.A. Cetin [ID82](#),
 D. Chakraborty [ID116](#), J. Chan [ID17a](#), W.Y. Chan [ID154](#), J.D. Chapman [ID32](#), E. Chapon [ID136](#),
 B. Chargeishvili [ID150b](#), D.G. Charlton [ID20](#), M. Chatterjee [ID19](#), C. Chauhan [ID134](#), Y. Che [ID14c](#),
 S. Chekanov [ID6](#), S.V. Chekulaev [ID157a](#), G.A. Chelkov [ID38,a](#), A. Chen [ID107](#), B. Chen [ID152](#), B. Chen [ID166](#),
 H. Chen [ID14c](#), H. Chen [ID29](#), J. Chen [ID62c](#), J. Chen [ID143](#), M. Chen [ID127](#), S. Chen [ID154](#), S.J. Chen [ID14c](#),
 X. Chen [ID62c,136](#), X. Chen [ID14b,ac](#), Y. Chen [ID62a](#), C.L. Cheng [ID171](#), H.C. Cheng [ID64a](#), S. Cheong [ID144](#),
 A. Cheplakov [ID38](#), E. Cheremushkina [ID48](#), E. Cherepanova [ID115](#), R. Cherkaoui El Moursli [ID35e](#),
 E. Cheu [ID7](#), K. Cheung [ID65](#), L. Chevalier [ID136](#), V. Chiarella [ID53](#), G. Chiarelli [ID74a](#), N. Chiedde [ID103](#),
 G. Chiodini [ID70a](#), A.S. Chisholm [ID20](#), A. Chitan [ID27b](#), M. Chitishvili [ID164](#), M.V. Chizhov [ID38](#),
 K. Choi [ID11](#), Y. Chou [ID139](#), E.Y.S. Chow [ID114](#), K.L. Chu [ID170](#), M.C. Chu [ID64a](#), X. Chu [ID14a,14e](#),

J. Chudoba ¹³², J.J. Chwastowski ⁸⁷, D. Cieri ¹¹¹, K.M. Ciesla ^{86a}, V. Cindro ⁹⁴, A. Ciocio ^{17a},
 F. Cirotto ^{72a,72b}, Z.H. Citron ¹⁷⁰, M. Citterio ^{71a}, D.A. Ciubotaru ^{27b}, A. Clark ⁵⁶, P.J. Clark ⁵²,
 N. Clarke Hall ⁹⁷, C. Clarry ¹⁵⁶, J.M. Clavijo Columbie ⁴⁸, S.E. Clawson ⁴⁸, C. Clement ^{47a,47b},
 J. Clercx ⁴⁸, Y. Coadou ¹⁰³, M. Cobal ^{69a,69c}, A. Coccaro ^{57b}, R.F. Coelho Barrue ^{131a},
 R. Coelho Lopes De Sa ¹⁰⁴, S. Coelli ^{71a}, B. Cole ⁴¹, J. Collot ⁶⁰, P. Conde Muiño ^{131a,131g},
 M.P. Connell ^{33c}, S.H. Connell ^{33c}, E.I. Conroy ¹²⁷, F. Conventi ^{72a,ae}, H.G. Cooke ²⁰,
 A.M. Cooper-Sarkar ¹²⁷, F.A. Corchia ^{23b,23a}, A. Cordeiro Oudot Choi ¹²⁸, L.D. Corpe ⁴⁰,
 M. Corradi ^{75a,75b}, F. Corriveau ^{105,v}, A. Cortes-Gonzalez ¹⁸, M.J. Costa ¹⁶⁴, F. Costanza ⁴,
 D. Costanzo ¹⁴⁰, B.M. Cote ¹²⁰, J. Couthures ⁴, G. Cowan ⁹⁶, K. Cranmer ¹⁷¹,
 D. Cremonini ^{23b,23a}, S. Crépe-Renaudin ⁶⁰, F. Crescioli ¹²⁸, M. Cristinziani ¹⁴²,
 M. Cristoforetti ^{78a,78b}, V. Croft ¹¹⁵, J.E. Crosby ¹²², G. Crosetti ^{43b,43a}, A. Cueto ¹⁰⁰, Z. Cui ⁷,
 W.R. Cunningham ⁵⁹, F. Curcio ¹⁶⁴, J.R. Curran ⁵², P. Czodrowski ³⁶, M.M. Czurylo ³⁶,
 M.J. Da Cunha Sargedas De Sousa ^{57b,57a}, J.V. Da Fonseca Pinto ^{83b}, C. Da Via ¹⁰²,
 W. Dabrowski ^{86a}, T. Dado ⁴⁹, S. Dahbi ¹⁴⁹, T. Dai ¹⁰⁷, D. Dal Santo ¹⁹, C. Dallapiccola ¹⁰⁴,
 M. Dam ⁴², G. D'amen ²⁹, V. D'Amico ¹¹⁰, J. Damp ¹⁰¹, J.R. Dandoy ³⁴, D. Dannheim ³⁶,
 M. Danninger ¹⁴³, V. Dao ¹⁴⁶, G. Darbo ^{57b}, S.J. Das ^{29,af}, F. Dattola ⁴⁸, S. D'Auria ^{71a,71b},
 A. D'avanzo ^{72a,72b}, C. David ^{33a}, T. Davidek ¹³⁴, I. Dawson ⁹⁵, H.A. Day-hall ¹³³, K. De ⁸,
 R. De Asmundis ^{72a}, N. De Biase ⁴⁸, S. De Castro ^{23b,23a}, N. De Groot ¹¹⁴, P. de Jong ¹¹⁵,
 H. De la Torre ¹¹⁶, A. De Maria ^{14c}, A. De Salvo ^{75a}, U. De Sanctis ^{76a,76b}, F. De Santis ^{70a,70b},
 A. De Santo ¹⁴⁷, J.B. De Vivie De Regie ⁶⁰, D.V. Dedovich ³⁸, J. Degens ⁹³, A.M. Deiana ⁴⁴,
 F. Del Corso ^{23b,23a}, J. Del Peso ¹⁰⁰, F. Del Rio ^{63a}, L. Delagrangé ¹²⁸, F. Deliot ¹³⁶,
 C.M. Delitzsch ⁴⁹, M. Della Pietra ^{72a,72b}, D. Della Volpe ⁵⁶, A. Dell'Acqua ³⁶,
 L. Dell'Asta ^{71a,71b}, M. Delmastro ⁴, P.A. Delsart ⁶⁰, S. Demers ¹⁷³, M. Demichev ³⁸,
 S.P. Denisov ³⁷, L. D'Eramo ⁴⁰, D. Derendarz ⁸⁷, F. Derue ¹²⁸, P. Dervan ⁹³, K. Desch ²⁴,
 C. Deutsch ²⁴, F.A. Di Bello ^{57b,57a}, A. Di Ciaccio ^{76a,76b}, L. Di Ciaccio ⁴,
 A. Di Domenico ^{75a,75b}, C. Di Donato ^{72a,72b}, A. Di Girolamo ³⁶, G. Di Gregorio ³⁶,
 A. Di Luca ^{78a,78b}, B. Di Micco ^{77a,77b}, R. Di Nardo ^{77a,77b}, K.F. Di Pettillo ³⁹,
 M. Diamantopoulou ³⁴, F.A. Dias ¹¹⁵, T. Dias Do Vale ¹⁴³, M.A. Diaz ^{138a,138b},
 F.G. Diaz Capriles ²⁴, M. Didenko ¹⁶⁴, E.B. Diehl ¹⁰⁷, S. Díez Cornell ⁴⁸, C. Diez Pardos ¹⁴²,
 C. Dimitriadi ^{162,24}, A. Dimitrievska ²⁰, J. Dingfelder ²⁴, I-M. Dinu ^{27b}, S.J. Dittmeier ^{63b},
 F. Dittus ³⁶, M. Divisek ¹³⁴, F. Djama ¹⁰³, T. Djobava ^{150b}, C. Doglioni ^{102,99},
 A. Dohnalova ^{28a}, J. Dolejsi ¹³⁴, Z. Dolezal ¹³⁴, K. Domijan ^{86a}, K.M. Dona ³⁹,
 M. Donadelli ^{83d}, B. Dong ¹⁰⁸, J. Donini ⁴⁰, A. D'Onofrio ^{72a,72b}, M. D'Onofrio ⁹³,
 J. Dopke ¹³⁵, A. Doria ^{72a}, N. Dos Santos Fernandes ^{131a}, P. Dougan ¹⁰², M.T. Dova ⁹¹,
 A.T. Doyle ⁵⁹, M.A. Dragnet ¹²⁷, E. Dreyer ¹⁷⁰, I. Drivas-koulouris ¹⁰, M. Drnevich ¹¹⁸,
 M. Drozdova ⁵⁶, D. Du ^{62a}, T.A. du Pree ¹¹⁵, F. Dubinin ³⁷, M. Dubovsky ^{28a}, E. Duchovni ¹⁷⁰,
 G. Duckeck ¹¹⁰, O.A. Ducu ^{27b}, D. Duda ⁵², A. Dudarev ³⁶, E.R. Duden ²⁶, M. D'uffizi ¹⁰²,
 L. Duflost ⁶⁶, M. Dührssen ³⁶, I. Duminica ^{27g}, A.E. Dumitriu ^{27b}, M. Dunford ^{63a}, S. Dungs ⁴⁹,
 K. Dunne ^{47a,47b}, A. Duperrin ¹⁰³, H. Duran Yildiz ^{3a}, M. Düren ⁵⁸, A. Durglishvili ^{150b},
 B.L. Dwyer ¹¹⁶, G.I. Dyckes ^{17a}, M. Dyndal ^{86a}, B.S. Dziedzic ³⁶, Z.O. Earnshaw ¹⁴⁷,
 G.H. Eberwein ¹²⁷, B. Eckerova ^{28a}, S. Eggebrecht ⁵⁵, E. Egidio Purcino De Souza ¹²⁸,
 L.F. Ehrke ⁵⁶, G. Eigen ¹⁶, K. Einsweiler ^{17a}, T. Ekelof ¹⁶², P.A. Ekman ⁹⁹, S. El Farkh ^{35b},
 Y. El Ghazali ^{35b}, H. El Jarrari ³⁶, A. El Moussaouy ^{35a}, V. Ellajosyula ¹⁶², M. Ellert ¹⁶²,
 F. Ellinghaus ¹⁷², N. Ellis ³⁶, J. Elmsheuser ²⁹, M. Elsayy ^{117a}, M. Elsing ³⁶,
 D. Emelianov ¹³⁵, Y. Enari ¹⁵⁴, I. Ene ^{17a}, S. Epari ¹³, P.A. Erland ⁸⁷,
 D. Ernani Martins Neto ⁸⁷, M. Errenst ¹⁷², M. Escalier ⁶⁶, C. Escobar ¹⁶⁴, E. Etzion ¹⁵²,
 G. Evans ^{131a}, H. Evans ⁶⁸, L.S. Evans ⁹⁶, A. Ezhilov ³⁷, S. Ezzarqtouni ^{35a}, F. Fabbri ^{23b,23a},

L. Fabbri [ID23b,23a](#), G. Facini [ID97](#), V. Fadeyev [ID137](#), R.M. Fakhruddinov [ID37](#), D. Fakoudis [ID101](#),
 S. Falciano [ID75a](#), L.F. Falda Ulhoa Coelho [ID36](#), F. Fallavollita [ID111](#), G. Falsetti [ID43b,43a](#), J. Faltova [ID134](#),
 C. Fan [ID163](#), Y. Fan [ID14a](#), Y. Fang [ID14a,14e](#), M. Fanti [ID71a,71b](#), M. Faraj [ID69a,69b](#), Z. Farazpay [ID98](#),
 A. Farbin [ID8](#), A. Farilla [ID77a](#), T. Farooque [ID108](#), S.M. Farrington [ID52](#), F. Fassi [ID35e](#), D. Fassouliotis [ID9](#),
 M. Faucci Giannelli [ID76a,76b](#), W.J. Fawcett [ID32](#), L. Fayard [ID66](#), P. Federic [ID134](#), P. Federicova [ID132](#),
 O.L. Fedin [ID37,a](#), M. Feickert [ID171](#), L. Feligioni [ID103](#), D.E. Fellers [ID124](#), C. Feng [ID62b](#), M. Feng [ID14b](#),
 Z. Feng [ID115](#), M.J. Fenton [ID160](#), L. Ferencz [ID48](#), R.A.M. Ferguson [ID92](#), S.I. Fernandez Luengo [ID138f](#),
 P. Fernandez Martinez [ID13](#), M.J.V. Fernoux [ID103](#), J. Ferrando [ID92](#), A. Ferrari [ID162](#), P. Ferrari [ID115,114](#),
 R. Ferrari [ID73a](#), D. Ferrere [ID56](#), C. Ferretti [ID107](#), D. Fiacco [ID75a,75b](#), F. Fiedler [ID101](#), P. Fiedler [ID133](#),
 A. Filipčič [ID94](#), E.K. Filmer [ID1](#), F. Filthaut [ID114](#), M.C.N. Fiolhais [ID131a,131c,c](#), L. Fiorini [ID164](#),
 W.C. Fisher [ID108](#), T. Fitschen [ID102](#), P.M. Fitzhugh [ID136](#), I. Fleck [ID142](#), P. Fleischmann [ID107](#), T. Flick [ID172](#),
 M. Flores [ID33d,aa](#), L.R. Flores Castillo [ID64a](#), L. Flores Sanz De Acedo [ID36](#), F.M. Follega [ID78a,78b](#),
 N. Fomin [ID16](#), J.H. Foo [ID156](#), A. Formica [ID136](#), A.C. Forti [ID102](#), E. Fortin [ID36](#), A.W. Fortman [ID17a](#),
 M.G. Foti [ID17a](#), L. Fountas [ID9,i](#), D. Fournier [ID66](#), H. Fox [ID92](#), P. Francavilla [ID74a,74b](#), S. Francescato [ID61](#),
 S. Franchellucci [ID56](#), M. Franchini [ID23b,23a](#), S. Franchino [ID63a](#), D. Francis [ID36](#), L. Franco [ID114](#),
 V. Franco Lima [ID36](#), L. Franconi [ID48](#), M. Franklin [ID61](#), G. Frattari [ID26](#), Y.Y. Frid [ID152](#), J. Friend [ID59](#),
 N. Fritzsche [ID50](#), A. Froch [ID54](#), D. Froidevaux [ID36](#), J.A. Frost [ID127](#), Y. Fu [ID62a](#),
 S. Fuenzalida Garrido [ID138f](#), M. Fujimoto [ID103](#), K.Y. Fung [ID64a](#), E. Furtado De Simas Filho [ID83e](#),
 M. Furukawa [ID154](#), J. Fuster [ID164](#), A. Gaa [ID55](#), A. Gabrielli [ID23b,23a](#), A. Gabrielli [ID156](#), P. Gadow [ID36](#),
 G. Gagliardi [ID57b,57a](#), L.G. Gagnon [ID17a](#), S. Gaid [ID161](#), S. Galantzan [ID152](#), E.J. Gallas [ID127](#),
 B.J. Gallop [ID135](#), K.K. Gan [ID120](#), S. Ganguly [ID154](#), Y. Gao [ID52](#), F.M. Garay Walls [ID138a,138b](#), B. Garcia [ID29](#),
 C. García [ID164](#), A. Garcia Alonso [ID115](#), A.G. Garcia Caffaro [ID173](#), J.E. García Navarro [ID164](#),
 M. Garcia-Sciveres [ID17a](#), G.L. Gardner [ID129](#), R.W. Gardner [ID39](#), N. Garelli [ID159](#), D. Garg [ID80](#),
 R.B. Garg [ID144](#), J.M. Gargan [ID52](#), C.A. Garner [ID156](#), C.M. Garvey [ID33a](#), V.K. Gassmann [ID159](#), G. Gaudio [ID73a](#),
 V. Gautam [ID13](#), P. Gauzzi [ID75a,75b](#), I.L. Gavrilenko [ID37](#), A. Gavrilyuk [ID37](#), C. Gay [ID165](#), G. Gaycken [ID48](#),
 E.N. Gazis [ID10](#), A.A. Geanta [ID27b](#), C.M. Gee [ID137](#), A. Gekow [ID120](#), C. Gemme [ID57b](#), M.H. Genest [ID60](#),
 A.D. Gentry [ID113](#), S. George [ID96](#), W.F. George [ID20](#), T. Geralis [ID46](#), P. Gessinger-Befurt [ID36](#),
 M.E. Geyik [ID172](#), M. Ghani [ID168](#), K. Ghorbanian [ID95](#), A. Ghosal [ID142](#), A. Ghosh [ID160](#), A. Ghosh [ID7](#),
 B. Giacobbe [ID23b](#), S. Giagu [ID75a,75b](#), T. Giani [ID115](#), P. Giannetti [ID74a](#), A. Giannini [ID62a](#), S.M. Gibson [ID96](#),
 M. Gignac [ID137](#), D.T. Gil [ID86b](#), A.K. Gilbert [ID86a](#), B.J. Gilbert [ID41](#), D. Gillberg [ID34](#), G. Gilles [ID115](#),
 L. Ginabat [ID128](#), D.M. Gingrich [ID2,ad](#), M.P. Giordani [ID69a,69c](#), P.F. Giraud [ID136](#), G. Giugliarelli [ID69a,69c](#),
 D. Giugni [ID71a](#), F. Giuli [ID36](#), I. Gkialas [ID9,i](#), L.K. Gladilin [ID37](#), C. Glasman [ID100](#), G.R. Gledhill [ID124](#),
 G. Glemža [ID48](#), M. Glisic [ID124](#), I. Gnesi [ID43b,e](#), Y. Go [ID29](#), M. Goblirsch-Kolb [ID36](#), B. Gocke [ID49](#),
 D. Godin [ID109](#), B. Gokturk [ID21a](#), S. Goldfarb [ID106](#), T. Golling [ID56](#), M.G.D. Gololo [ID33g](#), D. Golubkov [ID37](#),
 J.P. Gombas [ID108](#), A. Gomes [ID131a,131b](#), G. Gomes Da Silva [ID142](#), A.J. Gomez Delegido [ID164](#),
 R. Gonçalves [ID131a](#), L. Gonella [ID20](#), A. Gongadze [ID150c](#), F. Gonnella [ID20](#), J.L. Gonski [ID144](#),
 R.Y. González Andana [ID52](#), S. González de la Hoz [ID164](#), R. Gonzalez Lopez [ID93](#),
 C. Gonzalez Renteria [ID17a](#), M.V. Gonzalez Rodrigues [ID48](#), R. Gonzalez Suarez [ID162](#),
 S. Gonzalez-Sevilla [ID56](#), L. Goossens [ID36](#), B. Gorini [ID36](#), E. Gorini [ID70a,70b](#), A. Gorišek [ID94](#),
 T.C. Gosart [ID129](#), A.T. Goshaw [ID51](#), M.I. Gostkin [ID38](#), S. Goswami [ID122](#), C.A. Gottardo [ID36](#),
 S.A. Gotz [ID110](#), M. Gouighri [ID35b](#), V. Goumarre [ID48](#), A.G. Goussiou [ID139](#), N. Govender [ID33c](#),
 I. Grabowska-Bold [ID86a](#), K. Graham [ID34](#), E. Gramstad [ID126](#), S. Grancagnolo [ID70a,70b](#), C.M. Grant [ID1,136](#),
 P.M. Gravila [ID27f](#), F.G. Gravili [ID70a,70b](#), H.M. Gray [ID17a](#), M. Greco [ID70a,70b](#), C. Grefe [ID24](#),
 A.S. Grefsrud [ID16](#), I.M. Gregor [ID48](#), K.T. Greif [ID160](#), P. Grenier [ID144](#), S.G. Grewe [ID111](#), A.A. Grillo [ID137](#),
 K. Grimm [ID31](#), S. Grinstein [ID13,r](#), J.-F. Grivaz [ID66](#), E. Gross [ID170](#), J. Grosse-Knetter [ID55](#),
 J.C. Grundy [ID127](#), L. Guan [ID107](#), J.G.R. Guerrero Rojas [ID164](#), G. Guerrieri [ID69a,69c](#), R. Gugel [ID101](#),
 J.A.M. Guhit [ID107](#), A. Guida [ID18](#), E. Guilloton [ID168](#), S. Guindon [ID36](#), F. Guo [ID14a,14e](#), J. Guo [ID62c](#),

L. Guo ⁴⁸, Y. Guo ¹⁰⁷, R. Gupta ¹³⁰, S. Gurbuz ²⁴, S.S. Gurdasani ⁵⁴, G. Gustavino ^{75a,75b},
 M. Guth ⁵⁶, P. Gutierrez ¹²¹, L.F. Gutierrez Zagazeta ¹²⁹, M. Gutsche ⁵⁰, C. Gutschow ⁹⁷,
 C. Gwenlan ¹²⁷, C.B. Gwilliam ⁹³, E.S. Haaland ¹²⁶, A. Haas ¹¹⁸, M. Habedank ⁴⁸,
 C. Haber ^{17a}, H.K. Hadavand ⁸, A. Hadeef ⁵⁰, S. Hadzic ¹¹¹, A.I. Hagan ⁹², J.J. Hahn ¹⁴²,
 E.H. Haines ⁹⁷, M. Haleem ¹⁶⁷, J. Haley ¹²², J.J. Hall ¹⁴⁰, G.D. Hallewell ¹⁰³, L. Halser ¹⁹,
 K. Hamano ¹⁶⁶, M. Hamer ²⁴, G.N. Hamity ⁵², E.J. Hampshire ⁹⁶, J. Han ^{62b}, K. Han ^{62a},
 L. Han ^{14c}, L. Han ^{62a}, S. Han ^{17a}, Y.F. Han ¹⁵⁶, K. Hanagaki ⁸⁴, M. Hance ¹³⁷,
 D.A. Hangal ⁴¹, H. Hanif ¹⁴³, M.D. Hank ¹²⁹, J.B. Hansen ⁴², P.H. Hansen ⁴², K. Hara ¹⁵⁸,
 D. Harada ⁵⁶, T. Harenberg ¹⁷², S. Harkusha ³⁷, M.L. Harris ¹⁰⁴, Y.T. Harris ¹²⁷, J. Harrison ¹³,
 N.M. Harrison ¹²⁰, P.F. Harrison ¹⁶⁸, N.M. Hartman ¹¹¹, N.M. Hartmann ¹¹⁰, R.Z. Hasan ^{96,135},
 Y. Hasegawa ¹⁴¹, S. Hassan ¹⁶, R. Hauser ¹⁰⁸, C.M. Hawkes ²⁰, R.J. Hawkings ³⁶,
 Y. Hayashi ¹⁵⁴, S. Hayashida ¹¹², D. Hayden ¹⁰⁸, C. Hayes ¹⁰⁷, R.L. Hayes ¹¹⁵, C.P. Hays ¹²⁷,
 J.M. Hays ⁹⁵, H.S. Hayward ⁹³, F. He ^{62a}, M. He ^{14a,14e}, Y. He ¹⁵⁵, Y. He ⁴⁸, Y. He ⁹⁷,
 N.B. Heatley ⁹⁵, V. Hedberg ⁹⁹, A.L. Heggelund ¹²⁶, N.D. Hehir ^{95,*}, C. Heidegger ⁵⁴,
 K.K. Heidegger ⁵⁴, J. Heilman ³⁴, S. Heim ⁴⁸, T. Heim ^{17a}, J.G. Heinlein ¹²⁹, J.J. Heinrich ¹²⁴,
 L. Heinrich ^{111,ab}, J. Hejbal ¹³², A. Held ¹⁷¹, S. Hellesund ¹⁶, C.M. Helling ¹⁶⁵,
 S. Hellman ^{47a,47b}, R.C.W. Henderson ⁹², L. Henkelmann ³², A.M. Henriques Correia ³⁶, H. Herde ⁹⁹,
 Y. Hernández Jiménez ¹⁴⁶, L.M. Herrmann ²⁴, T. Herrmann ⁵⁰, G. Herten ⁵⁴, R. Hertenberger ¹¹⁰,
 L. Hervas ³⁶, M.E. Hesping ¹⁰¹, N.P. Hessey ^{157a}, M. Hidaoui ^{35b}, N. Hidic ¹³⁴, E. Hill ¹⁵⁶,
 S.J. Hillier ²⁰, J.R. Hinds ¹⁰⁸, F. Hinterkeuser ²⁴, M. Hirose ¹²⁵, S. Hirose ¹⁵⁸,
 D. Hirschbuehl ¹⁷², T.G. Hitchings ¹⁰², B. Hiti ⁹⁴, J. Hobbs ¹⁴⁶, R. Hobincu ^{27e}, N. Hod ¹⁷⁰,
 M.C. Hodgkinson ¹⁴⁰, B.H. Hodgkinson ¹²⁷, A. Hoecker ³⁶, D.D. Hofer ¹⁰⁷, J. Hofer ⁴⁸,
 T. Holm ²⁴, M. Holzbock ¹¹¹, L.B.A.H. Hommels ³², B.P. Honan ¹⁰², J.J. Hong ⁶⁸, J. Hong ^{62c},
 T.M. Hong ¹³⁰, B.H. Hooberman ¹⁶³, W.H. Hopkins ⁶, M.C. Hoppesch ¹⁶³, Y. Horii ¹¹²,
 S. Hou ¹⁴⁹, A.S. Howard ⁹⁴, J. Howarth ⁵⁹, J. Hoya ⁶, M. Hrabovsky ¹²³, A. Hrynevich ⁴⁸,
 T. Hryn'ova ⁴, P.J. Hsu ⁶⁵, S.-C. Hsu ¹³⁹, T. Hsu ⁶⁶, M. Hu ^{17a}, Q. Hu ^{62a}, S. Huang ^{64b},
 X. Huang ^{14a,14e}, Y. Huang ¹⁴⁰, Y. Huang ¹⁰¹, Y. Huang ^{14a}, Z. Huang ¹⁰², Z. Hubacek ¹³³,
 M. Huebner ²⁴, F. Huegging ²⁴, T.B. Huffman ¹²⁷, C.A. Hugli ⁴⁸, M. Huhtinen ³⁶,
 S.K. Huiberts ¹⁶, R. Hulsken ¹⁰⁵, N. Huseynov ¹², J. Huston ¹⁰⁸, J. Huth ⁶¹, R. Hyneman ¹⁴⁴,
 G. Iacobucci ⁵⁶, G. Iakovidis ²⁹, L. Iconomidou-Fayard ⁶⁶, J.P. Iddon ³⁶, P. Iengo ^{72a,72b},
 R. Iguchi ¹⁵⁴, Y. Iiyama ¹⁵⁴, T. Iizawa ¹²⁷, Y. Ikegami ⁸⁴, N. Ilic ¹⁵⁶, H. Imam ^{35a},
 M. Ince Lezki ⁵⁶, T. Ingebretsen Carlson ^{47a,47b}, G. Introzzi ^{73a,73b}, M. Iodice ^{77a},
 V. Ippolito ^{75a,75b}, R.K. Irwin ⁹³, M. Ishino ¹⁵⁴, W. Islam ¹⁷¹, C. Issever ^{18,48}, S. Istin ^{21a,ah},
 H. Ito ¹⁶⁹, R. Iuppa ^{78a,78b}, A. Ivina ¹⁷⁰, J.M. Izen ⁴⁵, V. Izzo ^{72a}, P. Jacka ¹³², P. Jackson ¹,
 C.S. Jagfeld ¹¹⁰, G. Jain ^{157a}, P. Jain ⁴⁸, K. Jakobs ⁵⁴, T. Jakoubek ¹⁷⁰, J. Jamieson ⁵⁹,
 M. Javurkova ¹⁰⁴, L. Jeanty ¹²⁴, J. Jejelava ^{150a,y}, P. Jenni ^{54,f}, C.E. Jessiman ³⁴, C. Jia ^{62b},
 J. Jia ¹⁴⁶, X. Jia ⁶¹, X. Jia ^{14a,14e}, Z. Jia ^{14c}, C. Jiang ⁵², S. Jiggins ⁴⁸, J. Jimenez Pena ¹³,
 S. Jin ^{14c}, A. Jinaru ^{27b}, O. Jinnouchi ¹⁵⁵, P. Johansson ¹⁴⁰, K.A. Johns ⁷, J.W. Johnson ¹³⁷,
 D.M. Jones ¹⁴⁷, E. Jones ⁴⁸, P. Jones ³², R.W.L. Jones ⁹², T.J. Jones ⁹³, H.L. Joos ^{55,36},
 R. Joshi ¹²⁰, J. Jovicevic ¹⁵, X. Ju ^{17a}, J.J. Junggeburth ¹⁰⁴, T. Junkermann ^{63a},
 A. Juste Rozas ^{13,r}, M.K. Juzek ⁸⁷, S. Kabana ^{138e}, A. Kaczmarek ⁸⁷, M. Kado ¹¹¹,
 H. Kagan ¹²⁰, M. Kagan ¹⁴⁴, A. Kahn ¹²⁹, C. Kahra ¹⁰¹, T. Kaji ¹⁵⁴, E. Kajomovitz ¹⁵¹,
 N. Kakati ¹⁷⁰, I. Kalaitzidou ⁵⁴, C.W. Kalderon ²⁹, N.J. Kang ¹³⁷, D. Kar ^{33g}, K. Karava ¹²⁷,
 M.J. Kareem ^{157b}, E. Karentzos ⁵⁴, O. Karkout ¹¹⁵, S.N. Karpov ³⁸, Z.M. Karpova ³⁸,
 V. Kartvelishvili ⁹², A.N. Karyukhin ³⁷, E. Kasimi ¹⁵³, J. Katzy ⁴⁸, S. Kaur ³⁴, K. Kawade ¹⁴¹,
 M.P. Kawale ¹²¹, C. Kawamoto ⁸⁸, T. Kawamoto ^{62a}, E.F. Kay ³⁶, F.I. Kaya ¹⁵⁹, S. Kazakos ¹⁰⁸,
 V.F. Kazanin ³⁷, Y. Ke ¹⁴⁶, J.M. Keaveney ^{33a}, R. Keeler ¹⁶⁶, G.V. Kehris ⁶¹, J.S. Keller ³⁴,

A.S. Kelly⁹⁷, J.J. Kempster ¹⁴⁷, P.D. Kennedy ¹⁰¹, O. Kepka ¹³², B.P. Kerridge ¹³⁵, S. Kersten ¹⁷²,
 B.P. Kerševan ⁹⁴, L. Keszeghova ^{28a}, S. Ketabchi Haghighat ¹⁵⁶, R.A. Khan ¹³⁰, A. Khanov ¹²²,
 A.G. Kharlamov ³⁷, T. Kharlamova ³⁷, E.E. Khoda ¹³⁹, M. Kholodenko ³⁷, T.J. Khoo ¹⁸,
 G. Khoriauli ¹⁶⁷, J. Khubua ^{150b,*}, Y.A.R. Khwaira ¹²⁸, B. Kibirige^{33g}, D.W. Kim ^{47a,47b},
 Y.K. Kim ³⁹, N. Kimura ⁹⁷, M.K. Kingston ⁵⁵, A. Kirchhoff ⁵⁵, C. Kirfel ²⁴, F. Kirfel ²⁴,
 J. Kirk ¹³⁵, A.E. Kiryunin ¹¹¹, C. Kitsaki ¹⁰, O. Kivernyk ²⁴, M. Klassen ¹⁵⁹, C. Klein ³⁴,
 L. Klein ¹⁶⁷, M.H. Klein ⁴⁴, S.B. Klein ⁵⁶, U. Klein ⁹³, P. Klimek ³⁶, A. Klimentov ²⁹,
 T. Klioutchnikova ³⁶, P. Kluit ¹¹⁵, S. Kluth ¹¹¹, E. Kneringer ⁷⁹, T.M. Knight ¹⁵⁶, A. Knue ⁴⁹,
 R. Kobayashi ⁸⁸, D. Kobylanskii ¹⁷⁰, S.F. Koch ¹²⁷, M. Kocian ¹⁴⁴, P. Kodyš ¹³⁴,
 D.M. Koeck ¹²⁴, P.T. Koenig ²⁴, T. Koffas ³⁴, O. Kolay ⁵⁰, I. Koletsou ⁴, T. Komarek ¹²³,
 K. Köneke ⁵⁴, A.X.Y. Kong ¹, T. Kono ¹¹⁹, N. Konstantinidis ⁹⁷, P. Kontaxakis ⁵⁶, B. Konya ⁹⁹,
 R. Kopeliansky ⁴¹, S. Koperny ^{86a}, K. Korcyl ⁸⁷, K. Kordas ^{153,d}, A. Korn ⁹⁷, S. Korn ⁵⁵,
 I. Korolkov ¹³, N. Korotkova ³⁷, B. Kortman ¹¹⁵, O. Kortner ¹¹¹, S. Kortner ¹¹¹,
 W.H. Kostecka ¹¹⁶, V.V. Kostyukhin ¹⁴², A. Kotsokechagia ¹³⁶, A. Kotwal ⁵¹, A. Koulouris ³⁶,
 A. Kourkoumeli-Charalampidi ^{73a,73b}, C. Kourkoumelis ⁹, E. Kourlitis ^{111,ab}, O. Kovanda ¹²⁴,
 R. Kowalewski ¹⁶⁶, W. Kozanecki ¹³⁶, A.S. Kozhin ³⁷, V.A. Kramarenko ³⁷, G. Kramberger ⁹⁴,
 P. Kramer ¹⁰¹, M.W. Krasny ¹²⁸, A. Krasznahorkay ³⁶, A.C. Kraus ¹¹⁶, J.W. Kraus ¹⁷²,
 J.A. Kremer ⁴⁸, T. Kresse ⁵⁰, J. Kretschmar ⁹³, K. Kreul ¹⁸, P. Krieger ¹⁵⁶,
 S. Krishnamurthy ¹⁰⁴, M. Krivos ¹³⁴, K. Krizka ²⁰, K. Kroeninger ⁴⁹, H. Kroha ¹¹¹, J. Kroll ¹³²,
 J. Kroll ¹²⁹, K.S. Krowpman ¹⁰⁸, U. Kruchonak ³⁸, H. Krüger ²⁴, N. Krumnack⁸¹, M.C. Kruse ⁵¹,
 O. Kuchinskaia ³⁷, S. Kудay ^{3a}, S. Kuehn ³⁶, R. Kuesters ⁵⁴, T. Kuhl ⁴⁸, V. Kukhtin ³⁸,
 Y. Kulchitsky ^{37,a}, S. Kuleshov ^{138d,138b}, M. Kumar ^{33g}, N. Kumari ⁴⁸, P. Kumari ^{157b},
 A. Kupco ¹³², T. Kupfer⁴⁹, A. Kupich ³⁷, O. Kuprash ⁵⁴, H. Kurashige ⁸⁵, L.L. Kurchaninov ^{157a},
 O. Kurdysh ⁶⁶, Y.A. Kurochkin ³⁷, A. Kurova ³⁷, M. Kuze ¹⁵⁵, A.K. Kvam ¹⁰⁴, J. Kvita ¹²³,
 T. Kwan ¹⁰⁵, N.G. Kyriacou ¹⁰⁷, L.A.O. Laatu ¹⁰³, C. Lacasta ¹⁶⁴, F. Lacava ^{75a,75b},
 H. Lacker ¹⁸, D. Lacour ¹²⁸, N.N. Lad ⁹⁷, E. Ladygin ³⁸, A. Lafarge ⁴⁰, B. Laforge ¹²⁸,
 T. Lagouri ¹⁷³, F.Z. Lahbabi ^{35a}, S. Lai ⁵⁵, J.E. Lambert ¹⁶⁶, S. Lammers ⁶⁸, W. Lampl ⁷,
 C. Lampoudis ^{153,d}, G. Lamprinoudis¹⁰¹, A.N. Lancaster ¹¹⁶, E. Lançon ²⁹, U. Landgraf ⁵⁴,
 M.P.J. Landon ⁹⁵, V.S. Lang ⁵⁴, O.K.B. Langrekken ¹²⁶, A.J. Lankford ¹⁶⁰, F. Lanni ³⁶,
 K. Lantzsck ²⁴, A. Lanza ^{73a}, J.F. Laporte ¹³⁶, T. Lari ^{71a}, F. Lasagni Manghi ^{23b},
 M. Lassnig ³⁶, V. Latonova ¹³², A. Laudrain ¹⁰¹, A. Laurier ¹⁵¹, S.D. Lawlor ¹⁴⁰,
 Z. Lawrence ¹⁰², R. Lazaridou¹⁶⁸, M. Lazzaroni ^{71a,71b}, B. Le¹⁰², E.M. Le Boulicaut ⁵¹,
 L.T. Le Pottier ^{17a}, B. Leban ^{23b,23a}, A. Lebedev ⁸¹, M. LeBlanc ¹⁰², F. Ledroit-Guillon ⁶⁰,
 S.C. Lee ¹⁴⁹, S. Lee ^{47a,47b}, T.F. Lee ⁹³, L.L. Leeuw ^{33c}, H.P. Lefebvre ⁹⁶, M. Lefebvre ¹⁶⁶,
 C. Leggett ^{17a}, G. Lehmann Miotto ³⁶, M. Leigh ⁵⁶, W.A. Leight ¹⁰⁴, W. Leinonen ¹¹⁴,
 A. Leisos ^{153,q}, M.A.L. Leite ^{83c}, C.E. Leitgeb ¹⁸, R. Leitner ¹³⁴, K.J.C. Leney ⁴⁴, T. Lenz ²⁴,
 S. Leone ^{74a}, C. Leonidopoulos ⁵², A. Leopold ¹⁴⁵, C. Leroy ¹⁰⁹, R. Les ¹⁰⁸, C.G. Lester ³²,
 M. Levchenko ³⁷, J. Levêque ⁴, L.J. Levinson ¹⁷⁰, G. Levrini ^{23b,23a}, M.P. Lewicki ⁸⁷,
 C. Lewis ¹³⁹, D.J. Lewis ⁴, A. Li ⁵, B. Li ^{62b}, C. Li ^{62a}, C-Q. Li ¹¹¹, H. Li ^{62a}, H. Li ^{62b},
 H. Li ^{14c}, H. Li ^{14b}, H. Li ^{62b}, J. Li ^{62c}, K. Li ¹³⁹, L. Li ^{62c}, M. Li ^{14a,14e}, S. Li ^{14a,14e},
 S. Li ^{62d,62c}, T. Li ⁵, X. Li ¹⁰⁵, Z. Li ¹²⁷, Z. Li ¹⁵⁴, Z. Li ^{14a,14e}, S. Liang ^{14a,14e},
 Z. Liang ^{14a}, M. Liberatore ¹³⁶, B. Liberti ^{76a}, K. Lie ^{64c}, J. Lieber Marin ^{83e}, H. Lien ⁶⁸,
 H. Lin ¹⁰⁷, K. Lin ¹⁰⁸, R.E. Lindley ⁷, J.H. Lindon ², E. Lipeles ¹²⁹, A. Lipniacka ¹⁶,
 A. Lister ¹⁶⁵, J.D. Little ⁶⁸, B. Liu ^{14a}, B.X. Liu ^{14d}, D. Liu ^{62d,62c}, E.H.L. Liu ²⁰, J.B. Liu ^{62a},
 J.K.K. Liu ³², K. Liu ^{62d}, K. Liu ^{62d,62c}, M. Liu ^{62a}, M.Y. Liu ^{62a}, P. Liu ^{14a}, Q. Liu ^{62d,139,62c},
 X. Liu ^{62a}, X. Liu ^{62b}, Y. Liu ^{14d,14e}, Y.L. Liu ^{62b}, Y.W. Liu ^{62a}, J. Llorente Merino ¹⁴³,
 S.L. Lloyd ⁹⁵, E.M. Lobodzinska ⁴⁸, P. Loch ⁷, T. Lohse ¹⁸, K. Lohwasser ¹⁴⁰, E. Loiacono ⁴⁸,

M. Lokajicek ^{132,*}, J.D. Lomas ²⁰, J.D. Long ¹⁶³, I. Longarini ¹⁶⁰, R. Longo ¹⁶³,
I. Lopez Paz ⁶⁷, A. Lopez Solis ⁴⁸, N. Lorenzo Martinez ⁴, A.M. Lory ¹¹⁰, M. Losada ^{117a},
G. Löschcke Centeno ¹⁴⁷, O. Loseva ³⁷, X. Lou ^{47a,47b}, X. Lou ^{14a,14e}, A. Lounis ⁶⁶,
P.A. Love ⁹², G. Lu ^{14a,14e}, M. Lu ⁶⁶, S. Lu ¹²⁹, Y.J. Lu ⁶⁵, H.J. Lubatti ¹³⁹, C. Luci ^{75a,75b},
F.L. Lucio Alves ^{14c}, F. Luehring ⁶⁸, I. Luise ¹⁴⁶, O. Lukianchuk ⁶⁶, O. Lundberg ¹⁴⁵,
B. Lund-Jensen ^{145,*}, N.A. Luongo ⁶, M.S. Lutz ³⁶, A.B. Lux ²⁵, D. Lynn ²⁹, R. Lysak ¹³²,
E. Lytken ⁹⁹, V. Lyubushkin ³⁸, T. Lyubushkina ³⁸, M.M. Lyukova ¹⁴⁶, M.Firdaus M. Soberi ⁵²,
H. Ma ²⁹, K. Ma ^{62a}, L.L. Ma ^{62b}, W. Ma ^{62a}, Y. Ma ¹²², J.C. MacDonald ¹⁰¹,
P.C. Machado De Abreu Farias ^{83e}, R. Madar ⁴⁰, T. Madula ⁹⁷, J. Maeda ⁸⁵, T. Maeno ²⁹,
H. Maguire ¹⁴⁰, V. Maiboroda ¹³⁶, A. Maio ^{131a,131b,131d}, K. Maj ^{86a}, O. Majersky ⁴⁸,
S. Majewski ¹²⁴, N. Makovec ⁶⁶, V. Maksimovic ¹⁵, B. Malaescu ¹²⁸, Pa. Malecki ⁸⁷,
V.P. Maleev ³⁷, F. Malek ^{60,m}, M. Mali ⁹⁴, D. Malito ⁹⁶, U. Mallik ⁸⁰, S. Maltezos ¹⁰,
S. Malyukov ³⁸, J. Mamuzic ¹³, G. Mancini ⁵³, M.N. Mancini ²⁶, G. Manco ^{73a,73b},
J.P. Mandalia ⁹⁵, I. Mandić ⁹⁴, L. Manhaes de Andrade Filho ^{83a}, I.M. Maniatis ¹⁷⁰,
J. Manjarres Ramos ⁹⁰, D.C. Mankad ¹⁷⁰, A. Mann ¹¹⁰, S. Manzoni ³⁶, L. Mao ^{62c},
X. Mapekula ^{33c}, A. Marantis ^{153,q}, G. Marchiori ⁵, M. Marcisovsky ¹³², C. Marcon ^{71a},
M. Marinescu ²⁰, S. Marium ⁴⁸, M. Marjanovic ¹²¹, A. Markhoos ⁵⁴, M. Markovitch ⁶⁶,
E.J. Marshall ⁹², Z. Marshall ^{17a}, S. Marti-Garcia ¹⁶⁴, J. Martin ⁹⁷, T.A. Martin ¹³⁵,
V.J. Martin ⁵², B. Martin dit Latour ¹⁶, L. Martinelli ^{75a,75b}, M. Martinez ^{13,r},
P. Martinez Agullo ¹⁶⁴, V.I. Martinez Outschoorn ¹⁰⁴, P. Martinez Suarez ¹³, S. Martin-Haugh ¹³⁵,
G. Martinovicova ¹³⁴, V.S. Martoiu ^{27b}, A.C. Martyniuk ⁹⁷, A. Marzin ³⁶, D. Mascione ^{78a,78b},
L. Masetti ¹⁰¹, T. Mashimo ¹⁵⁴, J. Masik ¹⁰², A.L. Maslennikov ³⁷, P. Massarotti ^{72a,72b},
P. Mastrandrea ^{74a,74b}, A. Mastroberardino ^{43b,43a}, T. Masubuchi ¹⁵⁴, T. Mathisen ¹⁶²,
J. Matousek ¹³⁴, N. Matsuzawa ¹⁵⁴, J. Maurer ^{27b}, A.J. Maury ⁶⁶, B. Maček ⁹⁴, D.A. Maximov ³⁷,
A.E. May ¹⁰², R. Mazini ¹⁴⁹, I. Maznas ¹¹⁶, M. Mazza ¹⁰⁸, S.M. Mazza ¹³⁷, E. Mazzeo ^{71a,71b},
C. Mc Ginn ²⁹, J.P. Mc Gowan ¹⁶⁶, S.P. Mc Kee ¹⁰⁷, C.C. McCracken ¹⁶⁵, E.F. McDonald ¹⁰⁶,
A.E. McDougall ¹¹⁵, J.A. Mcfayden ¹⁴⁷, R.P. McGovern ¹²⁹, R.P. Mckenzie ^{33g},
T.C. McLachlan ⁴⁸, D.J. McLaughlin ⁹⁷, S.J. McMahan ¹³⁵, C.M. Mcpartland ⁹³,
R.A. McPherson ^{166,v}, S. Mehlhase ¹¹⁰, A. Mehta ⁹³, D. Melini ¹⁶⁴, B.R. Mellado Garcia ^{33g},
A.H. Melo ⁵⁵, F. Meloni ⁴⁸, A.M. Mendes Jacques Da Costa ¹⁰², H.Y. Meng ¹⁵⁶, L. Meng ⁹²,
S. Menke ¹¹¹, M. Mentink ³⁶, E. Meoni ^{43b,43a}, G. Mercado ¹¹⁶, S. Merianos ¹⁵³,
C. Merlassino ^{69a,69c}, L. Merola ^{72a,72b}, C. Meroni ^{71a,71b}, J. Metcalfe ⁶, A.S. Mete ⁶,
E. Meuser ¹⁰¹, C. Meyer ⁶⁸, J-P. Meyer ¹³⁶, R.P. Middleton ¹³⁵, L. Mijović ⁵²,
G. Mikenberg ¹⁷⁰, M. Mikestikova ¹³², M. Mikuž ⁹⁴, H. Mildner ¹⁰¹, A. Milic ³⁶,
D.W. Miller ³⁹, E.H. Miller ¹⁴⁴, L.S. Miller ³⁴, A. Milov ¹⁷⁰, D.A. Milstead ^{47a,47b}, T. Min ^{14c},
A.A. Minaenko ³⁷, I.A. Minashvili ^{150b}, L. Mince ⁵⁹, A.I. Mincer ¹¹⁸, B. Mindur ^{86a},
M. Mineev ³⁸, Y. Mino ⁸⁸, L.M. Mir ¹³, M. Miralles Lopez ⁵⁹, M. Mironova ^{17a}, A. Mishima ¹⁵⁴,
M.C. Missio ¹¹⁴, A. Mitra ¹⁶⁸, V.A. Mitsou ¹⁶⁴, Y. Mitsumori ¹¹², O. Miu ¹⁵⁶,
P.S. Miyagawa ⁹⁵, T. Mkrtychyan ^{63a}, M. Mlinarevic ⁹⁷, T. Mlinarevic ⁹⁷, M. Mlynarikova ³⁶,
S. Mobius ¹⁹, P. Mogg ¹¹⁰, M.H. Mohamed Farook ¹¹³, A.F. Mohammed ^{14a,14e}, S. Mohapatra ⁴¹,
G. Mokgatitswane ^{33g}, L. Moleri ¹⁷⁰, B. Mondal ¹⁴², S. Mondal ¹³³, K. Mönig ⁴⁸,
E. Monnier ¹⁰³, L. Monsonis Romero ¹⁶⁴, J. Montejo Berlingen ¹³, M. Montella ¹²⁰,
F. Montekali ^{77a,77b}, F. Monticelli ⁹¹, S. Monzani ^{69a,69c}, N. Morange ⁶⁶,
A.L. Moreira De Carvalho ⁴⁸, M. Moreno Llácer ¹⁶⁴, C. Moreno Martinez ⁵⁶, P. Morettini ^{57b},
S. Morgenstern ³⁶, M. Morii ⁶¹, M. Morinaga ¹⁵⁴, F. Morodei ^{75a,75b}, L. Morvaj ³⁶,
P. Moschovakos ³⁶, B. Moser ³⁶, M. Mosidze ^{150b}, T. Moskalets ⁴⁴, P. Moskvitina ¹¹⁴,
J. Moss ^{31,j}, P. Moszkowicz ^{86a}, A. Moussa ^{35d}, E.J.W. Moyse ¹⁰⁴, O. Mtintsilana ^{33g},

S. Muanza ¹⁰³, J. Mueller ¹³⁰, D. Muenstermann ⁹², R. Müller ¹⁹, G.A. Mullier ¹⁶²,
 A.J. Mullin³², J.J. Mullin¹²⁹, D.P. Mungo ¹⁵⁶, D. Munoz Perez ¹⁶⁴, F.J. Munoz Sanchez ¹⁰²,
 M. Murin ¹⁰², W.J. Murray ^{168,135}, M. Muškinja ⁹⁴, C. Mwewa ²⁹, A.G. Myagkov ^{37,a},
 A.J. Myers ⁸, G. Myers ¹⁰⁷, M. Myska ¹³³, B.P. Nachman ^{17a}, O. Nackenhorst ⁴⁹, K. Nagai ¹²⁷,
 K. Nagano ⁸⁴, J.L. Nagle ^{29,af}, E. Nagy ¹⁰³, A.M. Nairz ³⁶, Y. Nakahama ⁸⁴, K. Nakamura ⁸⁴,
 K. Nakkalil ⁵, H. Nanjo ¹²⁵, E.A. Narayanan ¹¹³, I. Naryshkin ³⁷, L. Nasella ^{71a,71b},
 M. Naseri ³⁴, S. Nasri ^{117b}, C. Nass ²⁴, G. Navarro ^{22a}, J. Navarro-Gonzalez ¹⁶⁴, R. Nayak ¹⁵²,
 A. Nayaz ¹⁸, P.Y. Nechaeva ³⁷, S. Nechaeva ^{23b,23a}, F. Nechansky ⁴⁸, L. Nedic ¹²⁷, T.J. Neep ²⁰,
 A. Negri ^{73a,73b}, M. Negrini ^{23b}, C. Nellist ¹¹⁵, C. Nelson ¹⁰⁵, K. Nelson ¹⁰⁷, S. Nemecek ¹³²,
 M. Nessi ^{36,g}, M.S. Neubauer ¹⁶³, F. Neuhaus ¹⁰¹, J. Neundorf ⁴⁸, P.R. Newman ²⁰,
 C.W. Ng ¹³⁰, Y.W.Y. Ng ⁴⁸, B. Ngair ^{117a}, H.D.N. Nguyen ¹⁰⁹, R.B. Nickerson ¹²⁷,
 R. Nicolaidou ¹³⁶, J. Nielsen ¹³⁷, M. Niemeyer ⁵⁵, J. Niermann ⁵⁵, N. Nikiforou ³⁶,
 V. Nikolaenko ^{37,a}, I. Nikolic-Audit ¹²⁸, K. Nikolopoulos ²⁰, P. Nilsson ²⁹, I. Ninca ⁴⁸,
 G. Ninio ¹⁵², A. Nisati ^{75a}, N. Nishu ², R. Nisius ¹¹¹, J-E. Nitschke ⁵⁰, E.K. Nkadimeng ^{33g},
 T. Nobe ¹⁵⁴, T. Nommensen ¹⁴⁸, M.B. Norfolk ¹⁴⁰, B.J. Norman ³⁴, M. Noury ^{35a}, J. Novak ⁹⁴,
 T. Novak ⁹⁴, L. Novotny ¹³³, R. Novotny ¹¹³, L. Nozka ¹²³, K. Ntekas ¹⁶⁰,
 N.M.J. Nunes De Moura Junior ^{83b}, J. Ocariz ¹²⁸, A. Ochi ⁸⁵, I. Ochoa ^{131a}, S. Oerdek ^{48,s},
 J.T. Offermann ³⁹, A. Ogrodnik ¹³⁴, A. Oh ¹⁰², C.C. Ohm ¹⁴⁵, H. Oide ⁸⁴, R. Oishi ¹⁵⁴,
 M.L. Ojeda ⁴⁸, Y. Okumura ¹⁵⁴, L.F. Oleiro Seabra ^{131a}, I. Oleksiyuk ⁵⁶, S.A. Olivares Pino ^{138d},
 G. Oliveira Correa ¹³, D. Oliveira Damazio ²⁹, D. Oliveira Goncalves ^{83a}, J.L. Oliver ¹⁶⁰,
 Ö.O. Öncel ⁵⁴, A.P. O'Neill ¹⁹, A. Onofre ^{131a,131e}, P.U.E. Onyisi ¹¹, M.J. Oreglia ³⁹,
 G.E. Orellana ⁹¹, D. Orestano ^{77a,77b}, N. Orlando ¹³, R.S. Orr ¹⁵⁶, L.M. Osojnak ¹²⁹,
 R. Ospanov ^{62a}, G. Otero y Garzon ³⁰, H. Otono ⁸⁹, P.S. Ott ^{63a}, G.J. Ottino ^{17a}, M. Ouchrif ^{35d},
 F. Ould-Saada ¹²⁶, T. Ovsiannikova ¹³⁹, M. Owen ⁵⁹, R.E. Owen ¹³⁵, V.E. Ozcan ^{21a},
 F. Ozturk ⁸⁷, N. Ozturk ⁸, S. Ozturk ⁸², H.A. Pacey ¹²⁷, A. Pacheco Pages ¹³,
 C. Padilla Aranda ¹³, G. Padovano ^{75a,75b}, S. Pagan Griso ^{17a}, G. Palacino ⁶⁸, A. Palazzo ^{70a,70b},
 J. Pampel ²⁴, J. Pan ¹⁷³, T. Pan ^{64a}, D.K. Panchal ¹¹, C.E. Pandini ¹¹⁵, J.G. Panduro Vazquez ¹³⁵,
 H.D. Pandya ¹, H. Pang ^{14b}, P. Pani ⁴⁸, G. Panizzo ^{69a,69c}, L. Panwar ¹²⁸, L. Paolozzi ⁵⁶,
 S. Parajuli ¹⁶³, A. Paramonov ⁶, C. Paraskevopoulos ⁵³, D. Paredes Hernandez ^{64b},
 A. Pareti ^{73a,73b}, K.R. Park ⁴¹, T.H. Park ¹⁵⁶, M.A. Parker ³², F. Parodi ^{57b,57a}, E.W. Parrish ¹¹⁶,
 V.A. Parrish ⁵², J.A. Parsons ⁴¹, U. Parzefall ⁵⁴, B. Pascual Dias ¹⁰⁹, L. Pascual Dominguez ¹⁰⁰,
 E. Pasqualucci ^{75a}, S. Passaggio ^{57b}, F. Pastore ⁹⁶, P. Patel ⁸⁷, U.M. Patel ⁵¹, J.R. Pater ¹⁰²,
 T. Pauly ³⁶, C.I. Pazos ¹⁵⁹, J. Pearkes ¹⁴⁴, M. Pedersen ¹²⁶, R. Pedro ^{131a}, S.V. Peleganchuk ³⁷,
 O. Penc ³⁶, E.A. Pender ⁵², G.D. Penn ¹⁷³, K.E. Penski ¹¹⁰, M. Penzin ³⁷, B.S. Peralva ^{83d},
 A.P. Pereira Peixoto ¹³⁹, L. Pereira Sanchez ¹⁴⁴, D.V. Perepelitsa ^{29,af}, G. Perera ¹⁰⁴,
 E. Perez Codina ^{157a}, M. Perganti ¹⁰, H. Pernegger ³⁶, S. Perrella ^{75a,75b}, O. Perrin ⁴⁰,
 K. Peters ⁴⁸, R.F.Y. Peters ¹⁰², B.A. Petersen ³⁶, T.C. Petersen ⁴², E. Petit ¹⁰³, V. Petousis ¹³³,
 C. Petridou ^{153,d}, T. Petru ¹³⁴, A. Petrukhin ¹⁴², M. Pettee ^{17a}, A. Petukhov ³⁷, K. Petukhova ¹³⁴,
 R. Pezoa ^{138f}, L. Pezzotti ³⁶, G. Pezzullo ¹⁷³, T.M. Pham ¹⁷¹, T. Pham ¹⁰⁶, P.W. Phillips ¹³⁵,
 G. Piacquadio ¹⁴⁶, E. Pianori ^{17a}, F. Piazza ¹²⁴, R. Piegai ³⁰, D. Pietreanu ^{27b},
 A.D. Pilkington ¹⁰², M. Pinamonti ^{69a,69c}, J.L. Pinfeld ², B.C. Pinheiro Pereira ^{131a},
 A.E. Pinto Pinoargote ^{136,136}, L. Pintucci ^{69a,69c}, K.M. Piper ¹⁴⁷, A. Pirttikoski ⁵⁶, D.A. Pizzi ³⁴,
 L. Pizzimento ^{64b}, A. Pizzini ¹¹⁵, M.-A. Pleier ²⁹, V. Pleskot ¹³⁴, E. Plotnikova³⁸, G. Poddar ⁹⁵,
 R. Poettgen ⁹⁹, L. Poggioli ¹²⁸, I. Pokharel ⁵⁵, S. Polacek ¹³⁴, G. Polesello ^{73a}, A. Poley ^{143,157a},
 A. Polini ^{23b}, C.S. Pollard ¹⁶⁸, Z.B. Pollock ¹²⁰, E. Pompa Pacchi ^{75a,75b}, N.I. Pond ⁹⁷,
 D. Ponomarenko ¹¹⁴, L. Pontecorvo ³⁶, S. Popa ^{27a}, G.A. Popeneciu ^{27d}, A. Poreba ³⁶,
 D.M. Portillo Quintero ^{157a}, S. Pospisil ¹³³, M.A. Postill ¹⁴⁰, P. Postolache ^{27c}, K. Potamianos ¹⁶⁸,

P.A. Potepa ^{86a}, I.N. Potrap ³⁸, C.J. Potter ³², H. Potti ¹⁴⁸, J. Poveda ¹⁶⁴,
 M.E. Pozo Astigarraga ³⁶, A. Prades Ibanez ¹⁶⁴, J. Pretel ⁵⁴, D. Price ¹⁰², M. Primavera ^{70a},
 M.A. Principe Martin ¹⁰⁰, R. Privara ¹²³, T. Procter ⁵⁹, M.L. Proffitt ¹³⁹, N. Proklova ¹²⁹,
 K. Prokofiev ^{64c}, G. Proto ¹¹¹, J. Proudfoot ⁶, M. Przybycien ^{86a}, W.W. Przygoda ^{86b},
 A. Psallidas ⁴⁶, J.E. Puddefoot ¹⁴⁰, D. Pudzha ³⁷, D. Pyatiizbyantseva ³⁷, J. Qian ¹⁰⁷,
 D. Qichen ¹⁰², Y. Qin ¹³, T. Qiu ⁵², A. Quadt ⁵⁵, M. Queitsch-Maitland ¹⁰², G. Quetant ⁵⁶,
 R.P. Quinn ¹⁶⁵, G. Rabanal Bolanos ⁶¹, D. Rafanoharana ⁵⁴, F. Raffaelli ^{76a,76b}, F. Ragusa ^{71a,71b},
 J.L. Rainbolt ³⁹, J.A. Raine ⁵⁶, S. Rajagopalan ²⁹, E. Ramakoti ³⁷, I.A. Ramirez-Berend ³⁴,
 K. Ran ^{48,14e}, N.P. Rapheeha ^{33g}, H. Rasheed ^{27b}, V. Raskina ¹²⁸, D.F. Rassloff ^{63a},
 A. Rastogi ^{17a}, S. Rave ¹⁰¹, S. Ravera ^{57b,57a}, B. Ravina ⁵⁵, I. Ravinovich ¹⁷⁰, M. Raymond ³⁶,
 A.L. Read ¹²⁶, N.P. Readioff ¹⁴⁰, D.M. Rebutzi ^{73a,73b}, G. Redlinger ²⁹, A.S. Reed ¹¹¹,
 K. Reeves ²⁶, J.A. Reidelsturz ¹⁷², D. Reikher ¹⁵², A. Rej ⁴⁹, C. Rembser ³⁶, M. Renda ^{27b},
 M.B. Rendel ¹¹¹, F. Renner ⁴⁸, A.G. Rennie ¹⁶⁰, A.L. Rescia ⁴⁸, S. Resconi ^{71a},
 M. Ressegotti ^{57b,57a}, S. Rettie ³⁶, J.G. Reyes Rivera ¹⁰⁸, E. Reynolds ^{17a}, O.L. Rezanova ³⁷,
 P. Reznicek ¹³⁴, H. Riani ^{35d}, N. Ribaric ⁹², E. Ricci ^{78a,78b}, R. Richter ¹¹¹, S. Richter ^{47a,47b},
 E. Richter-Was ^{86b}, M. Ridel ¹²⁸, S. Ridouani ^{35d}, P. Rieck ¹¹⁸, P. Riedler ³⁶, E.M. Riefel ^{47a,47b},
 J.O. Rieger ¹¹⁵, M. Rijssenbeek ¹⁴⁶, M. Rimoldi ³⁶, L. Rinaldi ^{23b,23a}, P. Rincke ^{55,162},
 T.T. Rinn ²⁹, M.P. Rinnagel ¹¹⁰, G. Ripellino ¹⁶², I. Riu ¹³, J.C. Rivera Vergara ¹⁶⁶,
 F. Rizatdinova ¹²², E. Rizvi ⁹⁵, B.R. Roberts ^{17a}, S.H. Robertson ^{105,v}, D. Robinson ³²,
 C.M. Robles Gajardo ^{138f}, M. Robles Manzano ¹⁰¹, A. Robson ⁵⁹, A. Rocchi ^{76a,76b}, C. Roda ^{74a,74b},
 S. Rodriguez Bosca ³⁶, Y. Rodriguez Garcia ^{22a}, A. Rodriguez Rodriguez ⁵⁴,
 A.M. Rodríguez Vera ¹¹⁶, S. Roe ³⁶, J.T. Roemer ¹⁶⁰, A.R. Roepe-Gier ¹³⁷, J. Roggel ¹⁷²,
 O. Røhne ¹²⁶, R.A. Rojas ¹⁰⁴, C.P.A. Roland ¹²⁸, J. Roloff ²⁹, A. Romaniouk ³⁷,
 E. Romano ^{73a,73b}, M. Romano ^{23b}, A.C. Romero Hernandez ¹⁶³, N. Rompotis ⁹³, L. Roos ¹²⁸,
 S. Rosati ^{75a}, B.J. Rosser ³⁹, E. Rossi ¹²⁷, E. Rossi ^{72a,72b}, L.P. Rossi ⁶¹, L. Rossini ⁵⁴,
 R. Rosten ¹²⁰, M. Rotaru ^{27b}, B. Rottler ⁵⁴, C. Rougier ⁹⁰, D. Rousseau ⁶⁶, D. Rousso ⁴⁸,
 A. Roy ¹⁶³, S. Roy-Garand ¹⁵⁶, A. Rozanov ¹⁰³, Z.M.A. Rozario ⁵⁹, Y. Rozen ¹⁵¹,
 A. Rubio Jimenez ¹⁶⁴, A.J. Ruby ⁹³, V.H. Ruelas Rivera ¹⁸, T.A. Ruggeri ¹, A. Ruggiero ¹²⁷,
 A. Ruiz-Martinez ¹⁶⁴, A. Rummler ³⁶, Z. Rurikova ⁵⁴, N.A. Rusakovich ³⁸, H.L. Russell ¹⁶⁶,
 G. Russo ^{75a,75b}, J.P. Rutherford ⁷, S. Rutherford Colmenares ³², M. Rybar ¹³⁴, E.B. Rye ¹²⁶,
 A. Ryzhov ⁴⁴, J.A. Sabater Iglesias ⁵⁶, P. Sabatini ¹⁶⁴, H.F.W. Sadrozinski ¹³⁷,
 F. Safai Tehrani ^{75a}, B. Safarzadeh Samani ¹³⁵, S. Saha ¹, M. Sahinsoy ¹¹¹, A. Saibel ¹⁶⁴,
 M. Saimpert ¹³⁶, M. Saito ¹⁵⁴, T. Saito ¹⁵⁴, A. Sala ^{71a,71b}, D. Salamani ³⁶, A. Salnikov ¹⁴⁴,
 J. Salt ¹⁶⁴, A. Salvador Salas ¹⁵², D. Salvatore ^{43b,43a}, F. Salvatore ¹⁴⁷, A. Salzburger ³⁶,
 D. Sammel ⁵⁴, E. Sampson ⁹², D. Sampsonidis ^{153,d}, D. Sampsonidou ¹²⁴, J. Sánchez ¹⁶⁴,
 V. Sanchez Sebastian ¹⁶⁴, H. Sandaker ¹²⁶, C.O. Sander ⁴⁸, J.A. Sandesara ¹⁰⁴, M. Sandhoff ¹⁷²,
 C. Sandoval ^{22b}, L. Sanfilippo ^{63a}, D.P.C. Sankey ¹³⁵, T. Sano ⁸⁸, A. Sansoni ⁵³, L. Santi ^{36,75b},
 C. Santoni ⁴⁰, H. Santos ^{131a,131b}, A. Santra ¹⁷⁰, E. Sanzani ^{23b,23a}, K.A. Saoucha ¹⁶¹,
 J.G. Saraiva ^{131a,131d}, J. Sardain ⁷, O. Sasaki ⁸⁴, K. Sato ¹⁵⁸, C. Sauer ^{63b}, E. Sauvan ⁴,
 P. Savard ^{156,ad}, R. Sawada ¹⁵⁴, C. Sawyer ¹³⁵, L. Sawyer ⁹⁸, C. Sbarra ^{23b}, A. Sbrizzi ^{23b,23a},
 T. Scanlon ⁹⁷, J. Schaarschmidt ¹³⁹, U. Schäfer ¹⁰¹, A.C. Schaffer ^{66,44}, D. Schaile ¹¹⁰,
 R.D. Schamberger ¹⁴⁶, C. Scharf ¹⁸, M.M. Schefer ¹⁹, V.A. Schegelsky ³⁷, D. Scheirich ¹³⁴,
 M. Schernau ¹⁶⁰, C. Scheulen ⁵⁵, C. Schiavi ^{57b,57a}, M. Schioppa ^{43b,43a}, B. Schlag ^{144,1},
 K.E. Schleicher ⁵⁴, S. Schlenker ³⁶, J. Schmeing ¹⁷², M.A. Schmidt ¹⁷², K. Schmieden ¹⁰¹,
 C. Schmitt ¹⁰¹, N. Schmitt ¹⁰¹, S. Schmitt ⁴⁸, L. Schoeffel ¹³⁶, A. Schoening ^{63b},
 P.G. Scholer ³⁴, E. Schopf ¹²⁷, M. Schott ²⁴, J. Schovancova ³⁶, S. Schramm ⁵⁶, T. Schroer ⁵⁶,
 H-C. Schultz-Coulon ^{63a}, M. Schumacher ⁵⁴, B.A. Schumm ¹³⁷, Ph. Schune ¹³⁶, A.J. Schuy ¹³⁹,

H.R. Schwartz ¹³⁷, A. Schwartzman ¹⁴⁴, T.A. Schwarz ¹⁰⁷, Ph. Schwemling ¹³⁶,
 R. Schwienhorst ¹⁰⁸, A. Sciandra ²⁹, G. Sciolla ²⁶, F. Scuri ^{74a}, C.D. Sebastiani ⁹³,
 K. Sedlaczek ¹¹⁶, S.C. Seidel ¹¹³, A. Seiden ¹³⁷, B.D. Seidlitz ⁴¹, C. Seitz ⁴⁸, J.M. Seixas ^{83b},
 G. Sekhniaidze ^{72a}, L. Selem ⁶⁰, N. Semprini-Cesari ^{23b,23a}, D. Sengupta ⁵⁶, V. Senthilkumar ¹⁶⁴,
 L. Serin ⁶⁶, M. Sessa ^{76a,76b}, H. Severini ¹²¹, F. Sforza ^{57b,57a}, A. Sfyrta ⁵⁶, Q. Sha ^{14a},
 E. Shabalina ⁵⁵, A.H. Shah ³², R. Shaheen ¹⁴⁵, J.D. Shahinian ¹²⁹, D. Shaked Renous ¹⁷⁰,
 L.Y. Shan ^{14a}, M. Shapiro ^{17a}, A. Sharma ³⁶, A.S. Sharma ¹⁶⁵, P. Sharma ⁸⁰, P.B. Shatalov ³⁷,
 K. Shaw ¹⁴⁷, S.M. Shaw ¹⁰², Q. Shen ^{62c,5}, D.J. Sheppard ¹⁴³, P. Sherwood ⁹⁷, L. Shi ⁹⁷,
 X. Shi ^{14a}, C.O. Shimmin ¹⁷³, J.D. Shinner ⁹⁶, I.P.J. Shipsey ¹²⁷, S. Shirabe ⁸⁹,
 M. Shiyakova ^{38,t}, M.J. Shochet ³⁹, J. Shojaii ¹⁰⁶, D.R. Shope ¹²⁶, B. Shrestha ¹²¹,
 S. Shrestha ^{120,ag}, M.J. Shroff ¹⁶⁶, P. Sicho ¹³², A.M. Sickles ¹⁶³, E. Sideras Haddad ^{33g},
 A.C. Sidley ¹¹⁵, A. Sidoti ^{23b}, F. Siegert ⁵⁰, Dj. Sijacki ¹⁵, F. Sili ⁹¹, J.M. Silva ⁵²,
 I. Silva Ferreira ^{83b}, M.V. Silva Oliveira ²⁹, S.B. Silverstein ^{47a}, S. Simion ⁶⁶, R. Simoniello ³⁶,
 E.L. Simpson ¹⁰², H. Simpson ¹⁴⁷, L.R. Simpson ¹⁰⁷, N.D. Simpson ⁹⁹, S. Simsek ⁸²,
 S. Sindhu ⁵⁵, P. Sinervo ¹⁵⁶, S. Singh ¹⁵⁶, S. Sinha ⁴⁸, S. Sinha ¹⁰², M. Sioli ^{23b,23a}, I. Siral ³⁶,
 E. Sitnikova ⁴⁸, J. Sjölin ^{47a,47b}, A. Skaf ⁵⁵, E. Skorda ²⁰, P. Skubic ¹²¹, M. Slawinska ⁸⁷,
 V. Smakhtin ¹⁷⁰, B.H. Smart ¹³⁵, S.Yu. Smirnov ³⁷, Y. Smirnov ³⁷, L.N. Smirnova ^{37,a},
 O. Smirnova ⁹⁹, A.C. Smith ⁴¹, D.R. Smith ¹⁶⁰, E.A. Smith ³⁹, H.A. Smith ¹²⁷, J.L. Smith ¹⁰²,
 R. Smith ¹⁴⁴, M. Smizanska ⁹², K. Smolek ¹³³, A.A. Snesarev ³⁷, S.R. Snider ¹⁵⁶, H.L. Snoek ¹¹⁵,
 S. Snyder ²⁹, R. Sobie ^{166,v}, A. Soffer ¹⁵², C.A. Solans Sanchez ³⁶, E.Yu. Soldatov ³⁷,
 U. Soldevila ¹⁶⁴, A.A. Solodkov ³⁷, S. Solomon ²⁶, A. Soloshenko ³⁸, K. Solovieva ⁵⁴,
 O.V. Solovyanov ⁴⁰, P. Sommer ³⁶, A. Sonay ¹³, W.Y. Song ^{157b}, A. Sopczak ¹³³, A.L. Soppio ⁹⁷,
 F. Sopkova ^{28b}, J.D. Sorenson ¹¹³, I.R. Sotarriva Alvarez ¹⁵⁵, V. Sothilingam ^{63a},
 O.J. Soto Sandoval ^{138c,138b}, S. Sottocornola ⁶⁸, R. Soualah ¹⁶¹, Z. Soumami ^{35e}, D. South ⁴⁸,
 N. Soybelman ¹⁷⁰, S. Spagnolo ^{70a,70b}, M. Spalla ¹¹¹, D. Sperlich ⁵⁴, G. Spigo ³⁶, S. Spinali ⁹²,
 D.P. Spiteri ⁵⁹, M. Spousta ¹³⁴, E.J. Staats ³⁴, R. Stamen ^{63a}, A. Stampeki ²⁰, M. Standke ²⁴,
 E. Stanecka ⁸⁷, W. Stanek-Maslouska ⁴⁸, M.V. Stange ⁵⁰, B. Stanislaus ^{17a}, M.M. Stanitzki ⁴⁸,
 B. Stapf ⁴⁸, E.A. Starchenko ³⁷, G.H. Stark ¹³⁷, J. Stark ⁹⁰, P. Staroba ¹³², P. Starovoitov ^{63a},
 S. Stärz ¹⁰⁵, R. Staszewski ⁸⁷, G. Stavropoulos ⁴⁶, J. Steentoft ¹⁶², P. Steinberg ²⁹,
 B. Stelzer ^{143,157a}, H.J. Stelzer ¹³⁰, O. Stelzer-Chilton ^{157a}, H. Stenzel ⁵⁸, T.J. Stevenson ¹⁴⁷,
 G.A. Stewart ³⁶, J.R. Stewart ¹²², M.C. Stockton ³⁶, G. Stoicea ^{27b}, M. Stolarski ^{131a},
 S. Stonjek ¹¹¹, A. Straessner ⁵⁰, J. Strandberg ¹⁴⁵, S. Strandberg ^{47a,47b}, M. Stratmann ¹⁷²,
 M. Strauss ¹²¹, T. Streblor ¹⁰³, P. Strizenec ^{28b}, R. Ströhmer ¹⁶⁷, D.M. Strom ¹²⁴,
 R. Stroynowski ⁴⁴, A. Strubig ^{47a,47b}, S.A. Stucci ²⁹, B. Stugu ¹⁶, J. Stupak ¹²¹, N.A. Styles ⁴⁸,
 D. Su ¹⁴⁴, S. Su ^{62a}, W. Su ^{62d}, X. Su ^{62a}, D. Suchy ^{28a}, K. Sugizaki ¹⁵⁴, V.V. Sulin ³⁷,
 M.J. Sullivan ⁹³, D.M.S. Sultan ¹²⁷, L. Sultanaliyeva ³⁷, S. Sultansoy ^{3b}, T. Sumida ⁸⁸,
 S. Sun ¹⁷¹, O. Sunneborn Gudnadottir ¹⁶², N. Sur ¹⁰³, M.R. Sutton ¹⁴⁷, H. Suzuki ¹⁵⁸,
 M. Svatos ¹³², M. Swiatlowski ^{157a}, T. Swirski ¹⁶⁷, I. Sykora ^{28a}, M. Sykora ¹³⁴, T. Sykora ¹³⁴,
 D. Ta ¹⁰¹, K. Tackmann ^{48,s}, A. Taffard ¹⁶⁰, R. Tafirout ^{157a}, J.S. Tafoya Vargas ⁶⁶, Y. Takubo ⁸⁴,
 M. Talby ¹⁰³, A.A. Talyshev ³⁷, K.C. Tam ^{64b}, N.M. Tamir ¹⁵², A. Tanaka ¹⁵⁴, J. Tanaka ¹⁵⁴,
 R. Tanaka ⁶⁶, M. Tanasini ¹⁴⁶, Z. Tao ¹⁶⁵, S. Tapia Araya ^{138f}, S. Tapprogge ¹⁰¹,
 A. Tarek Abouelfadl Mohamed ¹⁰⁸, S. Tarem ¹⁵¹, K. Tariq ^{14a}, G. Tarna ^{27b}, G.F. Tartarelli ^{71a},
 M.J. Tartarin ⁹⁰, P. Tas ¹³⁴, M. Tasevsky ¹³², E. Tassi ^{43b,43a}, A.C. Tate ¹⁶³, G. Tateno ¹⁵⁴,
 Y. Tayalati ^{35e,u}, G.N. Taylor ¹⁰⁶, W. Taylor ^{157b}, R. Teixeira De Lima ¹⁴⁴, P. Teixeira-Dias ⁹⁶,
 J.J. Teoh ¹⁵⁶, K. Terashi ¹⁵⁴, J. Terron ¹⁰⁰, S. Terzo ¹³, M. Testa ⁵³, R.J. Teuscher ^{156,v},
 A. Thaler ⁷⁹, O. Theiner ⁵⁶, N. Themistokleous ⁵², T. Thevenaux-Pelzer ¹⁰³, O. Thielmann ¹⁷²,
 D.W. Thomas ⁹⁶, J.P. Thomas ²⁰, E.A. Thompson ^{17a}, P.D. Thompson ²⁰, E. Thomson ¹²⁹,

R.E. Thornberry ⁴⁴, C. Tian ^{62a}, Y. Tian ⁵⁵, V. Tikhomirov ^{37,a}, Yu.A. Tikhonov ³⁷, S. Timoshenko ³⁷, D. Timoshyn ¹³⁴, E.X.L. Ting ¹, P. Tipton ¹⁷³, A. Tishelman-Charny ²⁹, S.H. Tlou ^{33g}, K. Todome ¹⁵⁵, S. Todorova-Nova ¹³⁴, S. Todt ⁵⁰, L. Toffolin ^{69a,69c}, M. Togawa ⁸⁴, J. Tojo ⁸⁹, S. Tokár ^{28a}, K. Tokushuku ⁸⁴, O. Toldaiev ⁶⁸, R. Tombs ³², M. Tomoto ^{84,112}, L. Tompkins ^{144,1}, K.W. Topolnicki ^{86b}, E. Torrence ¹²⁴, H. Torres ⁹⁰, E. Torró Pastor ¹⁶⁴, M. Toscani ³⁰, C. Toscirci ³⁹, M. Tost ¹¹, D.R. Tovey ¹⁴⁰, I.S. Trandafir ^{27b}, T. Trefzger ¹⁶⁷, A. Tricoli ²⁹, I.M. Trigger ^{157a}, S. Trincaz-Duvoid ¹²⁸, D.A. Trischuk ²⁶, B. Trocmé ⁶⁰, L. Truong ^{33c}, M. Trzebinski ⁸⁷, A. Trzupiek ⁸⁷, F. Tsai ¹⁴⁶, M. Tsai ¹⁰⁷, A. Tsiamis ^{153,d}, P.V. Tsiareshka ³⁷, S. Tsigaridas ^{157a}, A. Tsirigotis ^{153,q}, V. Tsiskaridze ¹⁵⁶, E.G. Tskhadadze ^{150a}, M. Tsopoulou ¹⁵³, Y. Tsujikawa ⁸⁸, I.I. Tsukerman ³⁷, V. Tsulaia ^{17a}, S. Tsuno ⁸⁴, K. Tsurii ¹¹⁹, D. Tsybychev ¹⁴⁶, Y. Tu ^{64b}, A. Tudorache ^{27b}, V. Tudorache ^{27b}, A.N. Tuna ⁶¹, S. Turchikhin ^{57b,57a}, I. Turk Cakir ^{3a}, R. Turra ^{71a}, T. Turtuvshin ^{38,w}, P.M. Tuts ⁴¹, S. Tzamarias ^{153,d}, E. Tzovara ¹⁰¹, F. Ukegawa ¹⁵⁸, P.A. Ulloa Poblete ^{138c,138b}, E.N. Umaka ²⁹, G. Unal ³⁶, A. Undrus ²⁹, G. Unel ¹⁶⁰, J. Urban ^{28b}, P. Urrejola ^{138a}, G. Usai ⁸, R. Ushioda ¹⁵⁵, M. Usman ¹⁰⁹, Z. Uysal ⁸², V. Vacek ¹³³, B. Vachon ¹⁰⁵, T. Vafeiadis ³⁶, A. Vaitkus ⁹⁷, C. Valderanis ¹¹⁰, E. Valdes Santurio ^{47a,47b}, M. Valente ^{157a}, S. Valentinetti ^{23b,23a}, A. Valero ¹⁶⁴, E. Valiente Moreno ¹⁶⁴, A. Vallier ⁹⁰, J.A. Valls Ferrer ¹⁶⁴, D.R. Van Arneeman ¹¹⁵, T.R. Van Daalen ¹³⁹, A. Van Der Graaf ⁴⁹, P. Van Gemmeren ⁶, M. Van Rijnbach ³⁶, S. Van Stroud ⁹⁷, I. Van Vulpen ¹¹⁵, P. Vana ¹³⁴, M. Vanadia ^{76a,76b}, W. Vandelli ³⁶, E.R. Vandewall ¹²², D. Vannicola ¹⁵², L. Vannoli ⁵³, R. Vari ^{75a}, E.W. Varnes ⁷, C. Varni ^{17b}, T. Varol ¹⁴⁹, D. Varouchas ⁶⁶, L. Varriale ¹⁶⁴, K.E. Varvell ¹⁴⁸, M.E. Vasile ^{27b}, L. Vaslin ⁸⁴, G.A. Vasquez ¹⁶⁶, A. Vasyukov ³⁸, L.M. Vaughan ¹²², R. Vavricka ¹⁰¹, T. Vazquez Schroeder ³⁶, J. Veatch ³¹, V. Vecchio ¹⁰², M.J. Veen ¹⁰⁴, I. Veliscek ²⁹, L.M. Veloce ¹⁵⁶, F. Veloso ^{131a,131c}, S. Veneziano ^{75a}, A. Ventura ^{70a,70b}, S. Ventura Gonzalez ¹³⁶, A. Verbytskyi ¹¹¹, M. Verducci ^{74a,74b}, C. Vergis ⁹⁵, M. Verissimo De Araujo ^{83b}, W. Verkerke ¹¹⁵, J.C. Vermeulen ¹¹⁵, C. Vernieri ¹⁴⁴, M. Vessella ¹⁰⁴, M.C. Vetterli ^{143,ad}, A. Vgenopoulos ^{153,d}, N. Viaux Maira ^{138f}, T. Vickey ¹⁴⁰, O.E. Vickey Boeriu ¹⁴⁰, G.H.A. Viehhauser ¹²⁷, L. Vigani ^{63b}, M. Villa ^{23b,23a}, M. Villaplana Perez ¹⁶⁴, E.M. Villhauer ⁵², E. Vilucchi ⁵³, M.G. Vincter ³⁴, A. Visibile ¹¹⁵, C. Vittori ³⁶, I. Vivarelli ^{23b,23a}, E. Voevodina ¹¹¹, F. Vogel ¹¹⁰, J.C. Voigt ⁵⁰, P. Vokac ¹³³, Yu. Volkotrub ^{86b}, J. Von Ahnen ⁴⁸, E. Von Toerne ²⁴, B. Vormwald ³⁶, V. Vorobel ¹³⁴, K. Vorobev ³⁷, M. Vos ¹⁶⁴, K. Voss ¹⁴², M. Vozak ¹¹⁵, L. Vozdecky ¹²¹, N. Vranjes ¹⁵, M. Vranjes Milosavljevic ¹⁵, M. Vreeswijk ¹¹⁵, N.K. Vu ^{62d,62c}, R. Vuillermet ³⁶, O. Vujinovic ¹⁰¹, I. Vukotic ³⁹, S. Wada ¹⁵⁸, C. Wagner ¹⁰⁴, J.M. Wagner ^{17a}, W. Wagner ¹⁷², S. Wahdan ¹⁷², H. Wahlberg ⁹¹, M. Wakida ¹¹², J. Walder ¹³⁵, R. Walker ¹¹⁰, W. Walkowiak ¹⁴², A. Wall ¹²⁹, E.J. Wallin ⁹⁹, T. Wamorkar ⁶, A.Z. Wang ¹³⁷, C. Wang ¹⁰¹, C. Wang ¹¹, H. Wang ^{17a}, J. Wang ^{64c}, P. Wang ⁹⁷, R. Wang ⁶¹, R. Wang ⁶, S.M. Wang ¹⁴⁹, S. Wang ^{62b}, S. Wang ^{14a}, T. Wang ^{62a}, W.T. Wang ⁸⁰, W. Wang ^{14a}, X. Wang ^{14c}, X. Wang ¹⁶³, X. Wang ^{62c}, Y. Wang ^{62d}, Y. Wang ^{14c}, Z. Wang ¹⁰⁷, Z. Wang ^{62d,51,62c}, Z. Wang ¹⁰⁷, A. Warburton ¹⁰⁵, R.J. Ward ²⁰, N. Warrack ⁵⁹, S. Waterhouse ⁹⁶, A.T. Watson ²⁰, H. Watson ⁵⁹, M.F. Watson ²⁰, E. Watton ^{59,135}, G. Watts ¹³⁹, B.M. Waugh ⁹⁷, J.M. Webb ⁵⁴, C. Weber ²⁹, H.A. Weber ¹⁸, M.S. Weber ¹⁹, S.M. Weber ^{63a}, C. Wei ^{62a}, Y. Wei ⁵⁴, A.R. Weidberg ¹²⁷, E.J. Weik ¹¹⁸, J. Weingarten ⁴⁹, C. Weiser ⁵⁴, C.J. Wells ⁴⁸, T. Wenaus ²⁹, B. Wendland ⁴⁹, T. Wengler ³⁶, N.S. Wenke ¹¹¹, N. Wermes ²⁴, M. Wessels ^{63a}, A.M. Wharton ⁹², A.S. White ⁶¹, A. White ⁸, M.J. White ¹, D. Whiteson ¹⁶⁰, L. Wickremasinghe ¹²⁵, W. Wiedenmann ¹⁷¹, M. Wielers ¹³⁵, C. Wiglesworth ⁴², D.J. Wilbern ¹²¹, H.G. Wilkens ³⁶, J.J.H. Wilkinson ³², D.M. Williams ⁴¹, H.H. Williams ¹²⁹, S. Williams ³², S. Willocq ¹⁰⁴, B.J. Wilson ¹⁰², P.J. Windischhofer ³⁹, F.I. Winkel ³⁰, F. Winklmeier ¹²⁴, B.T. Winter ⁵⁴, J.K. Winter ¹⁰²,

M. Wittgen¹⁴⁴, M. Wobisch⁹⁸, T. Wojtkowski⁶⁰, Z. Wolffs¹¹⁵, J. Wollrath¹⁶⁰, M.W. Wolter⁸⁷, H. Wolters^{131a,131c}, M.C. Wong¹³⁷, E.L. Woodward⁴¹, S.D. Worm⁴⁸, B.K. Wosiek⁸⁷, K.W. Woźniak⁸⁷, S. Wozniowski⁵⁵, K. Wraight⁵⁹, C. Wu²⁰, M. Wu^{14d}, M. Wu¹¹⁴, S.L. Wu¹⁷¹, X. Wu⁵⁶, Y. Wu^{62a}, Z. Wu⁴, J. Wuerzinger^{111,ab}, T.R. Wyatt¹⁰², B.M. Wynne⁵², S. Xella⁴², L. Xia^{14c}, M. Xia^{14b}, J. Xiang^{64c}, M. Xie^{62a}, S. Xin^{14a,14e}, A. Xiong¹²⁴, J. Xiong^{17a}, D. Xu^{14a}, H. Xu^{62a}, L. Xu^{62a}, R. Xu¹²⁹, T. Xu¹⁰⁷, Y. Xu^{14b}, Z. Xu⁵², Z. Xu^{14c}, B. Yabsley¹⁴⁸, S. Yacoob^{33a}, Y. Yamaguchi¹⁵⁵, E. Yamashita¹⁵⁴, H. Yamauchi¹⁵⁸, T. Yamazaki^{17a}, Y. Yamazaki⁸⁵, J. Yan^{62c}, S. Yan⁵⁹, Z. Yan¹⁰⁴, H.J. Yang^{62c,62d}, H.T. Yang^{62a}, S. Yang^{62a}, T. Yang^{64c}, X. Yang³⁶, X. Yang^{14a}, Y. Yang⁴⁴, Y. Yang^{62a}, Z. Yang^{62a}, W-M. Yao^{17a}, H. Ye^{14c}, H. Ye⁵⁵, J. Ye^{14a}, S. Ye²⁹, X. Ye^{62a}, Y. Yeh⁹⁷, I. Yeletsikh³⁸, B.K. Yeo^{17b}, M.R. Yexley⁹⁷, T.P. Yildirim¹²⁷, P. Yin⁴¹, K. Yorita¹⁶⁹, S. Younas^{27b}, C.J.S. Young³⁶, C. Young¹⁴⁴, C. Yu^{14a,14e}, Y. Yu^{62a}, M. Yuan¹⁰⁷, R. Yuan^{62d,62c}, L. Yue⁹⁷, M. Zaazoua^{62a}, B. Zabinski⁸⁷, E. Zaid⁵², Z.K. Zak⁸⁷, T. Zakareishvili¹⁶⁴, N. Zakharchuk³⁴, S. Zambito⁵⁶, J.A. Zamora Saa^{138d,138b}, J. Zang¹⁵⁴, D. Zanzi⁵⁴, O. Zaplatilek¹³³, C. Zeitnitz¹⁷², H. Zeng^{14a}, J.C. Zeng¹⁶³, D.T. Zenger Jr²⁶, O. Zenin³⁷, T. Ženiš^{28a}, S. Zenz⁹⁵, S. Zerradi^{35a}, D. Zerwas⁶⁶, M. Zhai^{14a,14e}, D.F. Zhang¹⁴⁰, J. Zhang^{62b}, J. Zhang⁶, K. Zhang^{14a,14e}, L. Zhang^{62a}, L. Zhang^{14c}, P. Zhang^{14a,14e}, R. Zhang¹⁷¹, S. Zhang¹⁰⁷, S. Zhang⁹⁰, T. Zhang¹⁵⁴, X. Zhang^{62c}, X. Zhang^{62b}, Y. Zhang^{62c}, Y. Zhang⁹⁷, Y. Zhang^{14c}, Z. Zhang^{17a}, Z. Zhang^{62b}, Z. Zhang⁶⁶, H. Zhao¹³⁹, T. Zhao^{62b}, Y. Zhao¹³⁷, Z. Zhao^{62a}, Z. Zhao^{62a}, A. Zhemchugov³⁸, J. Zheng^{14c}, K. Zheng¹⁶³, X. Zheng^{62a}, Z. Zheng¹⁴⁴, D. Zhong¹⁶³, B. Zhou¹⁰⁷, H. Zhou⁷, N. Zhou^{62c}, Y. Zhou^{14b}, Y. Zhou^{14c}, Y. Zhou⁷, C.G. Zhu^{62b}, J. Zhu¹⁰⁷, X. Zhu^{62d}, Y. Zhu^{62c}, Y. Zhu^{62a}, X. Zhuang^{14a}, K. Zhukov³⁷, N.I. Zimine³⁸, J. Zinsser^{63b}, M. Ziolkowski¹⁴², L. Živković¹⁵, A. Zoccoli^{23b,23a}, K. Zoch⁶¹, T.G. Zorbas¹⁴⁰, O. Zormpa⁴⁶, W. Zou⁴¹, L. Zwalinski³⁶.

¹Department of Physics, University of Adelaide, Adelaide; Australia.

²Department of Physics, University of Alberta, Edmonton AB; Canada.

³(^a)Department of Physics, Ankara University, Ankara; (^b)Division of Physics, TOBB University of Economics and Technology, Ankara; Türkiye.

⁴LAPP, Université Savoie Mont Blanc, CNRS/IN2P3, Annecy; France.

⁵APC, Université Paris Cité, CNRS/IN2P3, Paris; France.

⁶High Energy Physics Division, Argonne National Laboratory, Argonne IL; United States of America.

⁷Department of Physics, University of Arizona, Tucson AZ; United States of America.

⁸Department of Physics, University of Texas at Arlington, Arlington TX; United States of America.

⁹Physics Department, National and Kapodistrian University of Athens, Athens; Greece.

¹⁰Physics Department, National Technical University of Athens, Zografou; Greece.

¹¹Department of Physics, University of Texas at Austin, Austin TX; United States of America.

¹²Institute of Physics, Azerbaijan Academy of Sciences, Baku; Azerbaijan.

¹³Institut de Física d'Altes Energies (IFAE), Barcelona Institute of Science and Technology, Barcelona; Spain.

¹⁴(^a)Institute of High Energy Physics, Chinese Academy of Sciences, Beijing; (^b)Physics Department, Tsinghua University, Beijing; (^c)Department of Physics, Nanjing University, Nanjing; (^d)School of Science, Shenzhen Campus of Sun Yat-sen University; (^e)University of Chinese Academy of Science (UCAS), Beijing; China.

¹⁵Institute of Physics, University of Belgrade, Belgrade; Serbia.

¹⁶Department for Physics and Technology, University of Bergen, Bergen; Norway.

- ¹⁷(*a*) Physics Division, Lawrence Berkeley National Laboratory, Berkeley CA; (*b*) University of California, Berkeley CA; United States of America.
- ¹⁸Institut für Physik, Humboldt Universität zu Berlin, Berlin; Germany.
- ¹⁹Albert Einstein Center for Fundamental Physics and Laboratory for High Energy Physics, University of Bern, Bern; Switzerland.
- ²⁰School of Physics and Astronomy, University of Birmingham, Birmingham; United Kingdom.
- ²¹(*a*) Department of Physics, Bogazici University, Istanbul; (*b*) Department of Physics Engineering, Gaziantep University, Gaziantep; (*c*) Department of Physics, Istanbul University, Istanbul; Türkiye.
- ²²(*a*) Facultad de Ciencias y Centro de Investigaciones, Universidad Antonio Nariño, Bogotá; (*b*) Departamento de Física, Universidad Nacional de Colombia, Bogotá; Colombia.
- ²³(*a*) Dipartimento di Fisica e Astronomia A. Righi, Università di Bologna, Bologna; (*b*) INFN Sezione di Bologna; Italy.
- ²⁴Physikalisches Institut, Universität Bonn, Bonn; Germany.
- ²⁵Department of Physics, Boston University, Boston MA; United States of America.
- ²⁶Department of Physics, Brandeis University, Waltham MA; United States of America.
- ²⁷(*a*) Transilvania University of Brasov, Brasov; (*b*) Horia Hulubei National Institute of Physics and Nuclear Engineering, Bucharest; (*c*) Department of Physics, Alexandru Ioan Cuza University of Iasi, Iasi; (*d*) National Institute for Research and Development of Isotopic and Molecular Technologies, Physics Department, Cluj-Napoca; (*e*) National University of Science and Technology Politehnica, Bucharest; (*f*) West University in Timisoara, Timisoara; (*g*) Faculty of Physics, University of Bucharest, Bucharest; Romania.
- ²⁸(*a*) Faculty of Mathematics, Physics and Informatics, Comenius University, Bratislava; (*b*) Department of Subnuclear Physics, Institute of Experimental Physics of the Slovak Academy of Sciences, Kosice; Slovak Republic.
- ²⁹Physics Department, Brookhaven National Laboratory, Upton NY; United States of America.
- ³⁰Universidad de Buenos Aires, Facultad de Ciencias Exactas y Naturales, Departamento de Física, y CONICET, Instituto de Física de Buenos Aires (IFIBA), Buenos Aires; Argentina.
- ³¹California State University, CA; United States of America.
- ³²Cavendish Laboratory, University of Cambridge, Cambridge; United Kingdom.
- ³³(*a*) Department of Physics, University of Cape Town, Cape Town; (*b*) iThemba Labs, Western Cape; (*c*) Department of Mechanical Engineering Science, University of Johannesburg, Johannesburg; (*d*) National Institute of Physics, University of the Philippines Diliman (Philippines); (*e*) University of South Africa, Department of Physics, Pretoria; (*f*) University of Zululand, KwaDlangezwa; (*g*) School of Physics, University of the Witwatersrand, Johannesburg; South Africa.
- ³⁴Department of Physics, Carleton University, Ottawa ON; Canada.
- ³⁵(*a*) Faculté des Sciences Ain Chock, Réseau Universitaire de Physique des Hautes Energies - Université Hassan II, Casablanca; (*b*) Faculté des Sciences, Université Ibn-Tofail, Kénitra; (*c*) Faculté des Sciences Semlalia, Université Cadi Ayyad, LPHEA-Marrakech; (*d*) LPMR, Faculté des Sciences, Université Mohamed Premier, Oujda; (*e*) Faculté des sciences, Université Mohammed V, Rabat; (*f*) Institute of Applied Physics, Mohammed VI Polytechnic University, Ben Guerir; Morocco.
- ³⁶CERN, Geneva; Switzerland.
- ³⁷Affiliated with an institute covered by a cooperation agreement with CERN.
- ³⁸Affiliated with an international laboratory covered by a cooperation agreement with CERN.
- ³⁹Enrico Fermi Institute, University of Chicago, Chicago IL; United States of America.
- ⁴⁰LPC, Université Clermont Auvergne, CNRS/IN2P3, Clermont-Ferrand; France.
- ⁴¹Nevis Laboratory, Columbia University, Irvington NY; United States of America.
- ⁴²Niels Bohr Institute, University of Copenhagen, Copenhagen; Denmark.
- ⁴³(*a*) Dipartimento di Fisica, Università della Calabria, Rende; (*b*) INFN Gruppo Collegato di Cosenza,

Laboratori Nazionali di Frascati; Italy.

⁴⁴Physics Department, Southern Methodist University, Dallas TX; United States of America.

⁴⁵Physics Department, University of Texas at Dallas, Richardson TX; United States of America.

⁴⁶National Centre for Scientific Research "Demokritos", Agia Paraskevi; Greece.

⁴⁷(^a) Department of Physics, Stockholm University; (^b) Oskar Klein Centre, Stockholm; Sweden.

⁴⁸Deutsches Elektronen-Synchrotron DESY, Hamburg and Zeuthen; Germany.

⁴⁹Fakultät Physik, Technische Universität Dortmund, Dortmund; Germany.

⁵⁰Institut für Kern- und Teilchenphysik, Technische Universität Dresden, Dresden; Germany.

⁵¹Department of Physics, Duke University, Durham NC; United States of America.

⁵²SUPA - School of Physics and Astronomy, University of Edinburgh, Edinburgh; United Kingdom.

⁵³INFN e Laboratori Nazionali di Frascati, Frascati; Italy.

⁵⁴Physikalisches Institut, Albert-Ludwigs-Universität Freiburg, Freiburg; Germany.

⁵⁵II. Physikalisches Institut, Georg-August-Universität Göttingen, Göttingen; Germany.

⁵⁶Département de Physique Nucléaire et Corpusculaire, Université de Genève, Genève; Switzerland.

⁵⁷(^a) Dipartimento di Fisica, Università di Genova, Genova; (^b) INFN Sezione di Genova; Italy.

⁵⁸II. Physikalisches Institut, Justus-Liebig-Universität Giessen, Giessen; Germany.

⁵⁹SUPA - School of Physics and Astronomy, University of Glasgow, Glasgow; United Kingdom.

⁶⁰LPSC, Université Grenoble Alpes, CNRS/IN2P3, Grenoble INP, Grenoble; France.

⁶¹Laboratory for Particle Physics and Cosmology, Harvard University, Cambridge MA; United States of America.

⁶²(^a) Department of Modern Physics and State Key Laboratory of Particle Detection and Electronics, University of Science and Technology of China, Hefei; (^b) Institute of Frontier and Interdisciplinary Science and Key Laboratory of Particle Physics and Particle Irradiation (MOE), Shandong University, Qingdao; (^c) School of Physics and Astronomy, Shanghai Jiao Tong University, Key Laboratory for Particle Astrophysics and Cosmology (MOE), SKLPPC, Shanghai; (^d) Tsung-Dao Lee Institute, Shanghai; (^e) School of Physics and Microelectronics, Zhengzhou University; China.

⁶³(^a) Kirchhoff-Institut für Physik, Ruprecht-Karls-Universität Heidelberg, Heidelberg; (^b) Physikalisches Institut, Ruprecht-Karls-Universität Heidelberg, Heidelberg; Germany.

⁶⁴(^a) Department of Physics, Chinese University of Hong Kong, Shatin, N.T., Hong Kong; (^b) Department of Physics, University of Hong Kong, Hong Kong; (^c) Department of Physics and Institute for Advanced Study, Hong Kong University of Science and Technology, Clear Water Bay, Kowloon, Hong Kong; China.

⁶⁵Department of Physics, National Tsing Hua University, Hsinchu; Taiwan.

⁶⁶IJCLab, Université Paris-Saclay, CNRS/IN2P3, 91405, Orsay; France.

⁶⁷Centro Nacional de Microelectrónica (IMB-CNM-CSIC), Barcelona; Spain.

⁶⁸Department of Physics, Indiana University, Bloomington IN; United States of America.

⁶⁹(^a) INFN Gruppo Collegato di Udine, Sezione di Trieste, Udine; (^b) ICTP, Trieste; (^c) Dipartimento Politecnico di Ingegneria e Architettura, Università di Udine, Udine; Italy.

⁷⁰(^a) INFN Sezione di Lecce; (^b) Dipartimento di Matematica e Fisica, Università del Salento, Lecce; Italy.

⁷¹(^a) INFN Sezione di Milano; (^b) Dipartimento di Fisica, Università di Milano, Milano; Italy.

⁷²(^a) INFN Sezione di Napoli; (^b) Dipartimento di Fisica, Università di Napoli, Napoli; Italy.

⁷³(^a) INFN Sezione di Pavia; (^b) Dipartimento di Fisica, Università di Pavia, Pavia; Italy.

⁷⁴(^a) INFN Sezione di Pisa; (^b) Dipartimento di Fisica E. Fermi, Università di Pisa, Pisa; Italy.

⁷⁵(^a) INFN Sezione di Roma; (^b) Dipartimento di Fisica, Sapienza Università di Roma, Roma; Italy.

⁷⁶(^a) INFN Sezione di Roma Tor Vergata; (^b) Dipartimento di Fisica, Università di Roma Tor Vergata, Roma; Italy.

⁷⁷(^a) INFN Sezione di Roma Tre; (^b) Dipartimento di Matematica e Fisica, Università Roma Tre, Roma; Italy.

- ⁷⁸(*a*) INFN-TIFPA; (*b*) Università degli Studi di Trento, Trento; Italy.
- ⁷⁹Universität Innsbruck, Department of Astro and Particle Physics, Innsbruck; Austria.
- ⁸⁰University of Iowa, Iowa City IA; United States of America.
- ⁸¹Department of Physics and Astronomy, Iowa State University, Ames IA; United States of America.
- ⁸²Istinye University, Sariyer, Istanbul; Türkiye.
- ⁸³(*a*) Departamento de Engenharia Elétrica, Universidade Federal de Juiz de Fora (UFJF), Juiz de Fora; (*b*) Universidade Federal do Rio De Janeiro COPPE/EE/IF, Rio de Janeiro; (*c*) Instituto de Física, Universidade de São Paulo, São Paulo; (*d*) Rio de Janeiro State University, Rio de Janeiro; (*e*) Federal University of Bahia, Bahia; Brazil.
- ⁸⁴KEK, High Energy Accelerator Research Organization, Tsukuba; Japan.
- ⁸⁵Graduate School of Science, Kobe University, Kobe; Japan.
- ⁸⁶(*a*) AGH University of Krakow, Faculty of Physics and Applied Computer Science, Krakow; (*b*) Marian Smoluchowski Institute of Physics, Jagiellonian University, Krakow; Poland.
- ⁸⁷Institute of Nuclear Physics Polish Academy of Sciences, Krakow; Poland.
- ⁸⁸Faculty of Science, Kyoto University, Kyoto; Japan.
- ⁸⁹Research Center for Advanced Particle Physics and Department of Physics, Kyushu University, Fukuoka ; Japan.
- ⁹⁰L2IT, Université de Toulouse, CNRS/IN2P3, UPS, Toulouse; France.
- ⁹¹Instituto de Física La Plata, Universidad Nacional de La Plata and CONICET, La Plata; Argentina.
- ⁹²Physics Department, Lancaster University, Lancaster; United Kingdom.
- ⁹³Oliver Lodge Laboratory, University of Liverpool, Liverpool; United Kingdom.
- ⁹⁴Department of Experimental Particle Physics, Jožef Stefan Institute and Department of Physics, University of Ljubljana, Ljubljana; Slovenia.
- ⁹⁵School of Physics and Astronomy, Queen Mary University of London, London; United Kingdom.
- ⁹⁶Department of Physics, Royal Holloway University of London, Egham; United Kingdom.
- ⁹⁷Department of Physics and Astronomy, University College London, London; United Kingdom.
- ⁹⁸Louisiana Tech University, Ruston LA; United States of America.
- ⁹⁹Fysiska institutionen, Lunds universitet, Lund; Sweden.
- ¹⁰⁰Departamento de Física Teórica C-15 and CIAFF, Universidad Autónoma de Madrid, Madrid; Spain.
- ¹⁰¹Institut für Physik, Universität Mainz, Mainz; Germany.
- ¹⁰²School of Physics and Astronomy, University of Manchester, Manchester; United Kingdom.
- ¹⁰³CPPM, Aix-Marseille Université, CNRS/IN2P3, Marseille; France.
- ¹⁰⁴Department of Physics, University of Massachusetts, Amherst MA; United States of America.
- ¹⁰⁵Department of Physics, McGill University, Montreal QC; Canada.
- ¹⁰⁶School of Physics, University of Melbourne, Victoria; Australia.
- ¹⁰⁷Department of Physics, University of Michigan, Ann Arbor MI; United States of America.
- ¹⁰⁸Department of Physics and Astronomy, Michigan State University, East Lansing MI; United States of America.
- ¹⁰⁹Group of Particle Physics, University of Montreal, Montreal QC; Canada.
- ¹¹⁰Fakultät für Physik, Ludwig-Maximilians-Universität München, München; Germany.
- ¹¹¹Max-Planck-Institut für Physik (Werner-Heisenberg-Institut), München; Germany.
- ¹¹²Graduate School of Science and Kobayashi-Maskawa Institute, Nagoya University, Nagoya; Japan.
- ¹¹³Department of Physics and Astronomy, University of New Mexico, Albuquerque NM; United States of America.
- ¹¹⁴Institute for Mathematics, Astrophysics and Particle Physics, Radboud University/Nikhef, Nijmegen; Netherlands.
- ¹¹⁵Nikhef National Institute for Subatomic Physics and University of Amsterdam, Amsterdam;

Netherlands.

¹¹⁶Department of Physics, Northern Illinois University, DeKalb IL; United States of America.

¹¹⁷^(a)New York University Abu Dhabi, Abu Dhabi;^(b)United Arab Emirates University, Al Ain; United Arab Emirates.

¹¹⁸Department of Physics, New York University, New York NY; United States of America.

¹¹⁹Ochanomizu University, Otsuka, Bunkyo-ku, Tokyo; Japan.

¹²⁰Ohio State University, Columbus OH; United States of America.

¹²¹Homer L. Dodge Department of Physics and Astronomy, University of Oklahoma, Norman OK; United States of America.

¹²²Department of Physics, Oklahoma State University, Stillwater OK; United States of America.

¹²³Palacký University, Joint Laboratory of Optics, Olomouc; Czech Republic.

¹²⁴Institute for Fundamental Science, University of Oregon, Eugene, OR; United States of America.

¹²⁵Graduate School of Science, Osaka University, Osaka; Japan.

¹²⁶Department of Physics, University of Oslo, Oslo; Norway.

¹²⁷Department of Physics, Oxford University, Oxford; United Kingdom.

¹²⁸LPNHE, Sorbonne Université, Université Paris Cité, CNRS/IN2P3, Paris; France.

¹²⁹Department of Physics, University of Pennsylvania, Philadelphia PA; United States of America.

¹³⁰Department of Physics and Astronomy, University of Pittsburgh, Pittsburgh PA; United States of America.

¹³¹^(a)Laboratório de Instrumentação e Física Experimental de Partículas - LIP, Lisboa;^(b)Departamento de Física, Faculdade de Ciências, Universidade de Lisboa, Lisboa;^(c)Departamento de Física, Universidade de Coimbra, Coimbra;^(d)Centro de Física Nuclear da Universidade de Lisboa, Lisboa;^(e)Departamento de Física, Universidade do Minho, Braga;^(f)Departamento de Física Teórica y del Cosmos, Universidad de Granada, Granada (Spain);^(g)Departamento de Física, Instituto Superior Técnico, Universidade de Lisboa, Lisboa; Portugal.

¹³²Institute of Physics of the Czech Academy of Sciences, Prague; Czech Republic.

¹³³Czech Technical University in Prague, Prague; Czech Republic.

¹³⁴Charles University, Faculty of Mathematics and Physics, Prague; Czech Republic.

¹³⁵Particle Physics Department, Rutherford Appleton Laboratory, Didcot; United Kingdom.

¹³⁶IRFU, CEA, Université Paris-Saclay, Gif-sur-Yvette; France.

¹³⁷Santa Cruz Institute for Particle Physics, University of California Santa Cruz, Santa Cruz CA; United States of America.

¹³⁸^(a)Departamento de Física, Pontificia Universidad Católica de Chile, Santiago;^(b)Millennium Institute for Subatomic physics at high energy frontier (SAPHIR), Santiago;^(c)Instituto de Investigación Multidisciplinario en Ciencia y Tecnología, y Departamento de Física, Universidad de La Serena;^(d)Universidad Andres Bello, Department of Physics, Santiago;^(e)Instituto de Alta Investigación, Universidad de Tarapacá, Arica;^(f)Departamento de Física, Universidad Técnica Federico Santa María, Valparaíso; Chile.

¹³⁹Department of Physics, University of Washington, Seattle WA; United States of America.

¹⁴⁰Department of Physics and Astronomy, University of Sheffield, Sheffield; United Kingdom.

¹⁴¹Department of Physics, Shinshu University, Nagano; Japan.

¹⁴²Department Physik, Universität Siegen, Siegen; Germany.

¹⁴³Department of Physics, Simon Fraser University, Burnaby BC; Canada.

¹⁴⁴SLAC National Accelerator Laboratory, Stanford CA; United States of America.

¹⁴⁵Department of Physics, Royal Institute of Technology, Stockholm; Sweden.

¹⁴⁶Departments of Physics and Astronomy, Stony Brook University, Stony Brook NY; United States of America.

- ¹⁴⁷Department of Physics and Astronomy, University of Sussex, Brighton; United Kingdom.
- ¹⁴⁸School of Physics, University of Sydney, Sydney; Australia.
- ¹⁴⁹Institute of Physics, Academia Sinica, Taipei; Taiwan.
- ¹⁵⁰^(a)E. Andronikashvili Institute of Physics, Iv. Javakhishvili Tbilisi State University, Tbilisi; ^(b)High Energy Physics Institute, Tbilisi State University, Tbilisi; ^(c)University of Georgia, Tbilisi; Georgia.
- ¹⁵¹Department of Physics, Technion, Israel Institute of Technology, Haifa; Israel.
- ¹⁵²Raymond and Beverly Sackler School of Physics and Astronomy, Tel Aviv University, Tel Aviv; Israel.
- ¹⁵³Department of Physics, Aristotle University of Thessaloniki, Thessaloniki; Greece.
- ¹⁵⁴International Center for Elementary Particle Physics and Department of Physics, University of Tokyo, Tokyo; Japan.
- ¹⁵⁵Department of Physics, Tokyo Institute of Technology, Tokyo; Japan.
- ¹⁵⁶Department of Physics, University of Toronto, Toronto ON; Canada.
- ¹⁵⁷^(a)TRIUMF, Vancouver BC; ^(b)Department of Physics and Astronomy, York University, Toronto ON; Canada.
- ¹⁵⁸Division of Physics and Tomonaga Center for the History of the Universe, Faculty of Pure and Applied Sciences, University of Tsukuba, Tsukuba; Japan.
- ¹⁵⁹Department of Physics and Astronomy, Tufts University, Medford MA; United States of America.
- ¹⁶⁰Department of Physics and Astronomy, University of California Irvine, Irvine CA; United States of America.
- ¹⁶¹University of Sharjah, Sharjah; United Arab Emirates.
- ¹⁶²Department of Physics and Astronomy, University of Uppsala, Uppsala; Sweden.
- ¹⁶³Department of Physics, University of Illinois, Urbana IL; United States of America.
- ¹⁶⁴Instituto de Física Corpuscular (IFIC), Centro Mixto Universidad de Valencia - CSIC, Valencia; Spain.
- ¹⁶⁵Department of Physics, University of British Columbia, Vancouver BC; Canada.
- ¹⁶⁶Department of Physics and Astronomy, University of Victoria, Victoria BC; Canada.
- ¹⁶⁷Fakultät für Physik und Astronomie, Julius-Maximilians-Universität Würzburg, Würzburg; Germany.
- ¹⁶⁸Department of Physics, University of Warwick, Coventry; United Kingdom.
- ¹⁶⁹Waseda University, Tokyo; Japan.
- ¹⁷⁰Department of Particle Physics and Astrophysics, Weizmann Institute of Science, Rehovot; Israel.
- ¹⁷¹Department of Physics, University of Wisconsin, Madison WI; United States of America.
- ¹⁷²Fakultät für Mathematik und Naturwissenschaften, Fachgruppe Physik, Bergische Universität Wuppertal, Wuppertal; Germany.
- ¹⁷³Department of Physics, Yale University, New Haven CT; United States of America.
- ^a Also Affiliated with an institute covered by a cooperation agreement with CERN.
- ^b Also at An-Najah National University, Nablus; Palestine.
- ^c Also at Borough of Manhattan Community College, City University of New York, New York NY; United States of America.
- ^d Also at Center for Interdisciplinary Research and Innovation (CIRI-AUTH), Thessaloniki; Greece.
- ^e Also at Centro Studi e Ricerche Enrico Fermi; Italy.
- ^f Also at CERN, Geneva; Switzerland.
- ^g Also at Département de Physique Nucléaire et Corpusculaire, Université de Genève, Genève; Switzerland.
- ^h Also at Departament de Física de la Universitat Autònoma de Barcelona, Barcelona; Spain.
- ⁱ Also at Department of Financial and Management Engineering, University of the Aegean, Chios; Greece.
- ^j Also at Department of Physics, California State University, Sacramento; United States of America.
- ^k Also at Department of Physics, King's College London, London; United Kingdom.
- ^l Also at Department of Physics, Stanford University, Stanford CA; United States of America.

- m* Also at Department of Physics, Stellenbosch University; South Africa.
- n* Also at Department of Physics, University of Fribourg, Fribourg; Switzerland.
- o* Also at Department of Physics, University of Thessaly; Greece.
- p* Also at Department of Physics, Westmont College, Santa Barbara; United States of America.
- q* Also at Hellenic Open University, Patras; Greece.
- r* Also at Institutio Catalana de Recerca i Estudis Avancats, ICREA, Barcelona; Spain.
- s* Also at Institut für Experimentalphysik, Universität Hamburg, Hamburg; Germany.
- t* Also at Institute for Nuclear Research and Nuclear Energy (INRNE) of the Bulgarian Academy of Sciences, Sofia; Bulgaria.
- u* Also at Institute of Applied Physics, Mohammed VI Polytechnic University, Ben Guerir; Morocco.
- v* Also at Institute of Particle Physics (IPP); Canada.
- w* Also at Institute of Physics and Technology, Mongolian Academy of Sciences, Ulaanbaatar; Mongolia.
- x* Also at Institute of Physics, Azerbaijan Academy of Sciences, Baku; Azerbaijan.
- y* Also at Institute of Theoretical Physics, Ilia State University, Tbilisi; Georgia.
- z* Also at Lawrence Livermore National Laboratory, Livermore; United States of America.
- aa* Also at National Institute of Physics, University of the Philippines Diliman (Philippines); Philippines.
- ab* Also at Technical University of Munich, Munich; Germany.
- ac* Also at The Collaborative Innovation Center of Quantum Matter (CICQM), Beijing; China.
- ad* Also at TRIUMF, Vancouver BC; Canada.
- ae* Also at Università di Napoli Parthenope, Napoli; Italy.
- af* Also at University of Colorado Boulder, Department of Physics, Colorado; United States of America.
- ag* Also at Washington College, Chestertown, MD; United States of America.
- ah* Also at Yeditepe University, Physics Department, Istanbul; Türkiye.
- * Deceased